MINISTÉRIO DA CIÊNCIA, TECNOLOGIA, INOVAÇÕES E COMUNICAÇÕES
INSTITUTO NACIONAL DE PESQUISAS ESPACIAIS

sid.inpe.br/mtc-m21b/2017/05.29.14.21-TDI

BIOMASS BURNING AND NATURAL EMISSIONS IN THE BRAZILIAN AMAZON RAINFOREST: IMPACT ON THE OXIDATIVE CAPACITY OF THE ATMOSPHERE

Fernando Cavalcante dos Santos

Doctorate Thesis of the Graduate Course in Earth System Science, guided by Drs. Karla Maria Longo de Freitas, and Alex Guenther, approved in May 31, 2017.

URL of the original document:
<http://urlib.net/8JMKD3MGP3W34P/3P26AFB>

INPE
São José dos Campos
2017

PUBLISHED BY:

Instituto Nacional de Pesquisas Espaciais - INPE
Gabinete do Diretor (GB)
Serviço de Informação e Documentação (SID)
Caixa Postal 515 - CEP 12.245-970
São José dos Campos - SP - Brasil
Tel.:(012) 3208-6923/6921
E-mail: pubtc@inpe.br

COMMISSION OF BOARD OF PUBLISHING AND PRESERVATION OF INPE INTELLECTUAL PRODUCTION (DE/DIR-544):
Chairperson:
Maria do Carmo de Andrade Nono - Conselho de Pós-Graduação (CPG)
Members:
Dr. Plínio Carlos Alvalá - Centro de Ciência do Sistema Terrestre (CST)
Dr. André de Castro Milone - Coordenação de Ciências Espaciais e Atmosféricas (CEA)
Dra. Carina de Barros Melo - Coordenação de Laboratórios Associados (CTE)
Dr. Evandro Marconi Rocco - Coordenação de Engenharia e Tecnologia Espacial (ETE)
Dr. Hermann Johann Heinrich Kux - Coordenação de Observação da Terra (OBT)
Dr. Marley Cavalcante de Lima Moscati - Centro de Previsão de Tempo e Estudos Climáticos (CPT)
Silvia Castro Marcelino - Serviço de Informação e Documentação (SID) **DIGITAL LIBRARY:**
Dr. Gerald Jean Francis Banon
Clayton Martins Pereira - Serviço de Informação e Documentação (SID)
DOCUMENT REVIEW:
Simone Angélica Del Ducca Barbedo - Serviço de Informação e Documentação (SID)
Yolanda Ribeiro da Silva Souza - Serviço de Informação e Documentação (SID)
ELECTRONIC EDITING:
Marcelo de Castro Pazos - Serviço de Informação e Documentação (SID)
André Luis Dias Fernandes - Serviço de Informação e Documentação (SID)

MINISTÉRIO DA CIÊNCIA, TECNOLOGIA, INOVAÇÕES E COMUNICAÇÕES
INSTITUTO NACIONAL DE PESQUISAS ESPACIAIS

sid.inpe.br/mtc-m21b/2017/05.29.14.21-TDI

BIOMASS BURNING AND NATURAL EMISSIONS IN THE BRAZILIAN AMAZON RAINFOREST: IMPACT ON THE OXIDATIVE CAPACITY OF THE ATMOSPHERE

Fernando Cavalcante dos Santos

Doctorate Thesis of the Graduate Course in Earth System Science, guided by Drs. Karla Maria Longo de Freitas, and Alex Guenther, approved in May 31, 2017.

URL of the original document:
<http://urlib.net/8JMKD3MGP3W34P/3P26AFB>

INPE
São José dos Campos
2017

Cataloging in Publication Data

Santos, Fernando Cavalcante dos.

Sa59b Biomass burning and natural emissions in the brazilian amazon rainforest: impact on the oxidative capacity of the atmosphere / Fernando Cavalcante dos Santos. – São José dos Campos : INPE, 2017.

xxii + 116 p. ; (sid.inpe.br/mtc-m21b/2017/05.29.14.21-TDI)

Thesis (Doctorate in Earth System Science) – Instituto Nacional de Pesquisas Espaciais, São José dos Campos, 2017.

Guiding : Drs. Karla Maria Longo de Freitas, and Alex Guenther.

1. Biogenic volatile organic compounds. 2. Observation and modeling. 3. Oxidative capacity. I.Title.

CDU 504.7:630*43(811.3)

Esta obra foi licenciada sob uma Licença Creative Commons Atribuição-NãoComercial 3.0 Não Adaptada.

This work is licensed under a Creative Commons Attribution-NonCommercial 3.0 Unported License.

Aluno (a): *Fernando Cavalcante dos Santos*

"BIOMASS BURNING AND NATURAL EMISSIONS IN THE BRAZILIAN AMAZON RAINFOREST: IMPACT ON THE OXIDATIVE CAPACITY OF THE ATMOSPHERE"

Aprovado (a) pela Banca Examinadora em cumprimento ao requisito exigido para obtenção do Título de *Doutor(a)* em

Ciência do Sistema Terrestre

Dr. Celso von Randow

Presidente / INPE / São José dos Campos - SP

Dra. Karla Maria Longo de Freitas

Orientador(a) / NASA / Washington, D.C. - USA

Dr. Alex Guenther

Orientador(a) / Uni. of California / California - USA

Dr. Jose Oscar William Vega Bustillos

Convidado(a) / IPEN / São Paulo - SP

Dr. Demerval Soares Moreira

Convidado(a) / UNESP / Bauru - SP

Este trabalho foi aprovado por:

( ) maioria simples

(x) unanimidade

São José dos Campos, 31 de maio de 2017

ACKNOWLEDGEMENTS

We thank the Group Modeling of the Atmosphere and Its Interfaces: Demerval Moreira, Rodrigo Braz, Luiz Flavio, Madeleine Gácita, Megan Bela, Daniela França, Ricardo Siqueira, Isilda Menezes and Dr. Saulo Freitas; Eliane Gomes Alves; the National Center for Atmospheric Research for the infrastructure given during the period of internship and researchers Dr. Louisa Emmons, Dr. James Smith, Dr. Christine Wiedinmyer, Dr. Jeong-Hu Park, Dr. Peter Haley and Dr. Andrew Turnipseed especially for their assistance in the quantification of the samples; the Pacific Northwest National Laboratory for their support and infrastructure provided during the internship, postdoctoral students Dasa Gu, Haofei Yu, the researchers Dr. Rodica Lindenmaier, Dr. Manishkumar Shrivastava, Dr. John Shilling and Dr. Beat Schmid.

To my friends in São Paulo, São Carlos, São José dos Campos and other cities and countries that I lived during these years.

An especial thank to my friends from the Earth System Science Center program! Alex, Aline, Carla, Gilney, Karine, Lucia, Mabelis, Chica, Michelle, Minella, Pri e Sandro.

To Dr. Karla Longo and Dr. Alex Guenther for guidance, patience, friendship and motivation provided during the whole period of development of this work. Thank you for providing me with this personal growth opportunity that goes beyond the academic knowledge gained in these years of research.

To FAPESP for the financial support. To the NCAR and PNNL for all the financial support.

To my family for the dedication, love and patience they have had for all these years; especially in some difficult times.

And to all who contributed in some way to the accomplishment of this work

ABSTRACT

Emitted by vegetation, isoprene (2-methyl-1,3-butadiene) is the most abundant non-methane hydrocarbons, with an annual global emission calculated ranging from 440 to 660Tg carbon, depending on the driving variables like temperature, solar radiation, leaf area index and plant functional type. It is estimated, for example, that the natural compounds like isoprene and terpenes present in the troposphere are about 90% and 50%, respectively, removed from the atmosphere by oxidation performed by hydroxyl radical (OH). Furthermore, the oxidation products of isoprene may contribute to secondary organic aerosol (SOA) formation, affecting the climate and altering the properties and lifetimes of clouds. Considering the importance of these emissions and the hydroxyl radical reaction in the atmosphere, the SAMBBA (South American Biomass Burning Analysis) experiment, which occurred during the dry season (September 2012) in the Amazon Rainforest, provided information about the chemical composition of the atmosphere through airborne observations. Although primarily focused on biomass burning flights, the SAMBBA project carried out other flights providing indirect oxidative capacity data in different environments: natural emission dominated flights and biomass-burning flights with fresh plumes and aged plumes. In this study, we evaluate the oxidative capacity of the Amazon rainforest in different environments, both for the unpolluted and biomass-burning disturbed atmosphere using the ratio [MVK + MACR]/[Isoprene]. Beyond that, we propose an improvement on the formulation of indirect OH density calculation, using the photochemical aging $[O_3]/[CO]$ as a parameter. Using a synergistic approach, balancing numerical modeling and direct observations, the numerical model BRAMS was coupled to MEGAN emission model to get a better result for isoprene and OH in the atmosphere, representing the observations during SAMBBA field campaign. In relation to OH estimation, we observed an improvement in the concentration values using the modified sequential reaction model, for both biomass burning regimes and background environment. We also detected a long-range transport events of O_3 during SAMBBA experiment, considering the high levels of O_3 in aged plumes at high altitudes (5,500 – 6,500 m), and the detection of an O_3 inflow in the Amazon basin from Africa. These findings support the importance of long-range transport events as a source of O_3 into the troposphere in the Amazon basin, which could even alter the atmospheric composition within the planetary boundary layer and alter the oxidative capacity in the region. The model results showed a reasonable agreement for isoprene concentration, although more investigation needed for the OH simulation.

Keywords: Biogenic Volatile Organic Compounds. Observation and Modeling. Oxidative Capacity.

EMISSÕES NATURAIS E DE QUEIMADAS NA FLORESTA AMAZÔNIA: IMPACTO NA CAPACIDADE OXIDATIVA DA ATMOSFERA

RESUMO

Emitido pela vegetação, o isopreno (2-metil-1,3-butadieno) é o hidrocarboneto não-metânico mais abundante, com uma emissão global anual calculada entre 440 e 660Tg de carbono, dependendo de variáveis como temperatura, radiação solar, índice de área foliar e tipo funcional da planta. Estima-se, por exemplo, que os compostos naturais como isopreno e terpenos presentes na troposfera são cerca de 90% e 50%, respectivamente, removidos da atmosfera por oxidação realizada por radical hidroxila (OH). Além disso, os produtos de oxidação do isopreno podem contribuir para a formação de aerossóis orgânicos secundários (AOS), afetando o clima e alterando as propriedades e o ciclo hidrológico das nuvens. Considerando a importância dessas emissões e a reação do radical hidroxila na atmosfera, o experimento SAMBBA (do inglês, South American Biomass Burning Analysis), que ocorreu durante a estação seca (setembro de 2012) na Floresta Amazônica, forneceu informações sobre a composição química da atmosfera através de observações aéreas. Embora focado principalmente nos voos ocorridos durante a queima de biomassa, o projeto SAMBBA realizou outros voos que forneceram dados indiretos de capacidade oxidativa em diferentes ambientes: voos dominados por emissão natural e voos com queima de biomassa com plumas frescas e envelhecidas. Neste estudo, avaliamos a capacidade oxidativa da floresta amazônica em diferentes ambientes, tanto para a atmosfera não poluída quanto para atmosfera perturbada pela queima de biomassa usando a razão [MVK + MACR] / [Isoprene]. Além disso, propomos uma melhoria na formulação do cálculo da densidade indireta de OH, usando o envelhecimento fotoquímico [O_3] / [CO] como parâmetro. Usando uma abordagem sinérgica, balanceando modelagem numérica e observações diretas, o modelo numérico BRAMS foi acoplado ao modelo de emissão MEGAN para obter um melhor resultado para isopreno e OH na atmosfera, representando as observações durante a campanha do SAMBBA. Em relação à estimativa de OH, observamos uma melhora nos valores de concentração usando o modelo de reação sequencial modificada, tanto para os regimes de queima de biomassa quanto para região pristina. Também detectamos eventos de transporte de longo alcance de O_3 durante o experimento SAMBBA, considerando os altos níveis de O_3 em plumas envelhecidas em altitudes elevadas (5.500 - 6.500 m) e a detecção de um influxo de O_3 na bacia amazônica proveniente da África. Essas descobertas sustentam a importância dos eventos de transporte de longo alcance como fonte de O_3 na troposfera da bacia amazônica, o que poderia até alterar a composição atmosférica dentro da camada limite planetária e alterar a capacidade oxidativa da região. Os resultados do modelo mostraram uma correlação razoável para a concentração de isopreno, embora fosse necessária mais investigação para a simulação de OH.

Palavras-chaves: Compostos Orgânicos Voláteis Biogênicos. Observação e Modelagem. Capacidade Oxidativa.

LIST OF FIGURES

Pag.

LIST OF TABLES

Pag.

LIST OF ACRONYMS AND ABBREVIATIONS

ABLE	Amazon Boundary Layer Experiment
ACCENT	Atmospheric Composition Change the European Network of Excellence
AIRS	Atmospheric Infrared Sounder
AP	Aged plume
ATTO	Amazonian Tall Tower Observatory
AUTH-Nkua	Aristotle University of Thessalonik – National and Kapodistrian University of Athens
AVAPS	Airborne Vertical Atmospheric Profiling System
BARCA	Regional Carbon Balance in Amazonia
BG	Backgorund
BIOEMI	Biogenic Emission Model
BRAMS	Brazilian developments on the Regional Atmospheric Modelling System
BVOC	Biogenic Volatile Organic Compounds
CARMA	Community Aerosol and Radiation Model for Atmospheres
CCN	Cloud Condensation Nuclei
CESM	Community Earth System Model
CL	Cloud Layer
CLM	Community Land Model
CPC	Condensation Particle Counter
CPTEC	Centro de Previsão de Tempo e Estudos Climáticos
CTM	Chemistry Transport Models
ECD	Electron Capture Detection
EDGAR	Emission Database for Global Atmospheric Research
ER	Enhancement Ratio
FGGA	Fast Greenhouse Gas Analyzer
FORTRAN	FORmula TRANslation
FP	Fresh Plume
GABRIEL	Guyanas Atmosphere-Biosphere exchange and Radicals Intensive Experiment with a Learjet
GC-FID	Gas Chromatography with Flame Ionization detector

GC-MS	Gas Chromatography with Mass Spectrometry detector
GEIA	Global Emissions Inventories Activity
GFED	Global Fire Emissions Database
IIR	Imaging Infrared Radiometer
IN	Ice Nuclei
INPE	Instituto Nacional de Pesquisas Espaciais
ISOPOOH	Hydroxyhydroperoxides
JULES	JointUKLand Environment Simulator
LAI	Leaf Area Index
LIDAR	Light Detection And Ranging
MACR	Methacrolein
MEGAN	Model of Emissions of Gases and Aerosols from Nature
MMS	Monolithic Miniature Spectrometer
MODIS	Moderate-Resolution Imaging Spectroradiometer
MVK	Methyl Vinyl Ketone
NCAR	National Center for Atmospheric Research
NIST	National Institute of Standards and Technology
PAN	Peroxyacetyl Nitrate
PAR	Photosynthetically Active Radiation
PBL	Planetary Boundary Layer
PFT	Plant Functional Type
PNNL	Pacific Northwest National Laboratory
PSAP	Particle Soot Absorption Photometer
PTRMS	Proton Transfer Reaction – Mass Spectrometry
RACM	Regional Atmospheric Chemistry Mechanism
RAMS	Regional Atmospheric Modeling System
REA	Relaxed Eddy Accumulation
RELACS	Regional Lumped Atmospheric Chemical Scheme
RETRO	REanalysis of the TROpospheric
RTIE	Real Time Imaging Electronics
SAMBBA	South American Biomass Burning Analysis
SCAR-B	Smoke/Sulfates, Clouds and Radiation - Brazil

SHIMS	Spectral Hemispheric Irradiance
SID	Serviço de Informação e Documentação
SOA	Secondary Organic Aerosol
SPG	Serviço de Pós-Graduação
SWS	Short Wave Spectrometer
TDI	Teses e Dissertações Internas
TEB	Town Energy Budget
TROFFEE	Tropical Forest and Fire Emissions Experiment
UKMO	UK Met Office
UV	Ultraviolet
VBA	Visual Basic for Applications
VOC	Volatile Organic Compounds
WAS	Whole Air Sampling
WRF	Weather Research and Forecasting Model

SUMMARY

Pag.

1 INTRODUCTION AND THEORETICAL REFERENCE

1.1. Tropical forests and volatile organic compounds

The Amazon Rainforest is the largest tropical forest in the world encompassing eight countries (Bolivia, Peru, Ecuador, Colombia, Venezuela, Guyana, Suriname and French Guiana) in addition to Brazil. The Brazilian Amazon has approximately 4 million km², almost half of the national territory (8.5 million km^2), displaying a great diversity in its fauna and flora. Because it is a complex ecosystem, with a large territorial area, high biodiversity and still has regions where the main environmental characteristics are preserved, the Amazon Rainforest is the target of different studies in different areas of knowledge, constituting a singular region of the planet. Like the Amazon Rainforest, tropical forests all over the planet (Figure 1.1) have striking common characteristics, the main one being the wide variety of flora and fauna in the world.

Figure 1.1 Map of the rainforests in the world (dark green).

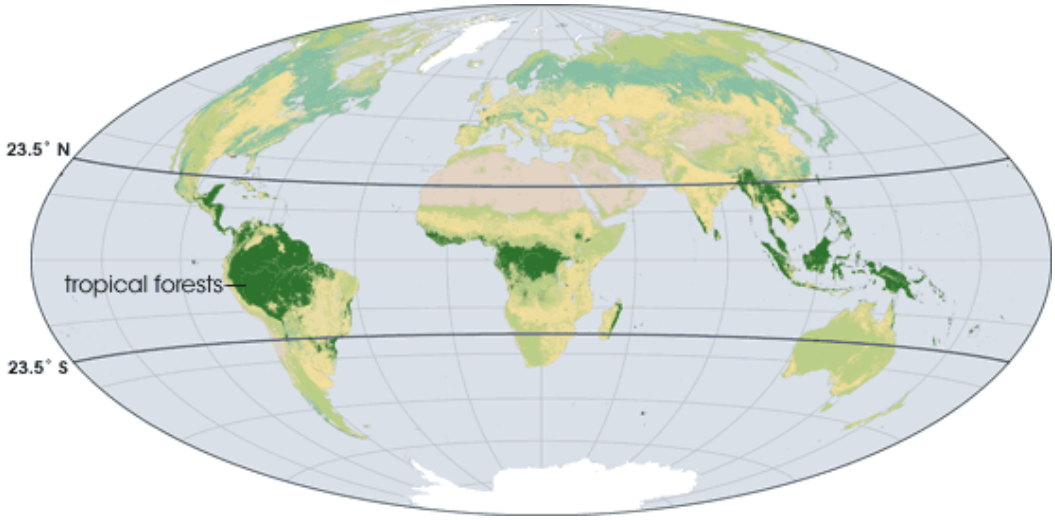

Source: Simmon (2007)

Tropical forests have the fundamental function of helping to maintain the planet's climatic stability, since they play an important role in biological, physical and chemical processes; and specifically, on the hydrological cycle and the chemical composition of the atmosphere. These complex and non-linear forest-atmosphere interactions can soften or amplify global climatic changes of anthropic origin (BONAN, 2008).

Observational and/or modeling studies conducted in different forest regions (HOFFMANN et al., 1997; THUNIS; CUVELIER, 2000; TOLL; BALDASANO, 2000; POTTER et al., 2001; XU; WESELY; PIERCE, 2002; KARLIK; CHUNG; WINER, 2003; BELL; ELLIS, 2004; SOLMON et al., 2004; YIN et al., 2004; BYUN et al., 2005; CARVALHO et al., 2005; CURCI et al., 2009; GUIMARÃES et al., 2009; FELDMAN et al., 2010; IM et al., 2011; SARTELET et al., 2012; YÁÑEZ-SERRANO et al., 2015; MISZTAL et al., 2016), with special attention to biogenic volatile organic compounds (BVOC), are useful for regional and global understanding of the chemistry of the atmosphere, carbon cycle and climate. The inclusion of BVOC emissions in numerical chemical transport models and a better understanding of the processes that control the emissions of these VOCs can result, for example, in an improvement in the description of the tropospheric ozone and secondary organic aerosol (SOA) formation processes (PIERCE et al., 1998; POTTER et al., 2001; BELL; ELLIS, 2004; IM et al., 2011; SARTELET et al., 2012; HERMANSSON et al., 2014).

Techniques of mass flow measurements above the canopy enable direct measurements of VOC fluxes using turbulent vortex covariance (BOWLING et al., 1998; NÖLSCHER et al., 2009; TURNIPSEED et al., 2009). Such systems allow for more accurate estimates of flow and continuous measurements, as well as the possibility of obtaining information for a wide variety of BVOCs. These measures assist in the assessment and validation of emission modeling procedures, and may also establish average emission factors in a given region with a high diversity of species (e.g. tropical forests) (REEVES et al., 2004).

The determination of BVOC in the atmospheric boundary layer assists in the determination of the degree of reactivity of many chemical compounds. Often, the concentration levels of VOCs observed in the environment are very low, but with significant emission flows. Such information is relevant because it indicates that the chemical compound studied has a considerable importance in the reactions that occur along its trajectory in the atmosphere, more precisely in the troposphere. Therefore, environmental concentration measurements are best used when combined with chemical emission and transport estimates in numerical models.

The Earth's land, oceans, and ecosystems daily release tons of trace gases and aerosol particles to the atmosphere, via both natural and anthropogenic processes. Terrestrial vegetation emits to the atmosphere a significant amount of biogenic volatile organic compounds (BVOCs), corresponding to 1,150 Tg Carbon per year. The most abundant BVOC is isoprene (C_5H_8), with an annual global emission ranging from 440 to 660 Tg Carbon per year, depending on driving variables such as temperature, solar radiation, leaf area index, and plant functional type (GUENTHER et al., 2012). In contrast, the global emission rate of anthropogenic volatile organic compounds (AVOCs) is around 145 Tg Carbon per year (JANSSENS-MAENHOUT et al., 2015). The BVOCs mixing ratios in the Amazon are variable, with the values ranging from 2.4 to 7.8 ppbv, depending on location, altitude, and seasonal behavior of radiation, temperature, and phenology (Yáñez-Serrano et al., 2015 and references therein). Harley et al. (2004), for example, estimated that about 38% of the plants in the Amazon forest emit isoprene. Also, studies have shown that the capacity of different plants for producing and storing isoprenoids is very specific (SHARKEY; WIBERLEY; DONOHUE, 2008; LAOTHAWORNKITKUL et al., 2009).

Most of the trace compounds that enter in the atmosphere through emissions from the surface are subjected to an oxidation process, producing chemical species such as sulfur dioxide (SO_2), sulfate (SO_4^{2-}), nitrogen oxide (NO), nitric acid (HNO_3), carbon

monoxide (CO) and carbon dioxide (CO_2). This effect of degradation that the atmosphere exerts on many chemical compounds, led to the stability in the concentration of the gases present in the current atmosphere, although the human activity is modifying its composition to a greater or lesser degree, depending on the species or chemical class of the emitted compound, as well as the intensity of its emission.

1.2. The oxidative capacity of the atmosphere

The overall concentration of the hydroxyl (OH) radical in the atmosphere is commonly used to express oxidative capacity and effectively represent the diurnal ability of the atmosphere to oxidize trace compounds. Due to this characteristic, the importance of the tropics in global oxidative capacity can be explained especially by the high levels of radiation and humidity in the atmosphere of these regions (MONKS, 2005; STOHL et al., 2009). In addition, the oxidative capacity of the atmosphere cannot be studied solely because of the chemical composition, since the formation of convective systems can transport species of short life to higher levels in the troposphere, influencing the availability of these compounds and consequently the occurrence of oxidative reactions at higher levels (PRINN, 2003). Due to this feature, we can note the importance of the combination of meteorological and chemical data in the analysis of numerical models.

The troposphere is responsible to chemically transform and remove trace gases due to a complex chemistry driven by solar UV radiation. This chemistry is also driven by emissions of gases, such as NO, CO and VOC, leading to the production of O_3 and OH. The hydroxyl radical is the most important oxidizer and a key measure of the capacity of the atmosphere to oxidize trace gases, influencing the climate, air pollution, and acid rain. The primary OH source involves water vapor that reacts with a singlet oxygen

atom O(1D) that comes from photodissociation of O_3 by solar UV radiation at wavelengths less than 310 nm (PRINN, 2014). In the presence of nitrogen oxides (NO and NO_2), which is a human-related source, significant amount of net production of O_3 is found in the troposphere, in agreement to the O_3 – NO_x – VOC chemistry. To summarize, the principal catalyzed reactions involving OH and O_3 in the troposphere are shown in equations 1.1 – 1.15.

$$O_3 + UV \rightarrow O_2 + O(^1D) \quad (1.1)$$

$$O(^1D) + H_2O \rightarrow 2OH \quad (1.2)$$

Net effect: $O_3 + H_2O \rightarrow O_2 + 2OH$ (1.3)

$$OH + CO \rightarrow H + CO_2 \quad (1.4)$$

$$H + O_2 \rightarrow HO_2 \quad (1.5)$$

$$HO_2 + NO \rightarrow OH + NO_2 \quad (1.6)$$

$$NO_2 + UV \rightarrow NO + O \quad (1.7)$$

$$O + O_2 \rightarrow O_3 \quad (1.8)$$

Net effect: $CO + 2O_2 \rightarrow CO_2 + O_3$ (1.9)

$$OH + RH \rightarrow R + H_2O \quad (1.10)$$

$$R + O_2 \rightarrow R_2 \quad (1.11)$$

$$RO_2 + NO \rightarrow RO + NO_2 \quad (1.12)$$

$$NO_2 + UV \rightarrow NO + O \quad (1.13)$$

$$O + O_2 \rightarrow O_3 \quad (1.14)$$

Net effect: $OH + RH + 2O_2 \rightarrow RO + H_2O + O_3$ (1.15)

The atmosphere of the Amazon, in its undisturbed state, oxidizes the BVOCs naturally emitted by the forest vegetation, recycling some OH and depositing reactive carbon back to the surface as several oxidation products, including as secondary organic aerosols (SOA) that has the potential to affect the climate and alter the properties and lifetimes of clouds. In this way, the cleaning process also acts as a local recycling mechanism, preventing the loss of essential nutrients from the forest (LELIEVELD et al., 2008). It is estimated that about 90% of the isoprene and 50% of the terpenes ($(C_5H_8)_n$) are removed from the atmosphere via oxidation by OH, followed by the deposition of oxidized VOC and SOA within a timescale of a few hours (MONKS, 2005). In fact, the isoprene is a key compound in many atmospheric chemistry studies, especially over forest regions, because of its abundance and high reactivity with OH (BARKET et al., 2004; PRINN, 2014).

For a long time, the traditional understanding was that the unpolluted atmosphere, defined by low levels of nitrogen oxides (NO_x), has low concentrations of OH during the midday, typically 1–5 x 10^5 molecules cm^{-3}. However, known discrepancies between atmospheric chemistry model results and observations raised the supposition of a missing sink for OH (WARNEKE et al., 2001; WHALLEY et al., 2013). Recently, airborne measurements carried out in an unpolluted atmosphere over the Amazon rainforest found unexpected high oxidative capacity levels, which, complemented laboratory and numerical modeling studies, led to a different hypothesis for OH

production (LELIEVELD et al., 2008). Concentrations of OH around 5.6 (±1.9) x 10^6 molecules cm^{-3} were measured in the planetary boundary layer (PBL) over the Amazon, concomitant with CO, NO, and O_3 mixing ratios of 113 (±13.9) ppbv, 0.02 (±0.02) ppbv, and 18.5 (±4.6) ppbv, respectively, values typical of the unpolluted atmosphere. This work pointed to the reaction of isoprene with peroxy radicals (HO_2) as an alternative pathway to produce OH in an unpolluted environment (LELIEVELD et al., 2008). The Figure 1.2 represents the major OH formation in the atmosphere and their subsequent reactions with VOCs.

Figure 1.2 OH recycling scheme. Photodissociation of ozone leads to primary OH formation and a subsequent OH reactions with carbon monoxide and VOCs produce peroxy radicals. In high-NO conditions, OH is recycled (pathway I). In low-NO conditions, the deposition of peroxides (pathway II) causes a net loss of OH. Pathway III was suggested by LELIEVELD et al. (2008) and detailed in equations 1.17-1.19. Pathway IV with unsaturated VOCs also occurs, with little influence on atmospheric OH.

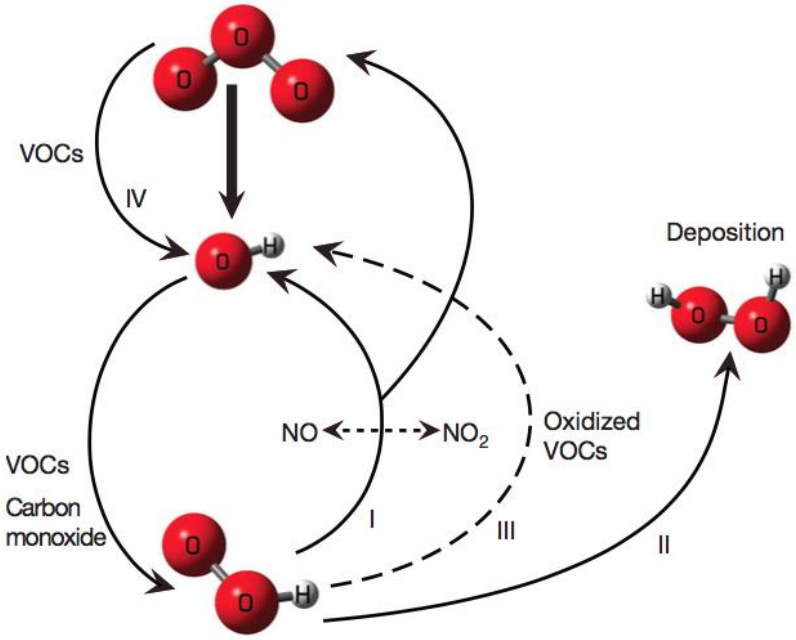

Source: Lelieveld et al. (2008).

The efficient OH recycling suggested by LELIEVELD et al., (2008) may explain how the atmospheric oxidation capacity could be sustained in geological warm periods with abundant vegetation. The equations x-y represents the OH recycling path, as well as the deposition of organic hydroperoxides under low-NO_x condition.

$$HO_2 + RO_2 \rightarrow ROOH + O_2 \qquad \text{[Deposition]} \qquad (1.16)$$

$$\text{Isoprene} + OH \rightarrow R \qquad (1.17)$$

$$R + O_2 \rightarrow RO_2 \qquad (1.18)$$

$$RO_{2(\text{from isoprene})} + HO_2 \rightarrow OH + {}_{\text{other products}} \qquad (1.19)$$

More recently, significant advances have been made with organic peroxy radicals produced as intermediates of atmospheric photochemistry, showing the importance of both HO_2 and NO pathways, even in considered low-NO regions to isoprene chemistry. An accurate understanding of the two pathways is needed for quantitative predictions of the concentrations of particulate matter, oxidation capacity, and consequent environmental and climate impacts in pristine forest regions (LIU et al., 2016).

In contrast, there are regions of Amazonia that have been strongly impacted by human activity. The ongoing deforestation, followed by vegetation burning to open areas for pasture and agriculture production is the most devastating example. During the austral winter (from July to October), the Amazonia climate is typically dry and is disturbed each year by extensive vegetation fires in areas of deforestation and agricultural/pasture land management, particularly along the so-called deforestation arc, an area of about 500,000 km^2 extending from the southwestern to the eastern border of the forest (ARTAXO et al., 2013). During the fire events, an intricate myriad of chemical and

physical processes occurs. The continuous increase in temperature of the fresh biomass caused by nearby fires can distill species absorbed by plants with low boiling point (*e.g.*, $T_{isoprene} \cong 307$ K), macromolecular bonds can be broken (*i.e.*, low-temperature pyrolysis), gasification reactions converting carbon in the solid char to CO and CO_2 can occur and the flames efficiently oxidize the volatile gases to species such as H_2O, CO_2, and NO_x (BERTSCHI et al., 2003; LONGO et al., 2009). The release of isoprene and other BVOCs is dependent on the different phases of biomass combustion, and different vegetation communities affect the amount and diversity of volatile organic compounds released (CICCIOLI; CENTRITTO; LORETO, 2014). In this disturbed atmosphere, the natural efficient OH recycling is affected, altering the oxidative capacity of the atmosphere. In the absence of biomass burning emissions, isoprene is the dominant reactive VOC in the pristine Amazon forest, and during the day, isoprene oxidation dominates the OH chemistry producing, amongst other products, methyl vinyl ketone (MVK), methacrolein (MACR), and hydroxyhydroperoxides (ISOPOOH) (KARL et al., 2007; RIVERA-RIOS et al., 2014; LIU et al., 2016).

1.3. Numerical modeling of atmospheric chemistry

Eulerian three-dimensional chemistry transport models (CTMs) are numerical tools that helps to understand the complex interactions between atmospheric emissions, meteorology and atmospheric chemistry. CTMs with transport solution, chemical mechanism and atmospheric aerosols, coupled to the solution of the atmospheric state, represent the state of the art of atmospheric composition modeling. In coupled models, the atmospheric transport of aerosol particles and trace gases is consistent with the atmospheric model due to the use of a single vertical and horizontal coordinate system; And the same physical parameterizations of the atmospheric model for the transport of trace compounds in the grid and sub-grid scales of the model. Another important

characteristic of the coupled, or integrated, CTMs is the feedback of the atmospheric state due to the disturbances initiated by the presence of pollutants. As examples of integrated CTMs, which follows this coupled numerical treatment, we can cite the model WRF-CHEM (*Weather Research and Forecasting Model*, GRELL et al., 2005; FAST et al., 2006) and BRAMS (*Brazilian Regional Atmospheric Modeling System*, LONGO et al., 2013, FREITAS et al., 2017).

Chemical mechanisms of gas phase reactions are vital components of the CTMs. Such chemical information is incorporated into modules that are used, for example, in the calculation of sources of ozone precursors, formation and sinks. The chemical mechanism is translated into the form of differential equations, which are coded into computational codes which in turn include numerical solutions used to simulate the evolution of chemical species in the atmosphere. Over the years, the chemical mechanisms for air quality modeling have improved and become more detailed according to the amount of observational data and supercomputers available. Although this development has taking place, it will not yet be possible to incorporate a detailed treatment of the reactions of all known chemical species because there are thousands of known organic or inorganic compounds emitted into the atmosphere. The gas-phase reaction mechanisms used in CTMs frequently have simplified or compressed kinetics. Detailed mechanisms are available, but their use can be impractical for large numbers of simulations, for either multiple box model calculations or the chemical integrations for a regional reaction/transport model. Due to this obstacle, some simplified methods become necessary for the execution of air quality modeling to be computationally possible (STOCKWELL et al., 2011).

In this context, the chemical mechanisms that are present in numerical atmospheric models can be classified in three different treatment methods; From the more complex (explicit mechanism) to the more simplified (aggregate mechanism). An explicit mechanism consists of explicit reactions to chemical species that are treated

individually. A replacement mechanism uses the explicit chemistry of some pre-selected organic chemical species to represent the atmospheric chemistry of all volatile organic compounds, for example. However, numerical air quality models use aggregate chemical mechanisms, with selected chemical species to represent the reactions of whole classes of organic compounds. The lower number of numerically treated chemical species results in a reduction of the computational resources required to perform numerical air quality models, but on the other hand, the reduction in the number of chemical species may limit the investigation of complex and/or specific processes which occur in the troposphere.

1.4. Numerical models of natural emissions

The methodologies commonly used by numerical models for the quantification of natural emissions require input data such as emissions based on measurements, meteorological and land use data (soil cover, leaf area index and etc.) derived from observations. Natural emissions estimates need to be adjusted in the grid, according to the chemical mechanism used in the air quality models and even with several studies (observational and modeling), uncertainties in natural emissions remain large, often overcoming the uncertainties associated with anthropogenic emissions. Biogenic emissions, for the most part, are calculated from emission models (MEGAN - *Model of Emissions of Gases and Aerosols from Nature*; BEIS3 – *Biogenic Emission Inventory System*, AUTH-Nkua – *Aristotle University of Thessalonik – National and Kapodistrian University of Athens* e BIOEMI – *Biogenic Emission Model*) and in some cases, from existing databases (GEIA/ACCENT, *Global Emissions Inventories Activity/Atmospheric Composition Change the European Network of Excellence*). The algorithms that are normally applied are those introduced by (GUENTHER et al., 1995), in which, isoprene emissions are temperature and solar radiation dependent, whereas

monoterpenes and other VOCs are temperature dependent only. Additional relevant processes in the emissions of biogenic compounds are described by some of the emission models. For example, the natural emission model BEIS3 provides species seasonally dependent on biogenic emission factors and leaf area index (LAI) for each type of land use, adjusting isoprene emissions to the effects of photosynthetically active radiation (PAR). Another example is the AUTH-Nkua model that considers the dependence of monoterpenes in relation to the solar radiation for some species of vegetation. The MEGAN model describes the variation of biogenic emissions as a function of innumerable environmental variables (temperature, solar radiation, humidity, wind speed in the canopy, leaf area index, leaf age and soil moisture), considering the loss and production component in the canopy.

Considering the importance of SAMBBA experiment to assess the BVOC mixing ratios and the contribution of hydroxyl radical reaction to the atmospheric composition, in this thesis I address three important issues to improve the understanding about the functioning of the oxidative capacity of the atmosphere in Amazonian forest using a synergistic approach, balancing numerical modeling and direct observations. The first issue is how to assess the impact of the anthropic disturbances like biomass burning activity on the oxidative capacity of the atmosphere of remote areas in the Amazon basin. The second issue is to obtain an appropriate method to estimate the OH concentration under the impact of different chemical regimes, with the results comparable with the observations in the study region. The third issue is what we can learn from the improvement in the estimated OH concentration in both biomass burning regimes and background environment, and to use such information to improve air quality models.

2 OBJECTIVES

The objective of this research project is to advance in the knowledge of oxidative capacity and determine the chemical composition of the atmosphere in the Amazon basin using a synergistic approach between numerical modeling and direct observations. It is proposed to use a 3D chemical model coupled with a natural emissions model to study the chemical mechanisms that control the atmospheric oxidative capacity in the Amazon Forest, seeking to represent in the numerical model the understanding obtained with the direct observations. The specific objectives of this project are listed below:

I. Understanding the oxidative capacity of the atmosphere in remote areas, evaluating the possible impacts of anthropic disturbances, mainly emissions from biomass burning.
II. To investigate the adequacy of the chemical mechanisms commonly used in air quality models.
III. To update the biogenic emissions in BRAMS numerical model, considering the environmental factors that alter the emission regime in the Amazon Forest.
IV. Contribute to the development of the Brazilian model of chemical transport and its suitability for the study region, with the introduction of a module of biogenic emissions in the current state of the art that contemplates the emissions of the Amazon Forest.

3 METHODS

The current thesis involves two observation platforms during SAMBBA field campaign and a numeric model development component. As a part to the observation platform, we conducted airborne measurements that capture different chemical composition in the atmosphere in the Amazon basin and tower observation that was restricted to measurements in the tower K-34 along three days. The numerical model development component focus on the implementation of a representative natural emission in BRAMS model, which was applied only for isoprene as a first step to a future complete implementation of MEGAN model into BRAMS.

The chapter is organized in three sub-chapters. In section 3.1, we present the SAMBBA field campaign, including the aircraft instrumentation, meteorological conditions and fire occurrence during the campaign period. The classification method of flight tracks, as well as the method for the indirect OH calculation, is also described in this section. In section 3.2, in addition to the airborne measurements, we also present the air sampling in a forest site, at the K-34 tower. Finally, the modeling tools, including the development of the coupling of MEGAN model within BRAMS, are presented in section 3.3, as well as the system configuration of the simulations during SAMBBA period.

3.1. SAMBBA field campaign

The SAMBBA field campaign was an airborne experiment carried out in the Brazilian Amazonian sector late in the dry season and during the transition from the dry to the wet season, from the 14th September to the 3rd October 2012. SAMBBA was a multidisciplinary and multinational joint effort of scientists from several institutions; a partnership between the UK Met Office (UKMO), the National Institute for Space

Research (INPE), a consortium of 7 UK Universities, and the University of Sao Paulo. Together, these institutions sought to assess and explore the predictive capability of aerosol and climate modeling across all scales. A synergistic approach to these activities has helped yield much greater outcomes, due to the great breadth of understanding between climate scientists, dynamical meteorologists, gas phase, aerosol and cloud observational scientists, process modelers and remote sensing experts. The SAMBBA aircraft campaign was the first deployment of a foreign atmospheric research aircraft in Brazil to measure biomass burning since Smoke/Sulfates, Clouds and Radiation - Brazil (SCAR-B) in 1995. Numerous atmospheric measurements were conducted on board the BAe-146 research aircraft, during 20 research flights, 67 flight hours in total. The BAe-146 research aircraft, from the Facility for Airborne Atmospheric Measurements (FAAM - http://www.faam.ac.uk), was based in Porto Velho - RO, but made use of other regional airports (Palmas - TO, Rio Branco - AC, and Manaus - AM airports) to extend the operational range of the aircraft (Figure 3.1).

Figure 3.1 Study area and SAMBBA flights tracks. The red dots indicate the airports locations.

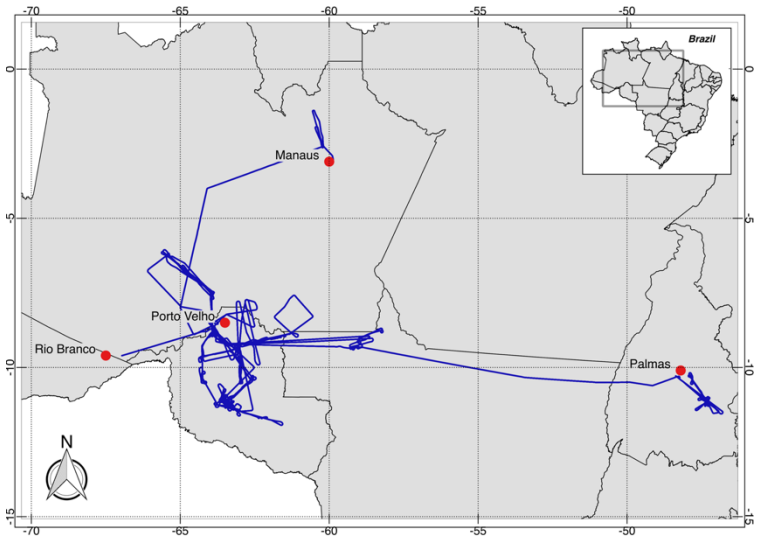

Source: Author's production.

The science drivers of the campaign are summarized by the following key objectives:

- Assess the impact of Amazonian biomass burning aerosol on the radiation budget via the direct, semi-direct and indirect effects.
- Assess the impact of the radiative forcing induced by biomass burning aerosol over Amazonia on the local energy budget, atmospheric dynamics and hydrological cycle.
- Assess the impact of the forcing and feedbacks arising from biomass burning aerosol on regional and global climate.
- Assess the impact of tropical biomass burning emissions upon the carbon cycle.
- Assess the impact of biomass burning aerosol on Numerical Weather Prediction forecasts via direct and semi-direct effects.
- Assess the impact of biomass burning air quality over Brazil.

Based on previous aircraft campaigns sampling biomass burning, and the likely synoptic/local conditions on the day, three types of science flights were conducted (Figure 3.2):

1. Single plume penetrations and cross plume raster sample patterns: allowed assessment of emission ratios close to source and to investigation of transformations of aerosols and their precursors in the plumes.
2. Closure studies of the direct radiative effect: Legs over the biomass burning pollution and underneath it to quantify the radiative fluxes.
3. Survey Flights: Carried out from the biomass burning region to regions of clear air to characterise the aerosol and its precursors in highly perturbed to clean background regimes.

Figure 3.2 Idealized flight patterns during SAMBBA field campaign.

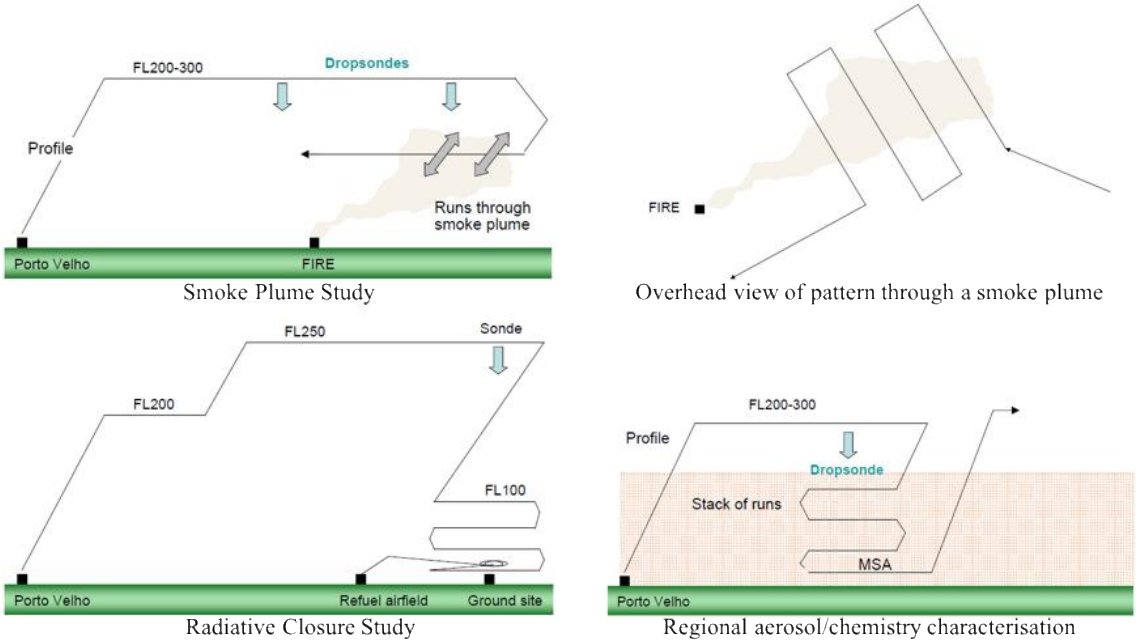

Source: Adapted from Darbyshire e Johnson (2012)

Table 3.1 gives an overview of the SAMBBA research flights, previously classified according to their scientific objectives as either biogenic or biomass burning flights. During the campaign, SAMBBA flights were carried out both in regions not, and directly affected by fire emissions, with parts of their tracks passing through unpolluted regions, smoke haze, or even interception of fresh smoke plumes. For this study, we selected 13 flights according to the gaseous chemistry data availability.

Table 3.1. SAMBBA research flights analyzed in this work. Reference locations are detailed in the appendix.

Flight	Date	Take-off and Landing Hour (local time)	Region *Directions from Porto Velho - RO	Objectives
B731	14 Sep 2012	10:00 14:35	East	Biomass burning
B732	15 Sep 2012	10:30 14:40	Surrounding Porto Velho-RO	Biomass burning
B734	18 Sep 2012	08:00 10:15	Southeast	Biomass burning
B735	19 Sep 2012	08:00 11:40	Northeast	Biogenic emissions
B737	20 Sep 2012	10:45 14:45	Southeast	Biomass burning
B740	25 Sep 2012	7:45 11:00	Surrounding Porto Velho-RO	Biomass burning
B742	27 Sep 2012	9:00 12:30	Southeast Palmas-TO	Biomass burning
B744	28 Sep 2012	9:00 12:30	Southeast	Biogenic emissions
B745	28 Sep 2012	14:00 17:30	Southeast	Biogenic emissions
B746	29 Sep 2012	09:00 13:00	East	Biomass burning
B748	02 Oct 2012	09:00 13:00	East	Biomass burning
B749	03 Oct 2012	10:00 13:30	Northwest	Biogenic emissions
B750	03 Oct 2012	15:00 18:30	Northwest	Biogenic emissions

3.1.1. Aircraft instrumentation

The BAe-146 flew with a comprehensive suite of instrumentation, capable of measuring aerosols, dynamics, cloud physics, chemical tracers, radiative fluxes, and additional meteorological variables. This instrumentation was composed of the ‘core’ instruments, which always fly on the aircraft as standard, and a host of other instruments provided and operated by institutions from across the UK. To perform the several chemicals analyzes of the atmosphere, the research aircraft Bae-146 was equipped with some analyzers: ozone, nitrogen oxides, carbon monoxide, sulfur dioxide, nitrogen oxides,

methane and carbon dioxide (greenhouse gases), methanol, acetonitrile, acetaldehyde, isoprene, monoterpenes, volatile organic compounds; and a system to collect air samples for later analysis in the laboratory. The instruments themselves are typically fitted to racks within the cabin area. Each rack can hold either a single instrument, which may consist of a number of separate components, or multiple instruments. The rack positions in the cabin can be altered to give the best position and combination of instruments for the science project. Each instrument has a sensor or sampling inlet on the exterior of the aircraft, control electronics or sampling pipes mounted close to the sensor or inlet and the main part of the instrument mounted on a rack. Figure 3.3 shows the research aircraft Bae-146 and a resume of the instrumentation onboard.

Figure 3.3 Aspects of the Research Aircraft.

The BAe-146


The Core Console

Cloud Physics Probes


Aerosol Mass Spectrometry Rack

Source: Author's production.

3.1.1.1. AVAPS Rack

Airborne Vertical Atmospheric Profiling System (AVAPS) records data from dropsondes which can be dropped from the aircraft via the dropsonde launch tube.

Figure 3.4 AVAPS/LIDAR rack and the dropsonde launch tube.

Source: Author's production.

The Vaisala Dropsonde RD94 is a general-purpose dropsonde for high-altitude deployment from a variety of aircraft. Slowed in its descent through the atmosphere by a special parachute, the RD94 measures the atmospheric profiles of pressure, temperature, relative humidity and wind from the point of launch to the surface. The RD94 transmits meteorological data via a 400 MHz meteorological band telemetry link

to the AVAPS receiving system onboard the aircraft. The AVAPS can be configured to track up to four RD94s simultaneously.

Figure 3.5 Vaisala Dropsonde RD94 equipped with a special parachute.

Source: Author's production.

3.1.1.2. Radiometer Rack

Contains the Imaging Infrared Radiometer (IIR). The radiometer itself is mounted on the exterior of the aircraft in the Large Radiometer Blister. The IIR system is a Phoenix radiometer with Real Time Imaging Electronics (RTIE) which functions in the

wavelength range between 8 and 9.2 µm. It also has a video camera co-located with it in the front of the large radiometer blister (in the DEIMOS position). The RTIE, power supply and control computer are located on Radiometer Rack. The instrument is operated from the Rear Core Console.

Figure 3.6 The Radiometer Rack is located in the center of the picture.

Source: Author's production.

3.1.1.3. Nephelometer/PSAP/Filters Rack

The aircraft FAAM BAe-146 has two TSI 563 three wavelength integrating nephelometers, designed to measure the light scattering coefficient of atmospheric aerosol. The aerosol sample will first be dehydrated and then passed through an integrating nephelometer that measures the scattering coefficient of red, green and blue

light. The sample is then passed down a humidifier tube where it is subjected to a controlled RH varying smoothly between 20 and 90%. The aerosol is then passed through a second nephelometer where the scattering coefficients are measured once again. The ratio of the wet to dry scattering coefficients as a function of applied relative humidity is the overall information that we require to help us understand the nature of the aerosol particles under different conditions of ambient relative humidity.

The Particle Soot Absorption Photometer (PSAP) is used to measure the optical extinction coefficient for absorption which can in also be used to estimate concentrations of black carbon. The instrument draws in air across a filter where particulate matter is deposited. The transmittance of a green (565 nm) LED light source through this medium is measured and compared to a reference cell, where the same light source is passed over the filter with no aerosol deposition. The filters used to collect particulate samples has a Millipore 47 and 90mm membrane size.

Figure 3.7 The Nephelometer/PSAP/Filters Rack.

Source: Author's production.

3.1.1.4. Core Chemistry Rack

The core chemistry rack contains three instruments:

- TEi49C, measures O_3 (ozone);
- AL5002, measures CO (carbon monoxide);
- Fast Greenhouse Gas Analyzer (FGGA), measures CO_2 & CH_4 (carbon dioxide and methane).

Calibration gases are supplied to the rack from the Gas Bottle Stowage situated at the rear of the cabin. Sampling of the atmosphere is via the Air Sample Pipes and a dedicated window-mounted inlet system. The rack also contains a data logger, inlet driers and pumps for drawing in samples to the rack instruments.

Figure 3.8 Core chemistry rack.

Source: Author's production.

3.1.1.5. CPC/CCN Rack

The water-filled 3786 CPC measures particles as small as 2.5 nm and operates on the principle of enlarging small particles using a condensation technique until they are large enough to be optically detected. A sample is drawn through a cooled saturator block and then into a heated condenser, where water vapor diffuses into the sample stream. Supersaturated conditions are created as water vapor diffuses to the center line of the condenser faster than heat. Particles greater than a critical radius in this region will serve as condensation nuclei for the water vapor and will quickly grow. These droplets are then counted by optical methods.

Figure 3.9 The CPC/CCN Rack (left) and the condensation particle counter (right).

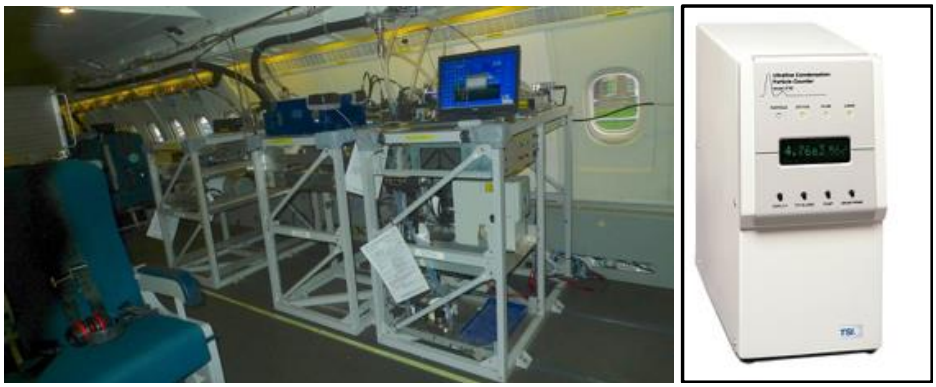

Source: Author's production.

The cloud condensation nuclei (CCN) counter measures the number of cloud condensation nuclei in a sample for a given set point supersaturation. The column operates on the principle that the diffusion of water vapor in air is quicker than heat allowing a region in the center of the CCN column to be supersaturated when a vertical temperature gradient in is maintained.

Figure 3.10 Droplet Measurement Technologies dual column cloud condensation nuclei counter.

Source: Author's production.

3.1.1.6. WAS Rack

A general purpose aerosol inlet is positioned just above the right-hand forward door (Figure 3.12, left). The interior components of the system are mounted both on the cabin walls and on the Low turbulence inlet and whole air sampling rack (Figure 3.12, right).

Figure 3.11 Low turbulence inlet and whole air sampling rack.

Source: Author's production.

Figure 3.12 Low turbulence inlet (left) and Interior components in the cabin (right)

Source: Author's production.

Whole Air Sampling (WAS) rack contains the sampling pump, control system and a source of Nitrogen gas used to operate control valves on a series of up to 64 silco steel air sampling cylinders that are stored in the rear cargo hold of the aircraft.

Figure 3.13 WAS cylinders, mounted in cases, in the rear cargo hold.

Source: Author's production.

The cylinders can thus take controlled samples of atmospheric air during flight, either at set time intervals or triggered manually as dictated by the flight requirements. The cylinders are later removed from the aircraft for analysis.

3.1.1.7. SWS/SHIMS Rack

The Short Wave Spectrometer (SWS) is used for measuring solar radiation, and is a visible/near infrared radiance spectrometer. In its concept, it is a combination of Monolithic Miniature Spectrometer (MMS) modules from Carl Zeiss Ltd with a scanning optic head and controlling software designed by the Met Office.

Figure 3.14 Short Wave Spectrometer and Spectral Hemispheric Irradiance Measurements rack.

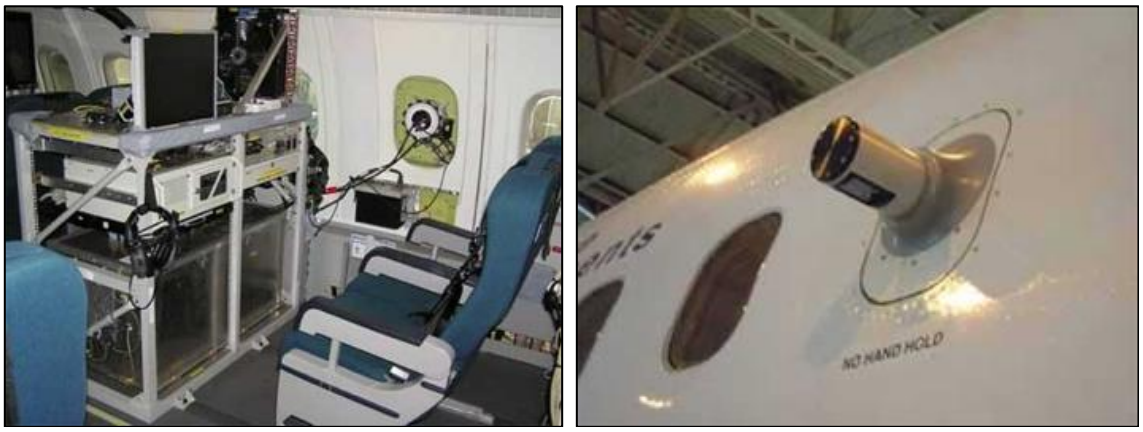

Source: Author's production.

The optical head is mounted on a window blank of the FAAM BAe-146 on the starboard side of the aircraft after the wings. The optic head can scan through 360 degrees, though some viewing angles are restricted by the wings of the airplane. The optic head reflects incoming light through 90 degrees onto two telescopes. Optical

fibers take the light from the telescopes to the spectrometer modules. The spectrometer modules are housed in a fridge to ensure temperature control of the electronic components which increases the signal to noise ratio.

The Spectral Hemispheric Irradiance (SHIMS) measures irradiance in the spectral range 303.4nm - 948.7nm (resolution 3.2nm) using existing broadband radiometer housings and optical fibers. The instruments, one on the top and one on the bottom of the aircraft, measure sky and surface irradiance (Figure 3.15).

Figure 3.15 Spectral Hemispheric Irradiance used during SAMBBA campaign.

Source: Author's production.

3.1.1.8. PTRMS Rack

The Proton Transfer Reaction – Mass Spectrometry (PTRMS) rack contains an instrument capable of measuring many important VOCs (volatile organic compounds) in the atmosphere at a high sampling rate. Compounds analyzed include isoprene and its oxidation products, selected OVOCs (oxygenated VOCs), aromatic hydrocarbons and acetonitrile, a useful tracer of biomass burning emissions.

3.1.1.9. Nitrate Rack

The Nitrate rack contains two instrument systems to measure NO_x and peroxyacetyl nitrate (PAN). The Air Quality Design NOx, is non core FAAM measurement for NO and NO_2. Measurements of PAN are carried out using a custom built two channel gas chromatograph (GC) with electron capture detection (ECD) (Ai Qualitek, Cambridge U.K.).

Figure 3.16 Nitrate rack used during SAMBBA campaign.

Source: Author's production.

3.1.1.10. GC-MS Rack

The gas chromatograph - mass spectrometer (GC-MS) was used for an in-situ measurement of a range of anthropogenic and biogenic volatile organic compounds (VOCs).

Figure 3.17 The gas chromatograph - mass spectrometer rack.

Source: Author's production.

In our study, we selected variables that are listed in the Table 3.2 and the respective instrument detail is also described. The Table 3.3 gives an overview of key instruments present in the aircraft.

Table 3.2. Instrumental information about selected variables used during the SAMBBA analysis.

INSTRUMENTATION	PRODUCT	TECHNICAL DETAILS
PTR-MS	Methanol Acetonitrile Acetaldehyde Acetone Isoprene Methyl Vinyl Ketone Methacrolein	Proton Transfer Reaction Mass Spectrometer containing a quadrupole detector. The instrument measured a range of hydrocarbons and oxygenated hydrocarbons with a typical cycle time of around 3–5 s. Isoprene was calibrated against gas standards provided by Apel-Reimer Environmental (Broomfield, CO, USA). The instrument was the same as used during OP3 and full instrumental, operational and calibration details are described in Murphy et al. (2010). Accuracy for isoprene is estimated at ±15% and data were validated against off-line gas chromatography analysis of samples taken using the aircraft's Whole Air Sampling (WAS) system.
NO_x Chemiluminescence	NO NO_2	NO measurements were conducted using a chemiluminescence instrument (Air Quality Design Inc, Wheat Ridge, CO, USA), with the NO_2 measured using a second channel after photolytic conversion to NO. The photolytic conversion eliminates the possible interference from NO_z on the NO_2 channel. The detection limits were close to 10 pptv for NO and 15 pptv for NO_2 for 10 s averaged data, with estimated accuracies of 15% for NO at 0.1 ppbv and 20% for NO_2 at 0.1 ppbv (Allan et al., 2014).
TEi49C AL5002 VUV	O_3 CO	The Ozone and CO analysis used, respectively, the TEi49C and AL5002 VUV Fast Fluorescence (Gerbig et al., 1996, 1999; Palmer et al., 2013) onboard instruments. Calibration gases were supplied to the rack from the gas bottle stowage, and the air sampling from the atmosphere was via the air sample pipes and a dedicated window-mounted inlet system.

Table 3.3. Key Instruments employed in the SAMBBA field campaign.

RADIATION			CLOUD PHYSICS			
IIR	SWS	SHIM	Core Cloud Phyics Rack	PCASP	SID2	CVI
Met Office	Met Office	Met Office	FAAM	FAAM	Hertfordshire	Met Office
Imaging Infrared Radiometer (IIR); this is mounted on the exterior of the aircraft in the Large Radiometer Blister	The Short-Wave Spectrometer (SWS) is used for measuring solar radiation; it is a visible/near infrared radiance spectrometer	The Spectral Hemispheric Irradiance Measurements (SHIMS) measures irradiance in the spectral range 303.4nm - 948.7nm	A rack which includes: The Cloud Droplet Probe (CDP), Cloud Imaging Probes (CIP15 & CIP100) and the 2DC	The PCASP is an optical particle counter which measures aerosol size distribution in the nominal range 0.1 to 3 micrometers.	The Small Ice Detector mark 2 provides in situ data on cloud particle concentration, size and shapeat high resolution	The Counter flow Virtual Impactor (CVI) is an inlet designed to initially separate cloud particles from the ambient atmosphere, it feeds into the CPC 3010 and PCASP and same sample can be distributed to the manchester aerosol rack

CORE		AEROSOL			
AVAPS Dropsondes	LIDAR	SP2	C-ToF AMS	PSAP	Nephelometers
FAAM	Met Office	U Mancehster	U Mancehster	FAAM	Met Office
Airborne Vertical Atmospheric Profiling System (AVAPS) records data from dropsondes - these are dropped from the aircraft and measure the atmospheric profiles of pressure, temperature, relative humidity and wind	UV aerosol backscatter LIDAR that provides information on distribution of aerosols / clouds below the aircraft	The Single Particle Soot Photometer (SP2) measures the soot content in individual airborne particles in the size range 200-1500nm	The Aerosol Time of Flight Mass Spectrometer measures the chemical and physical nature of aerosol particles online by delivering quantitative mass concentrations of the major non-refractory chemical species	The Particle Soot Absorption Photometer (PSAP) is used to measure the optical extinction coefficient for absorption which can be used to estimate concentrations of black carbon	Two integrating nephelometers measure the light scattering coefficient of atmospheric aerosols in a wet and dry sample

Core Chemistry	PAN	VACC	PTRMS	WAS	GCMS
FAAM	Leeds U	Leeds U	UEA	FGAM	York U
Contains three instruments: the TEi49C (O3), the AL5002 (CO) and the Fast Greenhouse Gas Analyzer (FGGA) which measures CO2 & CH4.	PAN Gas Chromatograph measures peroxyacetyl nitrate (PAN) using a custom built two channel gas chromatograph (GC)	The Volatile Aerosol Concentration and Composition (VACC) produces size distributions as a function of volatility and can thus provide information on the chemical composition in terms both number and size.	The Proton Transfer Reaction Mass Spectrometer (PTRMS) is capable of measuring VOCs (including isoprene, OVOCs, aromatic hydrocarbons and acetonitrile - a tracer of BBA)	Whole Air Sampling (WAS) are cylinders which take controlled samples of atmospheric air during flight, either at set time intervals or triggered manually	The Gas Chromatograph - Mass Spectrometer (GC-MS) is used for in-situ measurement of a range of anthropogenic and biogenic VOCs

3.1.2. Meteorological settings during SAMBBA

Figure 3.18 represent the average condition for total cloud cover and temperature during SAMBBA, with the respective anomalies corresponding to September, 2004-2014 comparisons. The data was obtained from European Centre for Medium-Range Weather Forecasts Re-Analysis Interim (ERA-Interim, DEE et al., 2011) The areas with negative anomalies of total cloud cover were intense mostly in the western and central Amazonia, while in the eastern sector the reduction in the total cloud cover was less intense. The temperature presented a positive anomaly in the southeast part of the Amazon forest, with values achieving up to 18°C, in contrast, negative anomalies were found in the north/northwest part of the forest. As a result, the combination of a reduced level of total cloud cover, high temperatures, intense fire activity and smoke in the southeast part of Amazonia, make the atmosphere in this region highly impacted in relation to the northwest sector. However, through the air masses transport in high altitudes, the recirculation of the air from eastern to western part of Amazon rainforest (Figure 3.19) can influence the atmospheric composition of the northwest part, previously defined as a potential clean area. Due to this recirculation, a simple regional classification method to analyze the SAMBBA data was not enough to discern between a clean and a biomass burning impacted region, as describe in the next chapter 3.1.3.

In addition to the internal influence of the biomass burning, the atmospheric composition of the Amazon basin is also affect by long range transport from African plumes and according to AGHEDO; SCHULTZ; RAST, (2007), Latin America experiences the highest impact of African emissions, including biogenic sources, biomass burning, lightning and anthropogenic emissions. Previous studies (AZEVEDO et al., 2010; LANGFORD et al., 2010; SRIVASTAVA; NAJA; THOURET, 2015) also found an evidence of long-range transport events of O_3, which could even alter the atmospheric composition within the planetary boundary layer.

Figure 3.18 On the left, average total column cloud fraction cover and temperature (^{o}C) during SAMBBA campaign in 2012. On the right, the respective anomalies relative to September, 2004-2014 period. Data from ERA-Interim global atmospheric reanalysis.

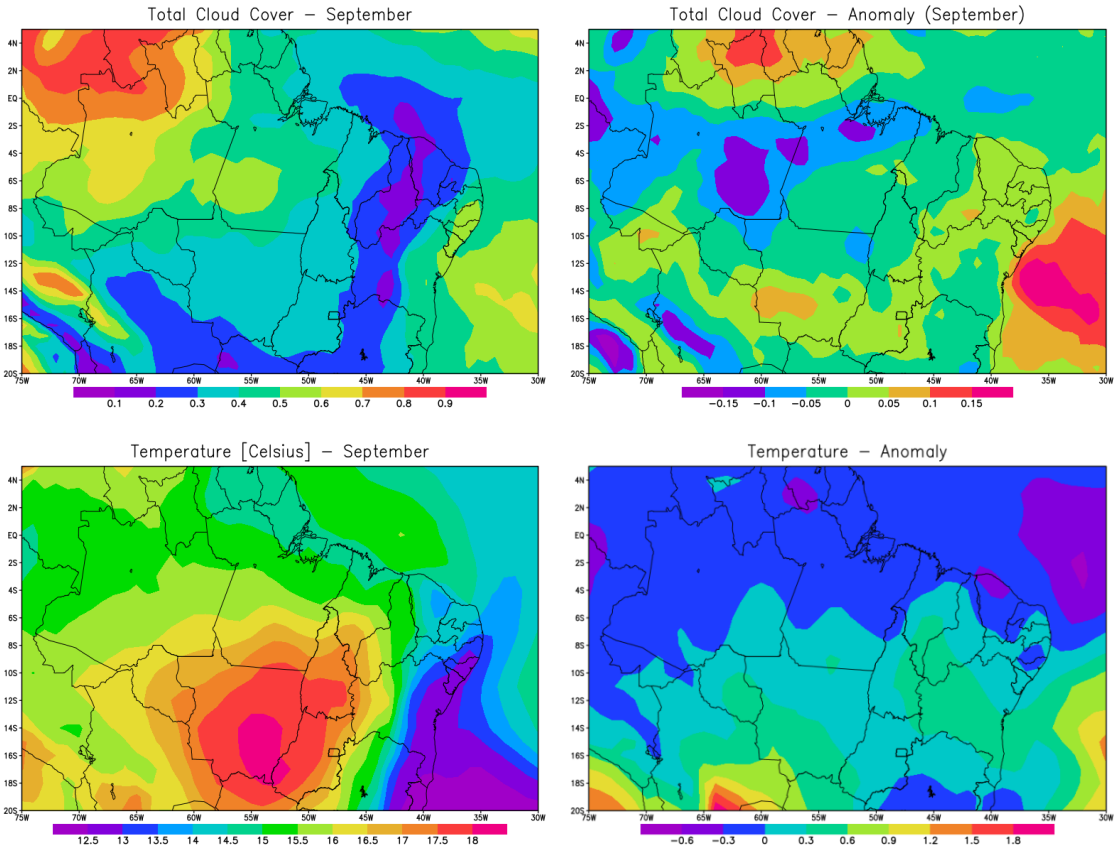

Source: Author's production.

Figure 3.19 Average surface wind field during SAMBBA campaign in 2012. Data from ERA-Interim global atmospheric reanalysis.

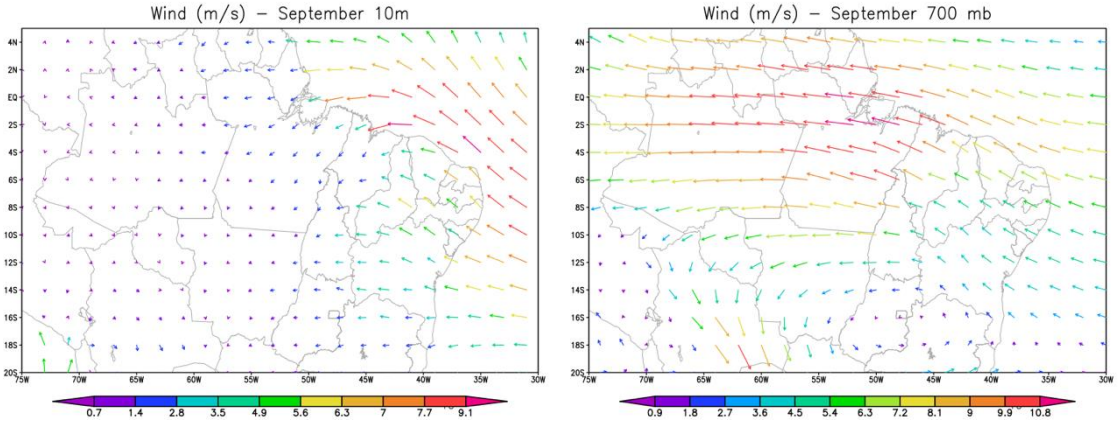

Source: Author's production.

Figure 3.20 shows the number of fires detected by Moderate-Resolution Imaging Spectroradiometer (MODIS) also aboard AQUA and the average CO mixing ratio derived from the Atmospheric Infrared Sounder (AIRS) (AUMANN; MILLER, 1995) measurements aboard AQUA satellite during in the SAMBBA domains and adjacent areas. During SAMBBA, the number of fires detected in the period (Figure 3.20.a) also followed the same pattern of the CO mixing ratio distribution (Figure 3.20.b), with the most intense and persistent fire activity occurring in the eastern part. AIRS data shows high levels of CO mixing ratio in the southeast sector, with values always above 200 ppbv at 500 hPa, peaking 220 ppbv. The northwest sector was representative of a cleaner area, with CO mixing ratio values about 130 ppbv. In fact, most SAMBBA flights with a biogenic emission objective were carried out in the northwest part, with some of them further south of Amazon rainforest.

Figure 3.20 (a) Number of fires detected from MODIS onboard AQUA and (b) average CO mixing ratio (ppmv) at 500 hPa from AIR sensor over Amazon during SAMBBA campaign in 2012.

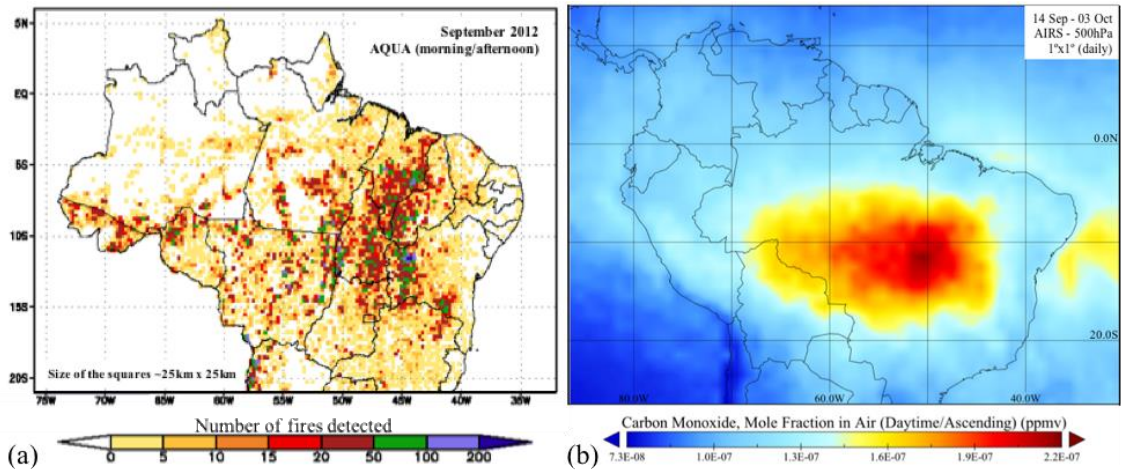

Source: Author's production.

3.1.3. Classification method of flight tracks

During the planning phase, SAMBBA flights were classified according to their scientific objectives as either biogenic or biomass burning flights. Additionally, we only considered the data collected below 2,000 m and between 11:00 am and 6:00 pm to capture the difference in the oxidative capacity activity along the planetary boundary layer (PBL) during daytime, since the OH concentration is regulated by photochemistry (ELSHORBANY et al., 2009). Some flights, despite the classification in the planning phase, had parts of their tracks passing through unpolluted regions, smoke haze, or even interception of fresh smoke plumes. To maximize the use of data, we classified parts of the flight tracks according to the CO mixing ratio values as background (BG) and biomass burning. According to Andreae et al. (2012) and several references therein, the Amazon rainforest atmosphere has a background level of CO mixing ratio typically around 100 ppbv. However, the mean CO inflow into the Amazon basin during the SAMBBA period at 500 hPa, retrieved from Atmospheric Infrared Sounder (AIRS) measurements onboard the AQUA satellite, ranged between 140 and 160 ppbv (Figure 3.21.a). Figure 3.21.b shows that this hemispheric inflow is quite homogeneous along the vertical column up to around 400 hPa and in fact, there were few SAMBBA samples with CO mixing ratio values below 100 ppbv. Therefore, we adopted a threshold of 150 ppbv to represent the background of CO in the Amazon atmosphere during SAMBBA campaign.

As O_3 is formed photochemically downwind during smoke aging, the enhancement ratio $ER_{[\Delta O_3]/[\Delta CO]}$ is acceptable as a reliable indicator of the smoke plume age (PARRISH et al., 1993; ANDREAE et al., 1994a). Furthermore, in the lack of NO_y/NO_x ratio in SAMBBA, we used the ratio of O_3 to CO as a proxy for smoke plume age. The biomass burning flights tracks with [CO] > 150 ppbv were then reclassified as fresh smoke plumes (FP) interceptions or as aged smoke plume (AP) according to the following Eq. (1):

$$ER_{\Delta O_3/\Delta CO} = \frac{[O_3]_{smoke} - [O_3]_{background}}{[CO]_{smoke} - [CO]_{background}} \quad (3.1)$$

During the BG flight tracks (CO ≤ 150 ppbv), the mean value of the O_3 mixing ratios near the surface (< 500 m) was 21 ±7 ppbv, which we then adopted as the O_3 mixing ratio background.

Figure 3.21 Time averaged CO (ppmv) over SAMBBA period (14th of September - 3rd of October 2012) from AIRS onboard AQUA satellite during daytime: (a) global map at 500 hPa, and (b) cross section of longitude-pressure within the region indicated on the map on top.

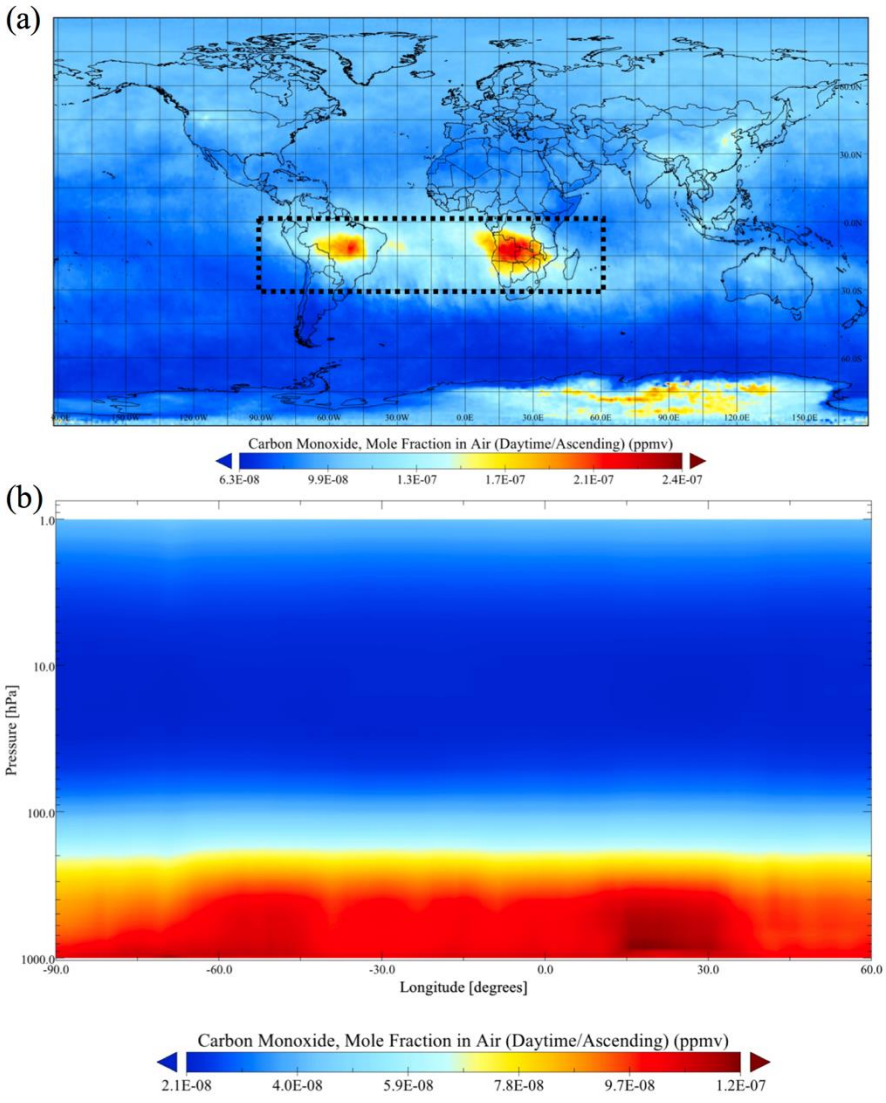

Source: Author's production

In Table 3.4, we list the values of the enhancement ratio of O_3 to CO and the estimated smoke plume age for several smoke measurements in Amazonia and Africa. Jost et al. (2003) found the value of 0.1 for the $ER_{[\Delta O_3]/[\Delta CO]}$ two hours after emission in Otavi, northern Namibia; and Andreae et al. (1988) found 0.08 for fresh biomass burning (650 m altitude) in the Amazon basin region.

Table 3.4. Observations of the ratio $\Delta O_3/\Delta CO$ and plume age in tropical and subtropical sites.

Tropics and subtropics region	**Plume age**	**Mean $\Delta O_3/\Delta CO$**	**Reference**
Southern Africa	< 30 min	0.09	Hobbs et al., 2003
Southern Africa	< 1 h	0.09	Yokelson et al., 2003
Mexico	< 2 h	0.08	Yokelson et al. 2009
Southern Africa	≈ 2 h	0.10	Jost et al., 2003
Northeast Brazil/Southern Africa	< 0.5 day	0.15	Mauzerall et al., 1998
Northeast Brazil/Southern Africa	0.5-1 day	0.32	Mauzerall et al., 1998
Southern Africa	< 1 day	0.01	Yokelson et al., 2003
Northern Africa	≤ 2 days	0.23	Jonquières et al., 1998
Southeast Asia	2 – 3 days	0.20	Kondo et al., 2004
Northeast Brazil/Southern Africa	1-5 days	0.71	Mauzerall et al., 1998
Southeast Asia	4-5 days	0.33	Bertschi et al. 2004
Northeast Brazil/Southern Africa	5-7 days	0.74	Mauzerall et al., 1998
South Africa/South America	≤ 10 days	0.75	Singh et al., 2000
Africa/South America	10 days	0.41	Andreae et al., 1994

Comparable values of $ER_{[\Delta O_3]/[\Delta CO]}$ (0.09) were observed in other young smoke plumes with 0.5–1.0 hour aged during the Southern African Regional Science Initiative 2000 - SAFARI 2000 (HOBBS et al., 2003; YOKELSON et al., 2003). Mauzerall et al. (1998) reported 0.15 for fresh smoke plumes with fewer than 4.8 hours over regions with active fires in the Northeast region of Brazil and Africa. In short, we classified the parts of the flight tracks as background (BG) when [CO] ≤ 150 ppbv, and the biomass burning

flights ([CO] > 150 ppbv) into two subgroups of fresh smoke plumes (FP), with $ER_{[\Delta O_3]/[\Delta CO]}$ < 0.1, and aged smoke plume (AP), with $ER_{[\Delta O_3]/[\Delta CO]} \geq 0.1$.

3.1.4. Method for the OH calculation

The OH concentrations from the [MVK+MACR+ISOPOOH]/[Isoprene] ratio using the sequential reaction model was originally developed by Apel, 2002 and Stroud et al., 2001 and modified according to the approach of Karl et al. (2007). This method can be used to investigate the impact of vertical transport, representing the processing time of the isoprene and its oxidation products from the surface to the atmosphere through the ratio of PBL depth and convective velocity scale. In order to have an OH estimation more accurate, we modified the processing time *t* to represent not only the vertical transport, but also the horizontal atmospheric transport time, by having *t* calculated as a function of the enhancement ratio $ER_{[\Delta O_3]/[\Delta CO]}$. This method is based on observations that the isoprene reaction rate with OH (rate coefficient ≅1.0 x 10^{-10}, lifetime ≅1.4 h) is more important than with O_3 (rate coefficient ≅1.3 x 10^{-17}, lifetime ≅1.3 d) during the daytime. Following the simplified sequential reaction model, we can estimate OH concentration, in molecules cm^{-3}, with the following analytical expression:

$$[OH] = \left[\ln\left(1 + \left(\frac{\frac{[MVK+MACR+ISOPOOH]}{[Isoprene]} * (K_{iso} - K_{prod})}{K_{is\square} * 0.55}\right)\right)\right] / ((K_{iso} - K_{prod}) * t) \qquad (3.2)$$

where k_{iso} and k_{prod} are, respectively, the reaction rate constants of isoprene + OH (1.1 x 10^{-10} cm^3 $molecules^{-1}$ sec^{-1}), and [MVK+MACR+ISOPOOH] + OH (6.1 x 10^{-11} cm^3 $molecules^{-1}$ sec^{-1}), and we are assuming a total yield of 0.55 of MVK+MACR+ISOPOOH from the OH + Isoprene reaction (BERTSCHI et al., 2002; KARL et al., 2007). We estimated the processing time as $t = 5.3e^{5.4 * ER_{[\Delta O_3]/[\Delta CO]}}$ (seconds), based on the fitting function of previous measurements of $ER_{[\Delta O_3]/[\Delta CO]}$ and plume age observations in tropical and subtropical sites (Table 3.4).

3.2. In situ observation: tower K-34

During the SAMBBA field campaign, in addition to the airborne measurements, we also collected air samples in a forest site, at the K-34 tower above the canopy (~50 m). The K-34 tower is located at the Forest Management Station ZF-2 (02° 36'S and 60° 12'W), 60 km north of Manaus (Figure 3.22). This activity was carried out in collaboration with Dr. Eliane Gomes Alves, currently a postdoc at National Institute of Amazonian Research.

Figure 3.22 Map showing the political boundaries of the Brazilian Amazon and a satellite image with the location of the sampling station tower K-34 (S-1) relative to Manaus location.

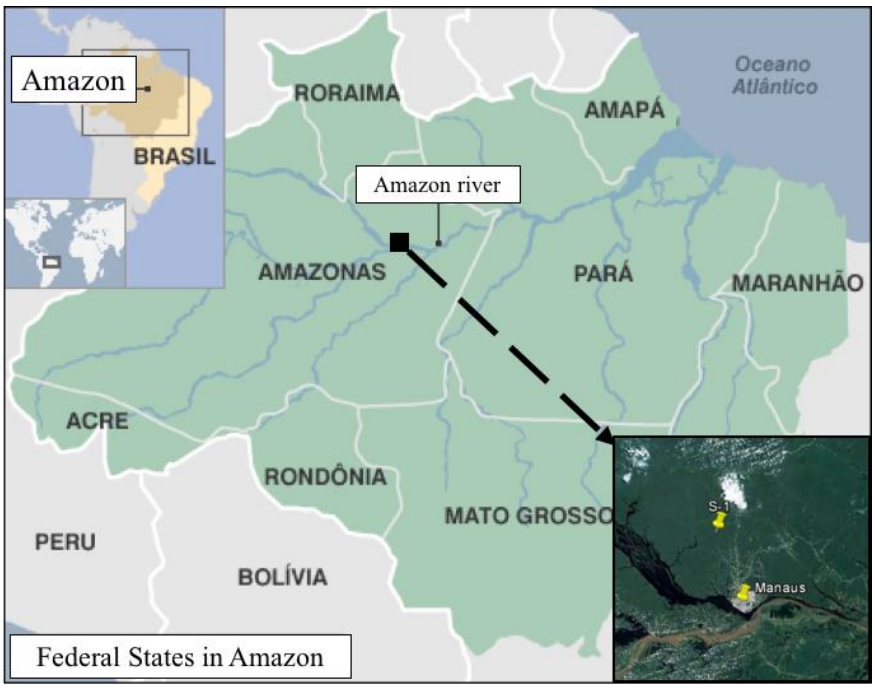

Source: Author's production.

The K-34 tower has 54 m of altitude and is deployed in a medium elevation plateau (130 m) in the Cuieiras Biological Reserve, a primary forest area represented in the Figure 3.23. The reserve has 22,735 ha of dense tropical rainforest area, typical of the central region of the Amazon. Despite this general classification, the region where the K-34 tower is located presents areas of forest with different environments, with

vegetation types being defined according to the stratification of the topography (RIBEIRO, 1999). In this region, the mean annual temperature is about 27°C and the mean annual precipitation is 2252 mm. The rainfall distribution presents two distinct seasons in the year: the dry season, which occurs between July and September, when precipitation is less than 100 mm per month; and the rainy season, which occurs between October and June, with March and April having the highest rainfall index.

Figure 3.23 Representation of the study site with the K34 tower location.

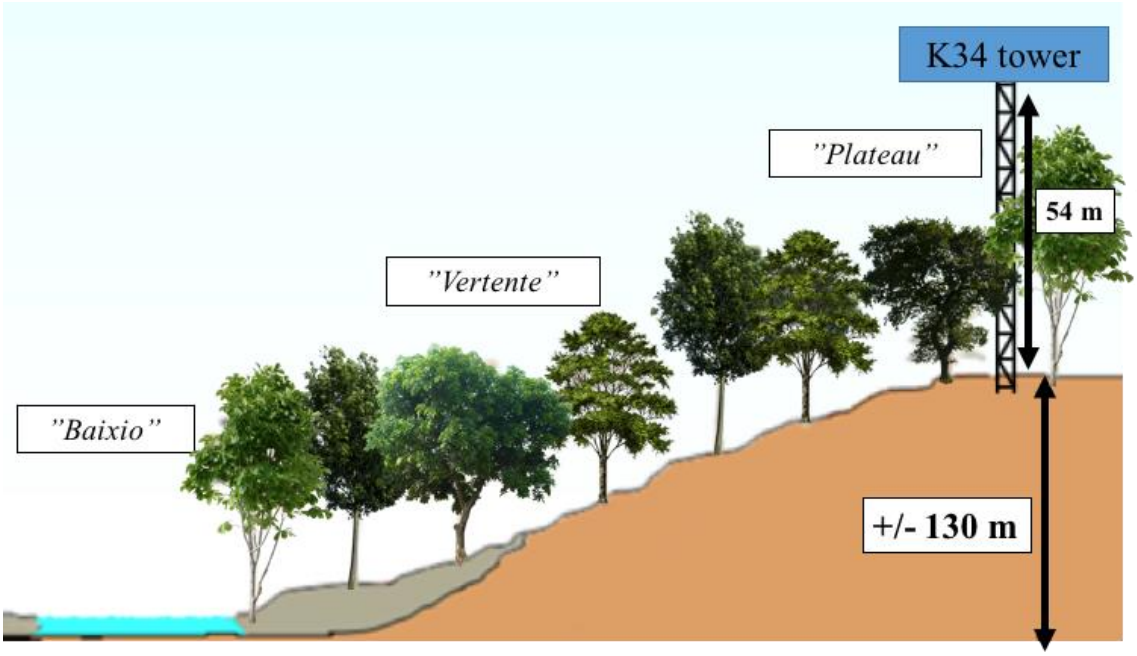

Source: Author's production.

The air sampling at the K-34 tower were carried out between the 19th and 21st of September aiming to coordinate the tower measurements with the SAMBBA flight B735 on the 20th of September. The B735 flight track was between Porto Velho and Manaus, with an extension of approximately 100 km north of Manaus to overpass the K-34 tower at about 8:30 am. Figure 3.24 shows pictures of the K-34 tower taken during the air sampling; including one of the Bae-146 aircraft overflying the K-34 tower during the flight B735. Previously SAMBBA field campaign, the K-34 sampling

measurements was developed to collect BVOCs emissions during a daytime cycle before and after the flight B735, in order to acquire precise information about the BVOCs emission flow into the atmosphere.

Figure 3.24 Photos of the tower k-34 (on the left), arrival of the sampling equipment by land (on the right top) and the aircraft Bae-146 overflying K-34 tower during flight B735 (on the right bottom).

Source: Author's production.

The air sampling system at the tower was designed to separate airflows based on the direction of the instantaneous vertical wind speed. The basic components of the sampling system flow are presented in Figure 3.25: (a) adsorbent cartridge, (b) main box containing the controller, battery, check valves and mass flow controller, and (c) a sonic anemometer (RM Young, Model 81000VRE) to measure wind speed. The use of a sonic anemometer allows the high frequency measurements of three velocity components of the wind (two horizontal and one vertical). The air samples were accumulated in two storage tanks (for approximately 30 minute), one facing up, and another facing down to measure downdrafts and updrafts, respectively. The selection of

reservoirs was based on the direction of the instantaneous vertical wind speed at the time of the sampling.

The Microcontroller indicated in the Figure 3.25.b initially activate (at 5 Hz) the sonic anemometer, which then responds with wind velocity and virtual temperature data. The Microcontroller then uses that information to determine whether there is an updraft or downdraft (or neutral) and then simultaneously opens both the upstream and downstream valves on the appropriate cartridge. The REA (Relaxed Eddy Accumulation) system is programmed to do three flux samples, of typically 30 minute each. During the first sample – air is sampled onto the cartridges labeled 1up, 1down and Neut. (see Figure 3.25.a). It then moves sequentially to 2up/2down and 3up/3down for the next two flux periods. The same neutral (N) cartridge is used for all 3 samples. The 8th cartridge is not sampled and is included as a blank sample to determine possible contamination.

Figure 3.25 Instrumentation used in the tower k-34: a) adsorbent cartridge, b) main box of the sampling system flow and c) anemometer.

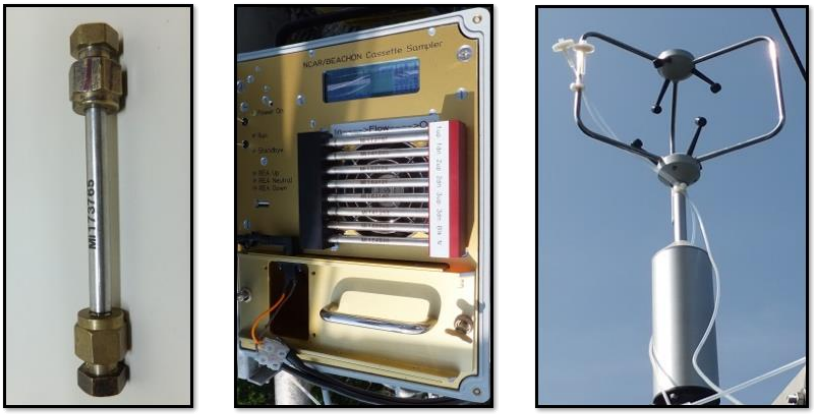

(a) (b) (c)

Source: Author's production.

The air samples from the adsorbing cartridges were stored for approximately 15 days at about -20°C, preventing the degradation of the matrix, and then transported to National Center for Atmospheric Research (NCAR) in Boulder, CO, US. At NCAR, the student

analyzed the chromatograms and mass spectra from the samples previously injected into the gas chromatography with mass spectrometry detector (GC-MS) and a gas chromatography with flame ionization detector (GC-FID) (Greenberg et al., 2004). During the sampling phase, was used cartridges made of stainless steel sampling tubes pre-packed with 2 sorbent beds, Tenax TA (Trapping Agent) and Carbograph 5TD (Thermal Desorption) with an air-sampling flow of about 200 sccm (standard cubic centimeters per minute). The air samples were analyzed for BVOC by thermal desorption (TD) followed by gas chromatographic separation and detection by both FID and MS detectors. Thermal desorption was carried via a 2-stage process, where the adsorbent cartridge was initially desorbed at 275°C while passing a flow of UHP (ultra high pressure) Helium through it using a commercial TD-autosampler (Markes Ltd, Model Ultra1). The sample was transferred via a heated line to a focusing trap that was packed with Tenax-TA and cooled to 0°C via peltier cell (Markes, Unity Series1). Once the entire sample was transferred to this intermediate trap, it was then rapidly heated to 300°C and injected onto the GC. The GC is cryofocused[1] to -30°C and then temperature is programmed to increase up to 275°C. The separation took place on a DB-5 (5% Phenyl 95% dimethylarylene siloxane) column (Restek, 250 micron) before the sample is split between the two detectors (FID and MS).

The system was calibrated daily by filling adsorbent cartridges with a secondary standard consisting of isoprene and camphene. This isoprene/camphene standard was calibrated with a National Institute of Standards and Technology (NIST)-certified butane/benzene gas standard, as well as a NIST-certified neohexane gas standard. Whenever possible, the FID was used to quantitate analyzes. Since the FID response is based on the number of carbon atoms within the molecule, its use allows a quantification of a wide range of carbon-containing compounds using a single standard compound. However, with the typical low mass loading of the tower K-34 samples, the quantification with the FID very often became problematic due to the interference and overlapping of the peaks. Analysis of these samples alongside isoprene/camphene

[1] To trap or detain gaseous compounds in a cryotrap.

standard allowed obtaining response factors relative to either the mass 68 ion of isoprene or the mass 93 ion of camphene (secondary standard). Due to the reduced number of α-pinene samples, the data presented here refer only to isoprene, although α-pinene was also collected.

Figure 3.26 Selected chromatogram (SIM mode) from a sample in the tower K-34 showing isoprene (a), alpha-pinene and other trace compounds (a and b), and a possible detection of sequiterpenes (SQT) in (c).

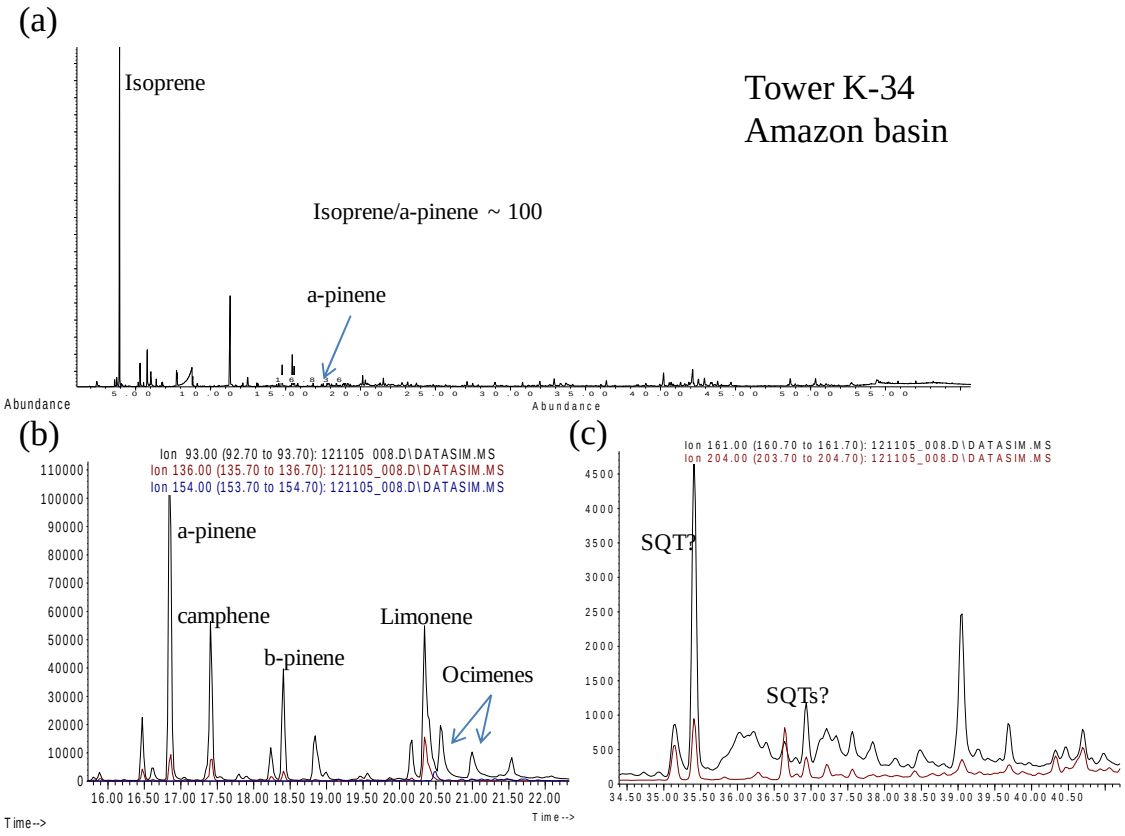

Source: Author's production.

The original plan was to collect air samples at the tower during SAMBBA field campaign, coordinating with the SAMBBA flights B735, and on the previous and next days characterizing the diurnal cycle. Unfortunately, there was a connection problem between sonic anemometer and the cassette sampler, and the air sampling in the 19th of September started only at 12:30 pm (local time), compromising the coordination with

the airborne measurements. Table 3.5 resume the sampling activities in the tower K-34 during SAMBBA field campaign. In addition, the limited number of cartridges available affected the sampling in the third day (21st of September), which had 2 cycles instead of 4 like the second day (20th of September).

Table 3.5. K-34 sampling during SAMBBA field campaign.

DATE	Nº of experiment	Nº of cycles	Hour (local time)
19 Sep 2012	1	3 (30 min./each)	12:30 14:30
20 Sep 2012*	1	3 (30 min./each)	09:00 10:30
	2	3 (30 min./each)	11:00 12:30
	3	3 (30 min./each)	13:00 14:30
	4	3 (30 min./each)	15:00 16:30
21 Sep 2012	1	3 (30 min./each)	08:00 09:30
	2	3 (30 min./each)	10:00 11:30

*B735 flight track that overpassed K-34 tower at about 8:30 am.

3.3. Modeling system

3.3.1. BRAMS

The Brazilian developments on the Regional Atmospheric Modeling System version 5.2 (BRAMS 5.2, (FREITAS et al., 2017)) is derived from the Regional Atmospheric Modeling System (RAMS, PIELKE et al., 1992; COTTON et al., 2003). The model RAMS was originally developed at Colorado State University in the USA. However, BRAMS diverged from RAMS with several new features and modifications that have been included mainly to improve the numerical representation of fundamental physical processes in tropical and subtropical regions (DE FREITAS et al., 2005; FREITAS et al., 2009). Additionally, BRAMS includes an urban surface scheme coupled with a photochemical model (DE FREITAS et al., 2005; FREITAS et al., 2009), a complete in-line module for atmospheric chemistry and aerosol processes (LONGO et al., 2013), as well as a state-of-the-art surface scheme to simulate the energy, water, carbon, and other biogeochemical cycles (MOREIRA et al., 2013), which extend RAMS original functionalities towards a fully integrated environmental model. The current BRAMS

version has capabilities analogous to the state-of-the-art limited area integrated atmospheric chemistry transport models such as WRF-Chem (GRELL et al., 2005) and COSMO-ART (ZANNONI et al., 2009). The Figure 3.27 resume several processes into the numerical model BRAMS.

Figure 3.27 Sub-grid processes resolved in BRAMS.

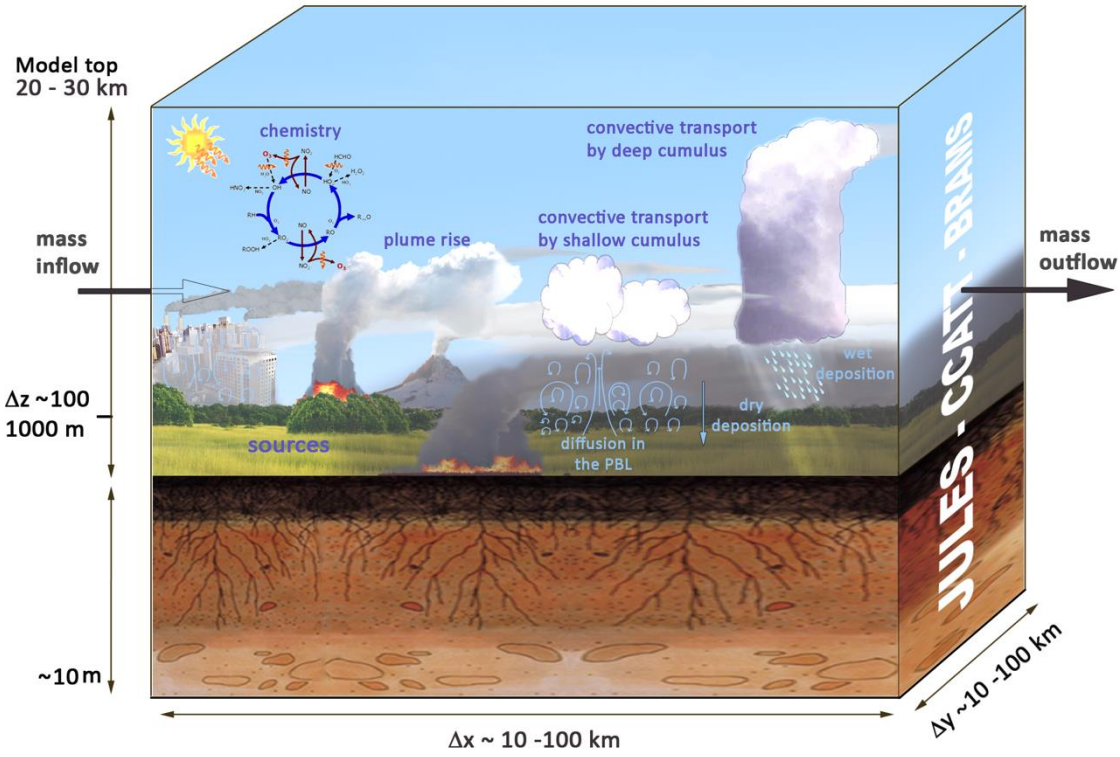

Source: Adapted from Moreira et al (2013).

In the Brazilian developments on the Regional Atmospheric Modelling System (BRAMS), the mass continuity equation is solved for each trace gas and aerosol. This equation can be expressed as a trend equation form:

$$\frac{\partial s}{\partial t} = \left(\frac{\partial s}{\partial t}\right) + \left(\frac{\partial s}{\partial t}\right) + \left(\frac{\partial s}{\partial t}\right) + \left(\frac{\partial s}{\partial t}\right) + W + R + Q + \left(\frac{\partial s}{\partial t}\right) \quad (3.3)$$

(1) (2) (3) (4) (5) (6) (7) (8) (9)

where ***s*** is the mean ratio of the trace gas mixture at the grid point. (1) term represents the local trend term, which is expressed as the sum of the wind advection terms on the grid scale (2), sub-grid turbulent transport within the planetary boundary layer (PBL) (3), deep convection (4) and shallow (5), wet deposition of particles (6), and dry deposition of aerosol particles (7), emission (8) (including the effects of removal of the plume emission in the case of burns emission), and finally, the chemical transformations (9), which can be both a source and sink of the concerned species. The term of chemical transformations is one of the most complexes to solve in the air quality modeling and the highest computational cost. In addition to BRAMS code itself, the modeling system also includes three pre-processing software tools for user-defined chemical mechanisms (M-SPACK, LONGO et al., 2013), aerosol and trace gas emissions fields (PREP-CHEM- SRC, FREITAS et al., 2011), and the interpolation of initial and boundary conditions for meteorology and chemistry (BC- PREP) (see Figure 3.28).

The PREP-CHEM-SRC tool provides emission fields interpolated onto the transport model grid. The preprocessor is coded using Fortran90 and C and is driven by a name list allowing the user to choose the type of emissions, databases and chemical species specification file from the M-SPACK. The emissions under consideration are from the most recent databases of urban/industrial, biogenic, biomass burning, volcanic, biofuel use and burning from agricultural waste sources. The current version includes anthropogenic emission inventories provided by "REanalysis of the TROpospheric chemical composition over the past 40 yr" (RETRO, http://retro.enes.org) for 26 species and is complemented by other species provided by the "Emission Database for Global Atmospheric Research – version 4.2" (EDGAR-4.2, http://edgar.jrc.ec.europa, OLIVIER et al., 1999). This version includes most direct greenhouse gases, 4 ozone precursor species and 3 acidifying gases, primary aerosol particles and stratospheric ozone depleting species. It also includes urban/industrial information specifically for the South American continent based on local inventories (ALONSO et al., 2010). Currently, all urban/industrial emissions are released in the lowest model layer. However, if emissions from point sources (e.g., stacks) are available, information on stack heights can be easily included. For biomass burning, the PREP-CHEM-SRC includes emissions provided by the Global Fire Emissions Database (GFEDv2), or emissions can also be

estimated directly from satellite remote sensing fire detections using the Brazilian Biomass Burning Emission Model (3BEM, LONGO et al., 2010) as included in the tool. In both cases, fire emissions are available for 107 different species. The biomass burning emission estimate is divided into two contributions, namely smoldering, which releases material in the lowest model layer, and flaming, which makes use of an embedded on-line 1-D cloud model in each column of the 3-D transport model to determine the vertical injection layer. In this case, the cloud model is integrated using current environmental conditions (temperature, water vapor mixing ratio and horizontal wind) provided by the host model (FREITAS; GEVAERD, 2006; FREITAS et al., 2007, 2010). Biogenic emissions are also considered via the Global Emissions Inventory Activity of the Atmospheric Composition Change: the European Network (GEIA/ACCENT, http://www.aero.jussieu.fr/projet/ACCENT/description.php) for 12 species and derived by the Model of Emissions of Gases and Aerosols from Nature (MEGAN, GUENTHER et al., 2012) for 15 species. Other emissions include volcanic ashes (MASTIN et al., 2009), volcanic degassing, biofuel use and agricultural waste burning inventories. The physical and chemical process present in BRAMS represents state-of-the-art in regional atmospheric models. The current version of the two-moment microphysical parameterization used in RAMS, version 6, has been implemented in BRAMS, providing prognostic equations for number concentration and mixing ratio for eight hydrometeor categories (cloud, drizzle, rain, pristine, snow, aggregates, graupel, and hail) (MEYERS et al., 1997; SALEEBY; COTTON, 2004; SALEEBY et al., 2008). The aerosol aware bulk microphysics scheme described in THOMPSON et al. (2008) and THOMPSON; EIDHAMMER (2014) was also implemented in BRAMS. The scheme treats five separate water species, mixing single- and double-moment treatment for different cloud species to minimize computational cost. It also includes the activation of aerosols as cloud condensation (CCN) and ice nuclei (IN) and, therefore, explicitly predicts the droplet number concentration of cloud water as well as the number concentrations of the two new aerosol variables (FREITAS et al., 2017).

The BRAMS radiation module includes two additional schemes to treat atmospheric radiative transfer consistently for both longwave and shortwave spectra. The first scheme, used in our simulations, is a modified version of the Community Aerosol and

Radiation Model for Atmospheres (CARMA) (TOON et al., 1989), and the second one is the Rapid Radiation Transfer Model version for global climate models (MLAWER et al., 1997; IACONO et al., 2008). The CARMA scheme solve the radiative transfer using the two-stream method and include all the major molecular absorbers (water vapor, carbon monoxide, ozone, oxygen) and aerosol extinction. CARMA also treats gaseous absorption coefficients using an exponential sum formulation (TOON et al., 1989). BRAMS also offers the possibility of using a combination of the LEAF surface scheme (WALKO et al., 2000) and the Town Energy Budget (TEB) (MASSON, 2000; FREITAS et al., 2006). TEB and LEAF schemes are activated simultaneously, and the surface fluxes of momentum and moisture, temperature, surface albedo, and emissivity are calculated by TEB wherever an urban grid point is identified, while LEAF is applied elsewhere (e.g. bare soil, water bodies, grass, forest, or any vegetation).

In terms of surface interactions, BRAMS has improved after the coupling of JointUKLand Environment Simulator (JULES) (MOREIRA et al., 2013). JULES contains the state-of- the-art numerical representation of surface processes and is able to simulate a number of soil–vegetation processes such as vegetation dynamics, photosynthesis, and plant respiration, and also transport of energy and mass in soils and plants, including a representation of urban elements. The coupling of JULES and BRAMS is fully two-way, with BRAMS providing atmospheric dynamics, thermodynamics, and chemical constituent information to JULES, which in turn responds with fluxes of horizontal momentum, water, energy, carbon, and other tracers exchanged between the atmosphere and the surface beneath.

To simulate the atmospheric composition and the related process, BRAMS has the Coupled Chemistry-Aerosol-Tracer Transport model (LONGO et al., 2013, hereafter CCATT) coupled with BRAMS and developed to simulate the transport, dispersion, chemical transformation, and removal processes of gases and aerosols for atmospheric composition and air pollution studies. CCATT computes the tracer transport in line with the simulation of the atmospheric state by BRAMS, using the same dynamical core, transport scheme, and physical parameterizations. The prognostic of the tracer mass mixing ratio includes the effects of sub-grid- scale turbulence in the planetary boundary layer and convective transports by shallow and deep moist convection, in addition to

grid-scale advective transport. The model also includes gaseous/aqueous chemistry, scavenging and dry depositions, and aerosol sedimentation.

Figure 3.28 A chart of the BRAMS system with the chemistry model component. The gray blocks and the black arrows indicate the codes that make up the BRAMS system and their outputs, respectively. The white blocks indicate either the input files for the pre-processing (first line) as the pre-processing outputs (third line), which are also input files for pre-processing emissions and boundary conditions and routines for composing the BRAMS model.

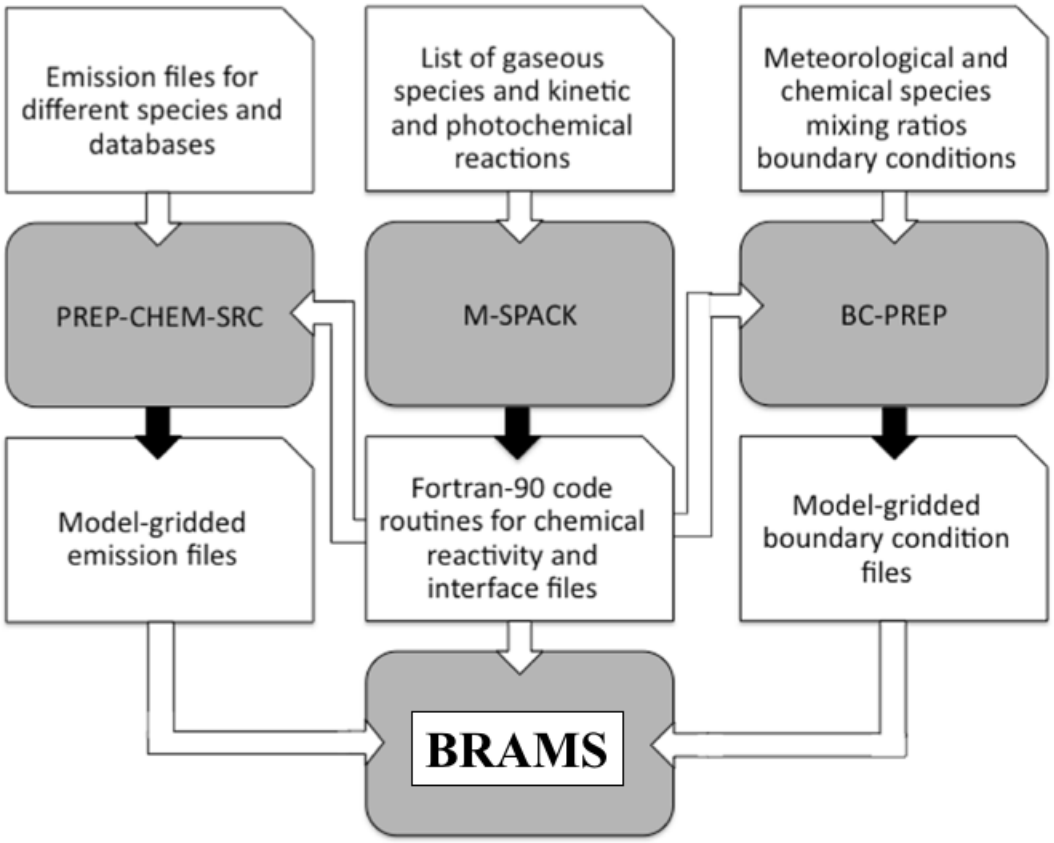

Source: Adapted from Longo et al. (2013).

The choice of different chemistry mechanisms in BRAMS is possible using a modified version of the SPACK pre-processing tool (Simplified Pre-processor for Atmospheric Chemical Kinetics, (DAMIAN, V., SANDU, A., DAMIAN, M., CARMICHAEL, G. R., AND POTRA; F A DAMIAN, 1995; DJOUAD; SPORTISSE; AUDIFFREN, 2002). In principle, M-SPACK allows the use of any chemical mechanism in BRAMS, though it requires building of the emissions interface. The current version of M-SPACK

includes three widely used tropospheric chemistry mechanisms: RACM, the Regional Atmospheric Chemistry Mechanism (STOCKWELL et al., 1997), Carbon Bond (G Z YARWOOD; YARWOOD, G., RAO, S., YOCKE, M., AND WHITTEN, 2005), and RELACS, the Regional Lumped Atmospheric Chemical Scheme (CRASSIER et al., 2000), which consider, respectively, 77, 36, and 37 chemical species.

3.3.2. MEGAN

The Model of Emissions of Gases and Aerosols from Nature version 2.1 (MEGAN2.1) is a modeling framework for estimating fluxes of biogenic compounds between terrestrial ecosystems and the atmosphere using simple mechanistic algorithms to account for the major known processes controlling biogenic emissions. MEGAN estimates emissions $\boldsymbol{F_i}$ of chemical species i from terrestrial landscapes as the product of these two components in units of (μg m^{-2} h^{-1}) for 19 compound classes $\boldsymbol{i}$ according to the equation:

$$F_i = \gamma_i \sum \varepsilon_{i,j} \chi_j \tag{3.4}$$

where $\boldsymbol{\varepsilon_{i,j}}$ is the emission factor at standard conditions for vegetation type $\boldsymbol{j}$ with fractional grid box areal coverage $\boldsymbol{\chi_j}$. The emission activity factor $\boldsymbol{\gamma_i}$ accounts for the processes controlling emission responses to environmental and phenological conditions. MEGAN is used to estimate emissions of compounds from urban, rural and agricultural ecosystems that can influence the atmosphere. The variables that are present in the model include land cover, climate and chemical composition of the atmosphere, and the model results are very sensitive to these driving variables (GUENTHER et al., 2006, 2012; HESS et al., 2008; ARNETH et al., 2011). The numerical system MEGAN is a global model with 1km (or less) spatial resolution, suitable for both regional air quality modeling and global earth system modeling studies. The model calculates hourly emissions of 19 categories of chemical compounds representing 147 individual

compounds (GUENTHER et al., 2012). MEGAN2.1 is available as an off-line code and as an integrated component of land surface and atmospheric chemistry models. As an example, MEGAN2.1 has been embedded into the Community Land Model (CLM4.0; LAWRENCE et al. (2009)) which can run off-line or as an on-line component of the Community Earth System Model (CESM; GENT et al. (2011)) which includes the chemistry model CAM-chem (LAMARQUE et al., 2011). The Figure 3.29 represents model components and driving variables (GUENTHER et al., 2012).

Figure 3.29 Schematic of MEGAN2.1 model components and driving variables.

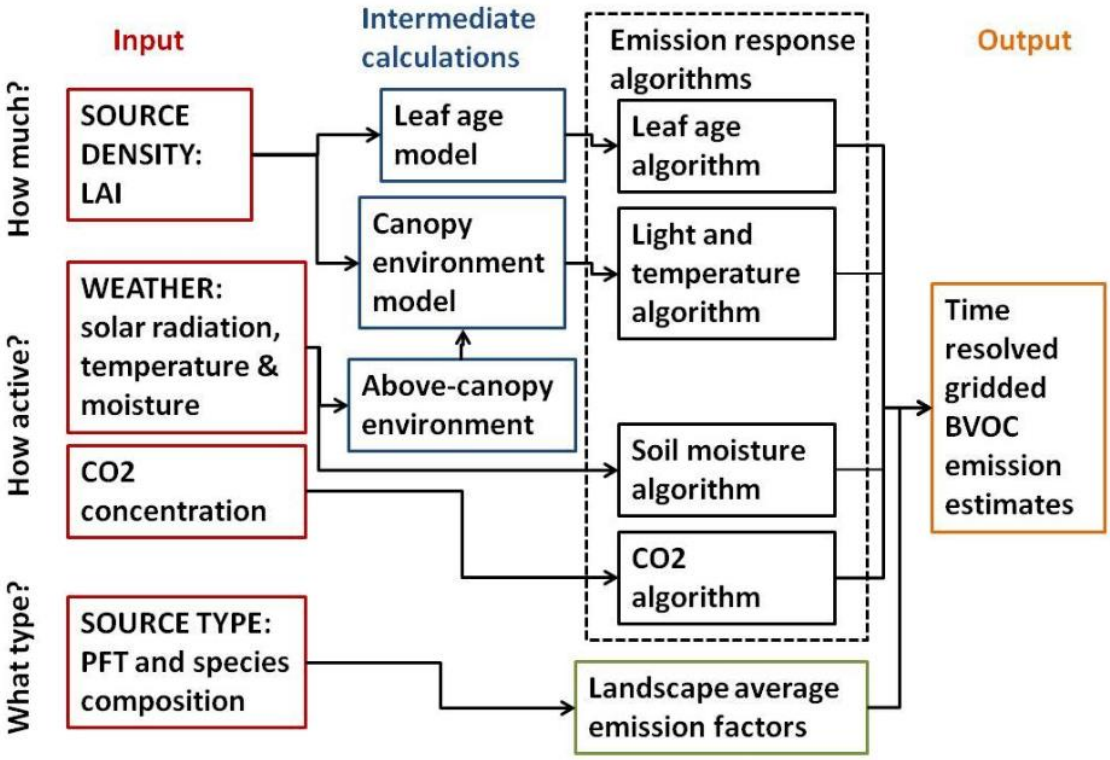

Source: Guenther et al. (2012)

Three types of input files are necessary: source density (monthly average LAI), meteorological data (solar radiation, temperature and moisture) and CO_2, and source type (Plant Functional Type and the corresponding Emission Factor) that must be the average for each grid point domain. Emissions estimated by the MEGAN model are

calculated for each plant functional type (PFT) and later added to estimate the total emissions in a region.

3.3.3. Model development: BRAMS and MEGAN coupling

BRAMS as described at LONGO et al. (2013) and (FREITAS et al., 2017) uses two off-line data options for biogenic emissions: GEIA and MEGAN. The GEIA database (*Global Emissions Inventories Activity*) has a spatial resolution of 1° x 1° and monthly temporal resolution. The data from MEGAN are global, with a spatial resolution of 0.5° × 0.5° resolution and monthly temporal, for the year 2000 (FREITAS et al., 2011). As part of this thesis, the coupling of MEGAN model with BRAMS was carried out aiming to have the biogenic emissions in BRAMS as a function of the environmental variables along the model execution.

The coupling of MEGAN model within BRAMS is schematically presented in Figure 3.30, in this way, the biogenic emissions respond to the atmospheric state simulated by BRAMS through an interface while the original code does not require any change in the previous method for natural emissions adopted before the coupling.

The development of the coupling was based on the excel version of MEGAN (MEGAN2.1beta06). The Visual Basic For Applications (VBA) code was translated to FORmula TRANslation (FORTRAN) program language during the internship at NCAR and PNNL (Pacific Northwest National Laboratory), and implemented later in one of the BRAMS subroutines (chem_source.f90).

Figure 3.30 Coupling scheme BRAMS/MEGAN. The current standard use of the MEGAN model outputs via emission module PREP-CHEM-SRC was preserved as an option for future simulations (gray box).

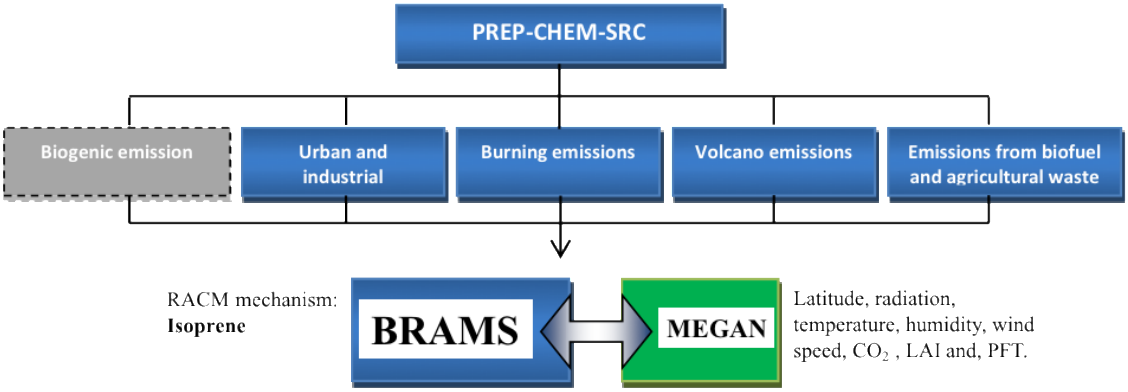

Source: Author's production

The MEGAN model inputs includes the latitude, solar radiation, temperature, humidity, wind speed, CO_2, plant functional type (PFT) and leaf area index (LAI). After receiving these information, MEGAN performs the estimation of the isoprene emission factor, and then BRAMS finally receives an updated isoprene emission from MEGAN, based on the BRAMS previous time-step informations.

Figure 3.31 presents the modeling development work accomplished: the MEGAN framework with subroutines, functions and variables representing the levels and calls inside the FORTRAN code built from the VBA MEGAN version.

Figure 3.31 MEGAN framework with subroutine, functions and variables representing the levels and calls inside the FORTRAN code built from the last MEGAN version.

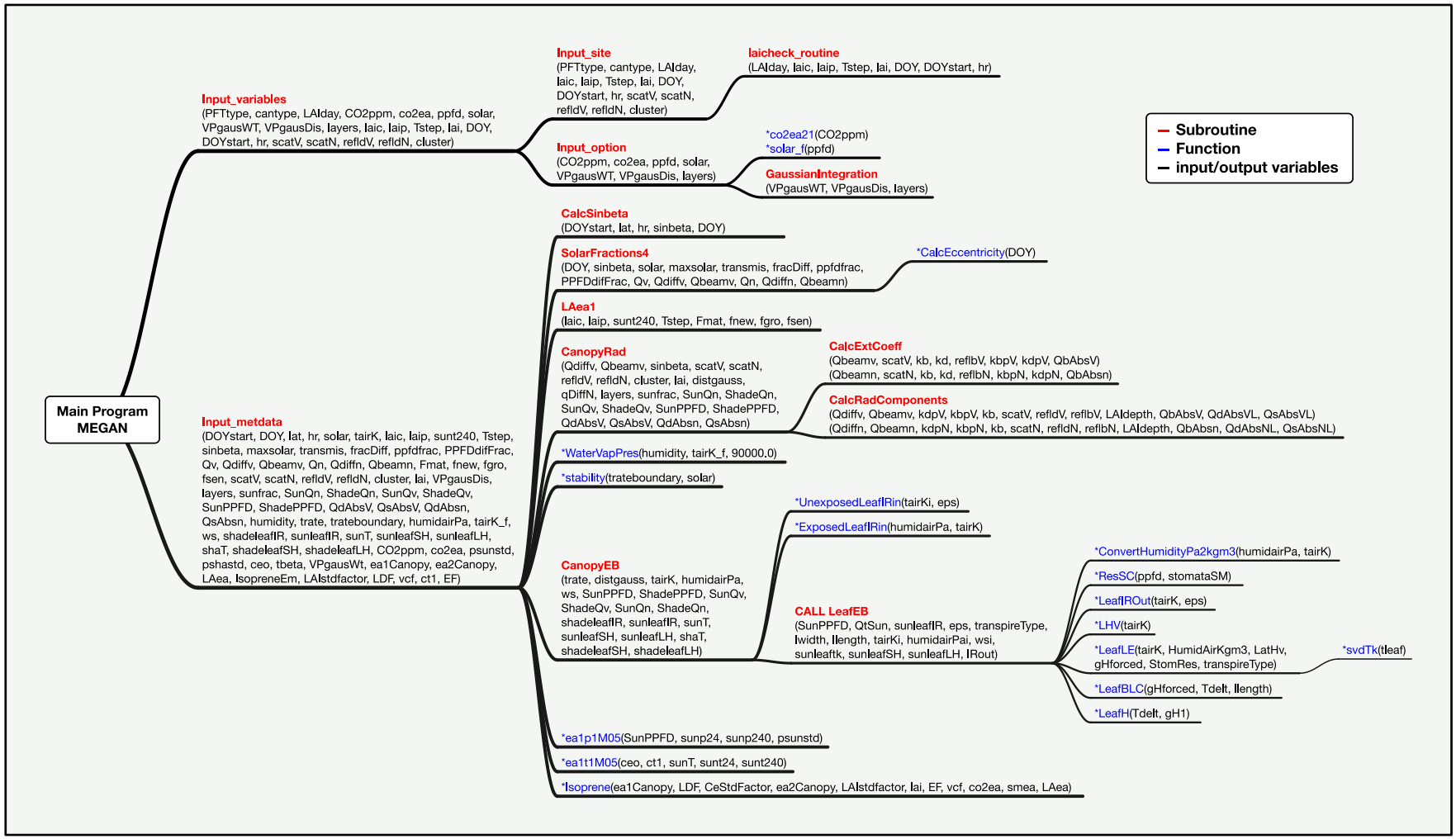

Source: Author's production.

3.3.4. Model configuration

Simulations for the SAMBBA period were conducted with the BRAMS numerical model, coupled with MEGAN both online and off-line, covering most of the Amazon basin (southwest corner: 14◦S 70◦W, northeast corner: 0◦S, 45◦W) with 10 km resolution as depicted in Figure 3.32. In addition to biogenic emissions, we used fire emissions from 3BEM (LONGO et al., 2010) as well as all the other sources described in Sect. 3.3.2.

Figure 3.32 Grid domains for SAMBBA simulations. Dash line represents the simulated domain.

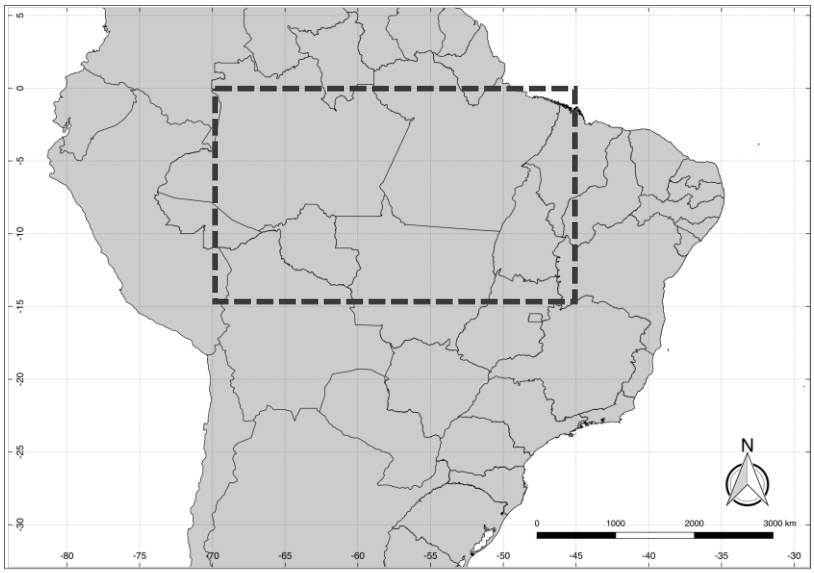

Source: Author's production

The physical parameterizations and modeling system configuration options that were used are summarized in Table 3.6. The SAMBBA simulations were initialized on 14 September 2012 00:00UTC and carried out until 4 October 2012 00:00UTC. The model parameterizations chosen for the simulations described in this section are detailed as follows. The surface scheme was the JULES (MOREIRA et al., 2013) and the RAMS parameterization for the unresolved turbulence in the PBL used in this simulation was

based on the MELLOR; YAMADA, (1982) formulation, which predicts turbulent kinetic energy (TKE). All radiative calculations were performed using CARMA (TOON et al., 1989) with aerosol optical properties prescribed accordingly to Rosario et al. (2013). For the microphysics, we used the single-moment bulk microphysics parameterization, which includes cloud water, rain, pristine ice, snow, aggregates, graupel and hail. It includes prognostic equations for the mixing ratios of rain and each ice category of total water and the concentration of pristine ice. Water vapor and cloud liquid mixing ratios are diagnosed from the prognostic variables using the saturation mixing ratio with respect to liquid water. The shallow and deep cumulus scheme is based on the mass-flux approach (GRELL and DÉVÉNYI, 2002). The RACM mechanism was used for the chemical integration.

The CPTEC/INPE global model T213 analysis provided initial and boundary conditions for the meteorological integration, and the MOCAGE (*Modélisation de la Chimie Atmosphérique Grande Echelle*) global chemistry forecast (JOSSE et al., 2004; BOUSSEREZ et al., 2007) provided boundary conditions for chemistry fields. Initial soil moisture was taken from the FREITAS; GEVAERD, (2006) estimation technique and the soil temperature was initialized assuming a vertically homogeneous field defined by the air temperature closest to the surface from the atmospheric initial data.

Table 3.6. System configuration for SAMBBA simulations.

	BRAMS
Grid resolution	10 km
Trace gas chemistry	RACM, (STOCKWELL et al., 1997)
Initial chemistry and boundary conditions	MOCAGE
Short/longwave radiation	Based on CARMA
Photolysis	FAST-TUV
shallow and deep convection	GRELL and DÉVÉNYI (2002)
PBL parameterization	(MELLOR; YAMADA, 1982)

For data analysis, the numerical simulations with BRAMS coupled with MEGAN online and off-line will be compared for isoprene and OH. Also, an assessment of the data time series and vertical profile along SAMBBA field campaign period will be conducted, using the observations in tower K-34 and airborne measurements as reference.

4 RESULTS

4.1. Tower K-34 measurements

The results for the isoprene mixing ratio, fluxes measured at the tower K-34 are presented in Figure 4.1, as well as the environmental variables. Figure 4.1 shows the data compilation for three days sampling period with the trend line for isoprene mixing ratio (ppbv) and fluxes (mg C m^{-2} h^{-1}). The isoprene flux in the morning was relatively high when compared with the observations during the afternoon, although most studies in Amazon basin present an increasing around 12-15 h (KARL et al., 2007; KUHN et al., 2007; YÁÑEZ-SERRANO et al., 2015). As mentioned previously, due a problem during tower sampling the diurnal isoprene cycle pattern was affected, compromising the signal in the chart. However, the magnitude of the results for isoprene flux and mixing ratio are consistent with other studies conducted in the Amazon rainforest. A study conducted in the tower K-34 by STEFANI et al. (2000) found isoprene flux around 1.1 mg C m^{-2} h^{-1} in for 30 ºC, 1100 µmol m^{-2} s^{-1} PAR, also using REA system. GREENBERG et al., (2004) found values ranging from 1.9 – 8.6 mg C m^{-2} h^{-1} in different sites in Amazon basin. Similar results was also reported by KUHN et al. (2007) at the K-34 tower, with a mean daytime flux ~2.1 mg C m^{-2} h^{-1} using REA system.

The isoprene mixing ratio in the tower K-34 achieved its maximum value approximately at 14:45 h, with 3.5 ppbv. In general, the values found in the Tower k-34 are close those reported by YÁÑEZ-SERRANO et al. (2015) at the Amazonian Tall Tower Observatory (ATTO) site, located in central Amazonia. The study showed during the wet season an isoprene mixing ratio ranging from 0.5 to 2.5 ppbv, with the maximum value at ~15:00 h. KUHN et al. (2007) also reported Isoprene mixing ratios ranging from 1 – 4 ppbv for altitudes up to 100 m during a flight campaign over a pristine tropical forest north of Manaus, in the central Amazon Basin. These values agree with our measurements for three days sampling in the K-34 tower, with isoprene interval from 0.5 – 3.5 ppbv.

Figure 4.1. Isoprene flux and mixing ratio for three days sampling in K-34 tower. Original data in red and trend line in blue. Photosynthetically active radiation and temperature conditions were obtained from BRAMS model.

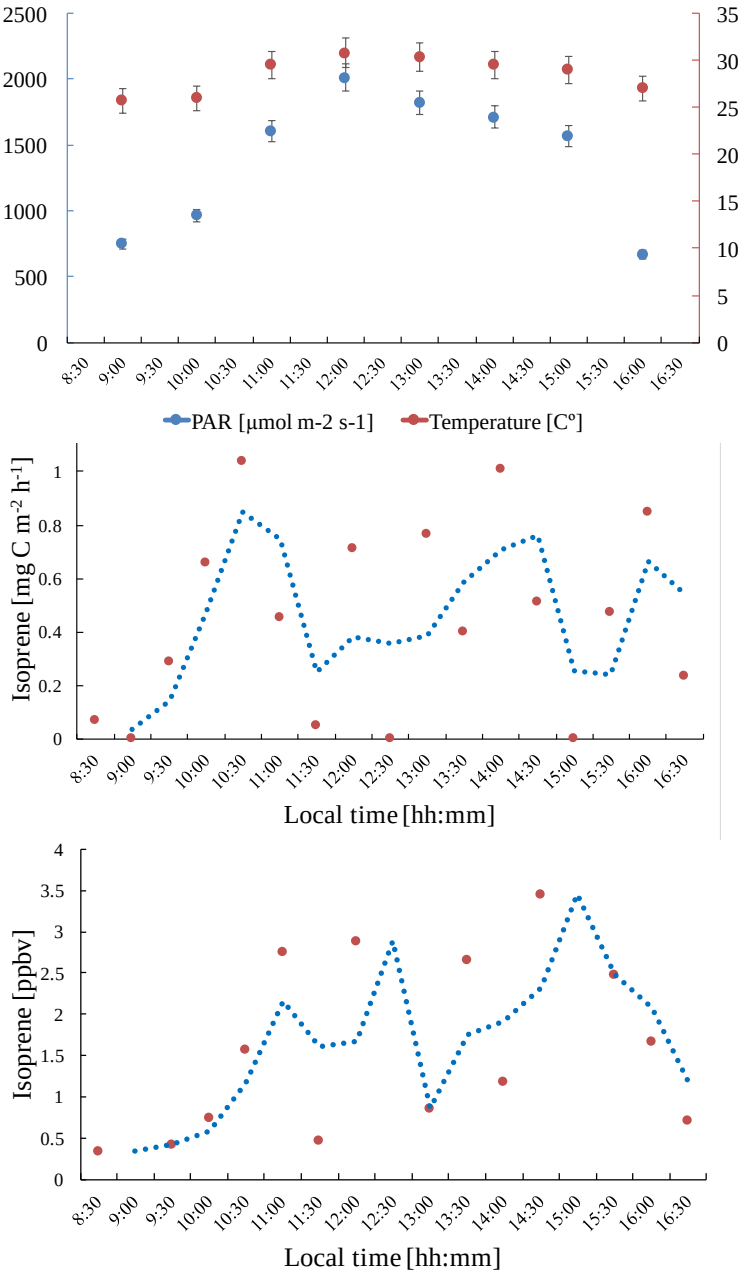

Source: Author's production.

4.2. SAMBBA airborne measurements

4.2.1. Ambient distributions of CO, NO_x and O_3

Figure 4.2 depicts CO, NO_x, and O_3 mixing ratios measured at different altitudes, up to 2 km, and time of the day, between 11:00 am and 6:00 pm. In Figure 4.2, the flight tracks are separated according to the BG, FP, and AP classification, while Table 4.1 shows typical values of CO, NO_x, and O_3 mixing ratios measured in this study and during several previous airborne campaigns in Amazonia and savannah areas in Brazil. During the SAMBBA field experiment, in BG condition (i.e., CO < 150 ppbv), the NO_x mixing ratio ranged from 50 pptv to 200 pptv. Torres and Buchan (1988) reported measurements of NO mixing ratios ranging between 20 and 35 pptv during the Amazon Boundary Layer Experiment (ABLE-2A) between July and August 1985. Modeling results of Jacob and Wofsy (1988) found NO_x mixing ratio values around 200 pptv, with the NO mixing ratio values similar to ABLE-2A observation that was conducted over the Amazon rainforest. Also in Brazilian Amazon basin during the wet season, aircraft measurements as part of the NASA Atmospheric Boundary Layer Experiment (ABLE 2B), showed NO_x mixing ratios ranging from 4 – 68 pptv (SINGH, 1990). Comparing our measurements with these previous studies, SAMBBA experiment showed a slightly influence from polluted regions. More recently, Liu et al. (2016) used four sets of different Master Chemical Mechanism and estimated that NO mixing ratio using the NO vs HO_2 isoprene chemistry (fHO_2:fNO ~ 0.6 – 1.4) would be around 20 – 40 pptv of NO based on measurement in the Amazon, lower than that obtained in our study. On the other hand, flight tracks in biomass burning areas showed high values of NO_x in FP (50-1,250 pptv) and AP (50-950 pptv) compared with other studies in forest areas of Amazonia, except for a study in cerrado area in Brazil (≤10,000 pptv) conducted by Crutzen et al. (1985) during the dry season.

Figure 4.2. Cross section of CO (on top), NO_x (middle) and O_3 (on bottom) mixing ratios (ppbv) for the three different groups: background environment (on the left), fresh smoke plume (t < 2 hours, on the middle) and aged smoke plume (t > 2 hours, on the right). The aircraft data was interpolated from the various vertical profile measurements using kriging correlation method. Grey lines show the flight tracks. Hour is presented in local time.

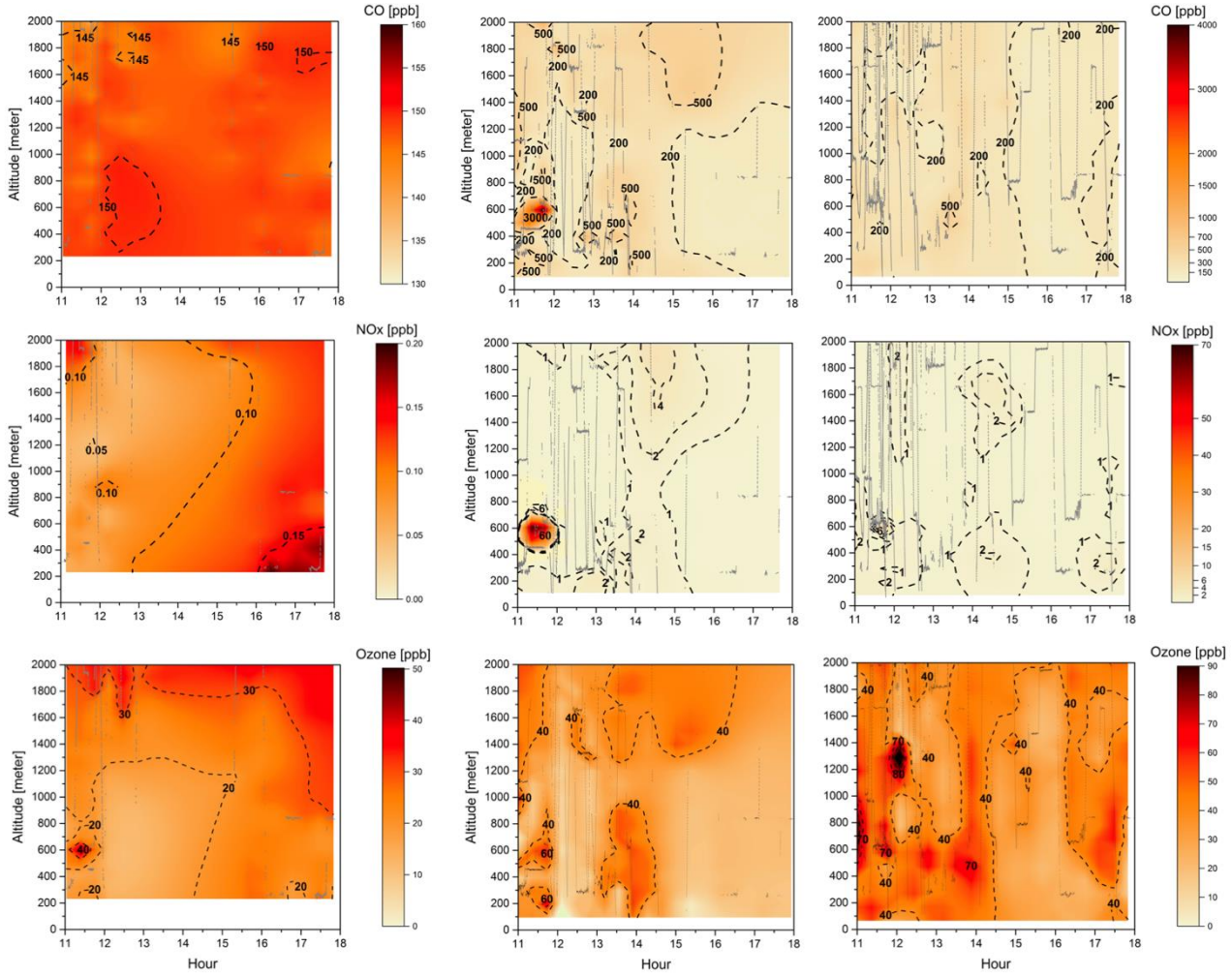

Source: Author's production

Table 4.1. Typical values of airborne measurements: CO, NO_x, and O_3 mixing ratios in Amazonia and cerrado areas in Brazil.

Month/Year	CO (ppbv)	NO_x (pptv)	O_3 (ppbv)	Biome and reference
Sep/2012	135-150[a]	50-200[a]	10-45[a]	Forest and grassland, BG, this work.
Sep/2012	150-900[b]	50-1,250[b]	10-75[b]	Forest and grassland, FP, this work.
Sep/2012	150-450[c]	50-950[c]	20-70[c]	Forest and grassland, AP, this work.
Aug/1979	70-500		40-65	Cerrado, Crutzen et al. (1985).
Aug/1980	100-400	-	20-55	Forest, Crutzen et al. (1985)
Jul/1985	150-600	74-102	20-50	Forest, Andreae et al. (1988).
Jul-Aug/1985	-	20-37	-	Amazon Basin TORRES; BUCHAN, (1988)
Apr/1987	84-118	4-68	10-57	Brazilian Amazon Basin (SINGH, 1990)
Sep/1989	150-600	-	25-80	Forest, Kaufman et al. (1992).
Sep/1992	100-400	-	-	Forest, Blake et al. (1996).
Aug/1995	440-763	-	95-102	Cerrado, Reid et al. (1998).
Aug/1995	482-566	-	61-70	Forest, Reid et al. (1998).
Aug/2004	100-600	-	10-30[a, c]	Forest, Yokelson et al. (2007).
Nov/2008	100-300[b, c]	-	40-60[c]	Forest, Andreae et al. (2012), Bela et al. (2014).
May/2009	60-110[a]	-	10-20[a]	Forest, Andreae et al. (2012), Bela et al. (2014).

Measurements in [a]background, [b]fresh plumes, and [c]aged plumes. The data without an index was collected without any particular criteria.

The O_3 mixing ratios in the BG environment reached 40 ppbv at about 600 m altitude during flight B735 (at 11:30 am, Figure 4.2), although typical values ranged from 10 to 45 ppbv (< 2000 m). This value of 40 ppbv is nearly double the mean value of O_3 mixing ratio that we used as background in the enhancement ratio, and even out of the range of the standard deviation (21 ppbv, SD=7). Bela et al. (2014) reported O_3 ranging from 10 to 20 ppbv during the wet-to-dry transition season (May/June 2009), measurements performed in a clean atmosphere during the *Regional Carbon Balance in Amazonia* (BARCA B) campaign. In contrast, during BARCA A campaign, in the dry-to-wet transition season (November/December 2008), the O_3 mixing ratio ranged from 40 to 60 ppbv in an area influenced by fires, values which are comparable with FP (10-75 ppbv) and AP (20-70 ppbv), and even in BG conditions (10-45 ppbv) during SAMBBA.

In terms of CO and NO_x, the flight tracks classified as FP were the most polluted of the campaign. The CO and NO_x mixing ratios for FP reached, respectively, values above 3,000 and 60 ppbv at 600 m from the surface between 11:00 am and 12:00 pm. The enhancement of CO and NO_x mixing ratios near the surface suggests an initial vertical transport due to the hot plume buoyancy, which may increase the tracer lifetime released to the atmosphere. The vertical transport can be observed mainly for CO at different altitudes and time of the day since the CO is preserved longer along the plume when compared with NO_x. The measurements in fresh biomass burning plumes also captured higher levels of CO mixing ratios (≅500 ppbv) at 1.4 km and 2 km of altitude. Yokelson et al. (2007), during the Tropical Forest and Fire Emissions Experiment (TROFFEE), reported a vertical transport mechanism, called a “mega-plume”, at 2km altitude during a flight in the south of the Amazon rainforest (from Manaus to Cuiabá), with CO mixing ratio reaching 1,200 ppbv. The TROFFEE experiment used airborne measurements during the 2004 Amazon dry season, and reported, on 8 September, the presence of a massive plume formed from numerous fires. During SAMBBA campaign, we also detected the presence of similar mega-plumes during the flight B742, classified mostly as FP, with a unique CO mixing ratio value, peaking ~5,000 ppbv at about 600 m. These results demonstrate the strength of vertical transport during a fresh biomass

burning event, with the plume injection height up to 2 km. Freitas et al. (2006, 2007, 2010) highlighted the importance of representing the injection height of biomass burning plumes in numerical models to describe the regional smoke distribution. Trentmann and Andreae (2003) also demonstrated a large impact of fire emissions on the chemical composition in a young biomass burning plume using a 3-D chemical transport model and direct observations. These authors reported simulated high values near the fire (z ≅150 m) for CO and NO_x, with mean values around 18,000 ppbv and 404 ppbv, respectively. On the other hand, Andreae et al. (2012) reported CO mixing ratios up to 300 ppbv in a smoky region in the southern Amazon basin during the BARCA experiment. The highest values were found at about 1,000 m altitude, late in the dry season (BARCA-A, November 2008). In this study, the CO mixing ratio measurements in FP and AP ranged from 150 to 900 ppbv and from 150 to 450 ppbv, respectively. The CO mixing ratios in FP (150-900 ppbv) are comparable with values found by Reid et al. (1998) in a cerrado area (440-763 ppbv) and some forest studies (up to 600 ppbv) conducted by Andreae et al. (1988), Kaufman et al. (1992) and Yokelson et al. (2007). The values found in AP were consistent with values of CO mixing ratios from forest areas, impacted by haze smoke plumes (Table 4.1).

In Figure 4.2, during most of the flight tracks classified as AP, the NO_x mixing ratio values were below 2 ppbv, except for a peak of 6 ppbv at 600 m from the surface between 11:30 am and 12:00 pm, a value below that observed in the FP environment (60 ppbv). On the other hand, the O_3 mixing ratio results in AP presented high levels (≅ 80 ppbv) around 12:10 pm at 1,300 m altitude. We also investigated the high levels of CO and NO_x mixing ratios found in FP corresponding to the same flight in which we also detected high levels of O_3 in AP. In fact, Figure 4.3 shows the track of flight B742 in a transition from a remote site impacted by FP to an urban site in Palmas-TO, with high levels of O_3 (≅ 80 ppbv).

Figure 4.3. On the left, the track of flight B742 that landed in Palmas – TO. The color bar is representing the measured O_3 mixing ratios (ppbv) along the flight track. On the right, from top to bottom, the altitude, and the CO, NO_x and O_3 mixing ratios (ppbv) measured along the same flight track. The red and blue dots are representing the parts of the flight track classified as fresh (FP) and aged (AP) smoke plumes, respectively.

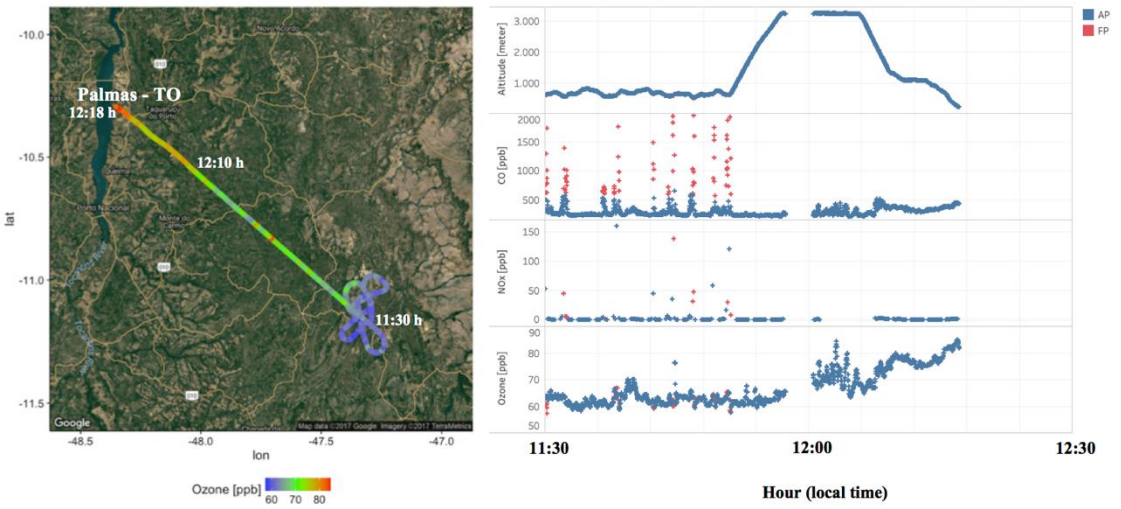

Source: Author's production.

The mean value of O_3 found in FP was 31 ppbv (SD = 14), which is 29% lower than measured for AP (44 ppbv, SD = 13 ppbv), since O_3 is produced as a secondary product from the interaction between VOCs and NO_x. The O_3 mixing ratios in FP peak at about 60 ppbv near the surface (200–600 m) and, for most cases, plumes with about 40 ppbv were observed both near the surface and in high altitudes (Figure 4.2). During the TROFFEE experiment, Yokelson et al. (2007) found O_3 mixing ratios of about 30 ppbv in smoke haze layers in Amazonia. Our results showed higher values for O_3 mixing ratios, ranging from 10 to 75 ppbv in FP and 20 to 70 ppbv in AP. Agreeing with the SAMBBA results, Reid et al. (1998) found O_3 mixing ratios ranging from 60 to 100 ppbv during SCAR-B experiment in 1995 dry season, and Kaufman et al. (1992) found similar levels of O_3 in a forest site in Amazonia during BASE A (Table 4.1).

4.2.2. Long-range transport of O_3

We analyzed the ozone vertical distribution for all SAMBBA flights following the methodology proposed by Greenslade et al. (2017). To identify a long-range transport event, we selected the flights excluding the first 0.5 km of altitude to avoid noise levels of ozone, characteristic in a region impacted by biomass burning. We also filtered the data ignoring high O_3 events within 0.5 km of the tropopause (> 8 km) to reduce uncertainties related with the variations in lower stratospheric and upper tropospheric layer. Then, after calculating the 99th percentile perturbation value, we separated the flights using the O_3 threshold (83.5 ppbv) as criteria to identify the long-range transport events.

The O_3 is formed photochemically during the smoke plume aging and we used the enhancement ratio $ER_{[\Delta O_3]/[\Delta CO]}$ as an indicator of the smoke plume age, according to the Eq. 3.1. The enhancement ratio $ER_{\Delta O_3/\Delta CO}$ allowed us to identify aged plumes during the analyzes, corroborating the influence of long range transport. Table 3.4 list values of $ER_{\Delta O_3/\Delta CO}$ and the estimated plume age for several measurements in tropical and subtropical sites.

Figure 4.4.a shows the vertical profile of O_3 mixing ratio for all SAMBBA flights and its approximate plume age through the $ER_{\Delta O_3/\Delta CO}$. The high values of O_3 mixing ratio (> 83.5 ppbv) found between 5,500 and 6,500 m of altitude, also presented high values for the enhancement ratio ($ER_{\Delta O_3/\Delta CO} > 2$), suggesting long-range transport of ozone. We detected two possible long-range ozone transport events between 5,500 – 6,500 m of altitude (O_3 > 83.5 ppbv), southward (flights B744 and B745) and westward (flight B746) from Porto Velho – RO. These scientific flights affected by long-range transport occurred on September 24 and 29, 2012 (Figure 4.4.b).

During this same period, the O_3 product retrieved from Atmospheric Infrared Sounder (AIRS) measurements onboard the AQUA satellite during daytime highlights the long-range ozone transport from biomass burning emissions in Africa, with an inflow into the Amazon basin at 500 hPa (Figure 4.5).

Figure 4.4. (a) Vertical profiles of O_3 with the altitude and as a function of $ER_{\Delta O_3/\Delta CO}$ (color scale) for all SAMBBA flights. (b) Flights identified as a long-range transport of ozone.

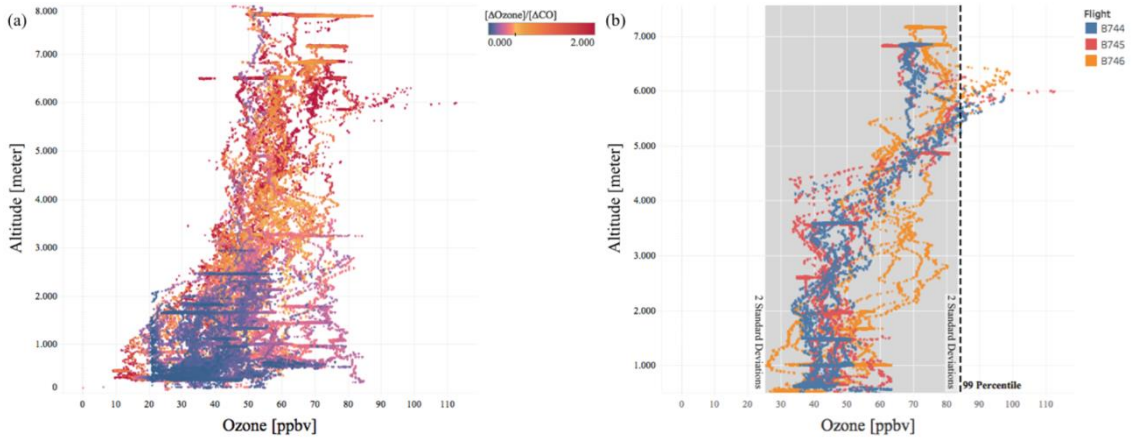

Source: Author's production.

Figure 4.5. Time averaged Ozone (ppmv) from September 24 to 29 2012 retrieved from AIRS onboard AQUA satellite during daytime at 500 hPa, with 1º x 1º spatial resolution.

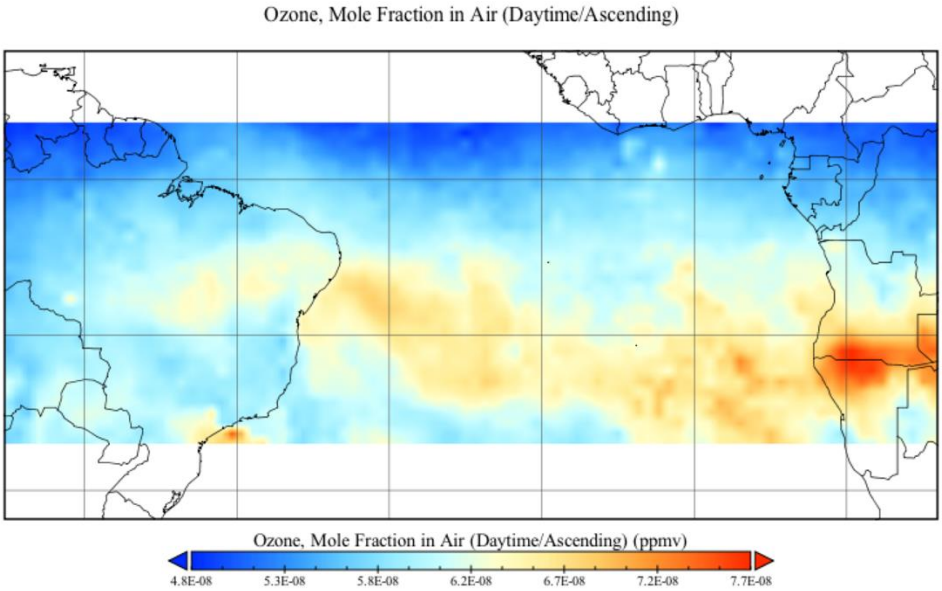

Source: Adapted from AIRS.

4.2.3. Isoprene and its oxidation ratio

Information about the isoprene transport and chemistry can be derived from the isoprene abundance in the atmosphere and the ratio of its oxidation products relative to isoprene, [MVK+MACR+ISOPOOH]/[isoprene]. During the day, the isoprene chemistry is affected mainly by the distance from the emission source (transport time), photochemical degradation and availability of OH, which reacts with isoprene to produce chemical species including MVK, MACR and ISOPOOH (KUHN et al., 2007; LIU et al., 2016). During SAMBBA, the mean isoprene mixing ratio in BG was 2.8 ppbv and 1.5 ppbv for the boundary layer and free troposphere, respectively. We also detected higher values of O_3 (40 ppbv at 600 m) in BG, shown in Figure 4.2, coinciding with the interpolated cross section of the isoprene (≤4 ppbv at 600 m), also in BG environment (Figure 4.6). As mentioned by Barket et al. (2004), in fact, a sequence of reactions initialized by the reaction of isoprene with OH leads to the production of organic peroxy radicals (RO_2), that then react with NO_x promoting the ozone formation observed during the BG flights tracks. Table 4.2 summarizes the mean values of isoprene and the oxidation ratio [MVK+MACR+ISOPOOH]/[isoprene] during SAMBBA, together with previously-reported airborne measurements in remote areas and biomass burning environments. The isoprene mixing ratios measured during SAMBBA in BG environment generally agree with values reported in pristine areas of the Amazon forest (Greenberg et al., 2004; Greenberg and Zimmerman, 1984; Gregory et al., 1986; Helmig et al., 1998; Kuhn et al., 2007; Lelieveld et al., 2008; Rasmussen and Khalil, 1988; Zimmerman et al., 1988). Some studies conducted in the Amazonian tropical forest, e.g., Greenberg et al. (2004) and Kuhn et al. (2007), have higher isoprene with reported values up to ~6 to 7 ppbv.

Figure 4.6. Cross section of the isoprene mixing ratio (ppbv) (top) and the [MVK+MACR+ISOPOOH]/[Isoprene] ratio (bottom) for the three different groups: background environment (on the left), fresh smoke plume (t < 2 hours, in the middle), and aged smoke plume (t > 2 hours, on the right). The aircraft data was interpolated from the various vertical profile measurements using kriging correlation method. White dashed lines show the flight tracks. Hour is presented in local time.

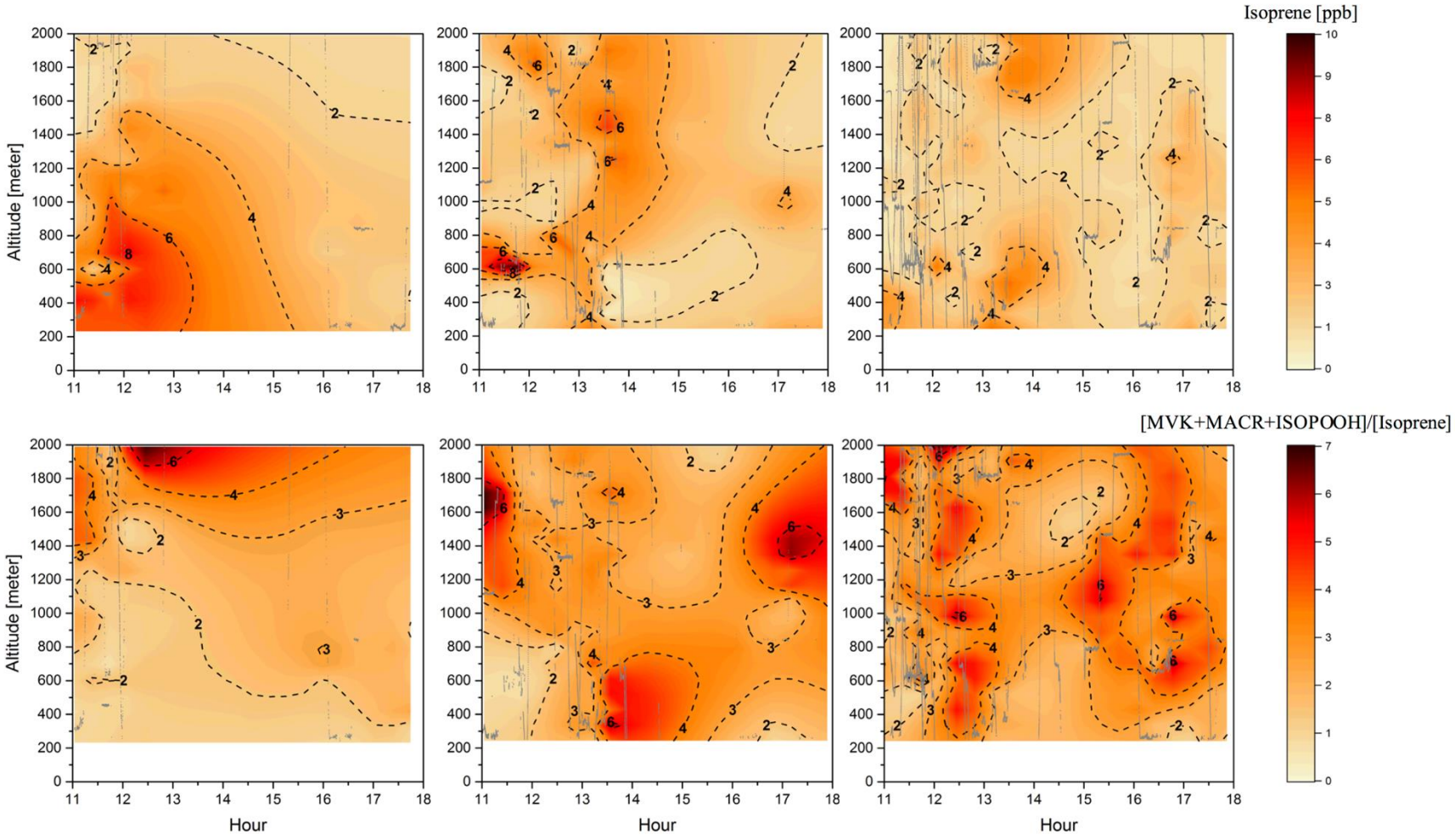

Source: Author's production.

Table 4.2. Airborne measurements of isoprene, oxidation ratio [MVK+MACR+ISOPOOH]/[isoprene], and OH in remote areas and biomass burning environments worldwide.

Month/Year	Isoprene (ppbv)	[MVK+MACR+ ISOPOOH]/ [Isoprene]	OH (10^6molec. cm^{-3})	Biome, location, and reference
Sep/2012	2.8[c] 1.5[d]	1.7[c] 3.3[d]	0.1[a, c] 0.5[a, d]	Tropical forest in Brazil, background, this work
Sep/2012	1.4[c] 1.6[d]	7.0[c] 6.1[d]	1.4[a, c] 1.2[a, d]	Tropical forest in Brazil, fresh smoke, this work
Sep/2012	2.4[c] 2.4[d]	2.3[c] 2.3[d]	0.1[a, c] 0.3[a, d]	Tropical forest in Brazil, aged smoke, this work
Sep/1979 Aug/1980	2.4[b] 2.3[c] 0.2[d]	-	-	Grassland/Tropical forest Brazil, Greenberg and Zimmerman, 1984
Jun/1984	2.3[b]	-	-	Tropical forest in Guyana, Gregory et al., 1986
Jul/1985	2-4[c]	-	-	Tropical forest in Brazil, Rasmussen & Khalil, 1988
Jul/1985	~2[c]	-	-	Tropical forest Brazil (north of Manaus), Zimmerman et al., 1988
Oct/1995	-	-	3-5[d]	Southern Ocean south of Tasmania, Mauldin et al., 1997
Jul/1996	3.1[b] 1.4[c] 0.2[d]	0.15[b] 0.19[c] 0.48[d]	-	Tropical forest in Peru, Helmig et al., 1998
May/1997	1-4[b]	-	8-13[c, a]	Boreal forest in USA (Sierra Nevada), Dreyfus et al., 2002
Aug/2000	-	-	~17[a]	Savanna in South Africa (Timbavati reserve), Hobbs et al., 2003
Jan/2000	0.4/0.7/0.5[f]	-	-	Tropical forest in Brazil (Tapajós), Greenberg et al., 2004
Mar/1998	1.7/2.9/3.1[f]	-	-	Tropical forest in Brazil (Balbina), Greenberg et al., 2004
Feb/1999	6.6/6.9/6.6[f]	-	-	Tropical forest in Brazil (Jaru reserve), Greenberg et al., 2004
Feb/1999	2.0/1.3/1.2[f]	-	-	Grassland in Brazil (FNS site), Greenberg et al., 2004
Jul/2001	1.1-5.8[c]	< 2[c] / 2-10[d]	5.5[c]	Tropical forest in Brazil (north of Manaus), Kuhn et al., 2007
Sep/2004	-	0.39[b]/0.61[c]/1.2[d]	0.2[b]-9[c]	Tropical forest in Brazil (north of Manaus), Karl et al., 2007
Oct/2005	2.0[c] 0.1[d]	-	11[c] 5[d]	Tropical forest in Suriname, Lelieveld et al., 2008
Oct/2005	-	-	4.4[c]	Pristine forest in Suriname, Kubistin et al., 2010

[a]Estimated values. Measurements at [b]surface, [c]boundary layer, [d]free troposphere, [e]cloud layer. [f]Measurements at 9-12h/12-15h/15-18h

On average, we found lower isoprene in FP (1.4 ppbv), and slightly lower in AP (2.4 ppbv), relative to the BG value (2.8 ppbv), within the PBL (<1,200 m), around 50% and 14%, respectively.

In contrast, above the PBL (> 1,2000 m) we observed a substantial increase of about 60% of the isoprene in AP (2.4 ppbv) relative to the BG value (1.5 ppbv), which is about the same mean value found in FP (1.6 ppbv). These high levels of isoprene at higher altitudes in air masses affected by biomass burning emissions, are likely to be associated with the heat released from vegetation fires affecting nearby plants that also release significant amounts of isoprene to the atmosphere, especially in tropical forest fires in Brazil (Ciccioli et al., 2014). Müller et al. (2016), for example, found isoprene mixing ratios up to 15 ppbv in a smoke plume from a small forest understory fire in Georgia, USA. We also found higher isoprene mixing ratios in upper levels (> 1,200 m) in smoke areas when compared with pristine mixed layer studies mentioned previously. These results reinforce the hypothesis that fire activity promoted the isoprene transport to higher altitudes both in fresh (≅ 6 ppbv, 1,700–2,000 m) and aged plumes (≅ 4 ppbv, 1,600–2,000 m) during SAMBBA flights (Figure 4.6). In Figure 4.7, we also verified the average isoprene mixing ratio (< 2,000 m) in AP (2.4 ppbv) was 71% higher than FP (1.4 ppbv) and similar to the mean value measured in BG (2.6 ppbv).

In fresh smoke plumes, biomass burning tracers, such as acetonitrile and acetaldehyde, are present at a relatively high concentration, while the [MVK+MACR+ ISOPOOH]/[isoprene] ratio is low. In contrast, aged smoke plumes typically have higher values for the [MVK+MACR+ISOPOOH]/[isoprene] ratio, since there is more time for the isoprene to degrade. Figure 4.8 presents the plume interception during the flight B732, between 10:00 am and 11:30 am, in which it is possible to observe the difference between FP and AP interceptions through the biomass burning tracers and [MVK+MACR+ISOPOOH]/[isoprene] ratio. In this study, we found the [MVK+MACR+ISOPOOH]/[isoprene] ratio mean value ranging from around 1.7 in the boundary layer to 3.3 in the free troposphere for BG conditions, with AP presenting a similar value (2.3) for both boundary layer and free troposphere.

Figure 4.7. Isoprene, acetonitrile and carbon monoxide mixing ratios (ppbv) as function of the daytime (local time) for the different chemical regimes previously classified as background (green dots), smoke fresh plume (red dots), and aged smoke plume (blue dots). Black dash lines, and the numbers next to them, are representing the mean values of the measurements taken below 2,000 m of altitude. Hour is presented in local time (11:00 – 18:00 h).

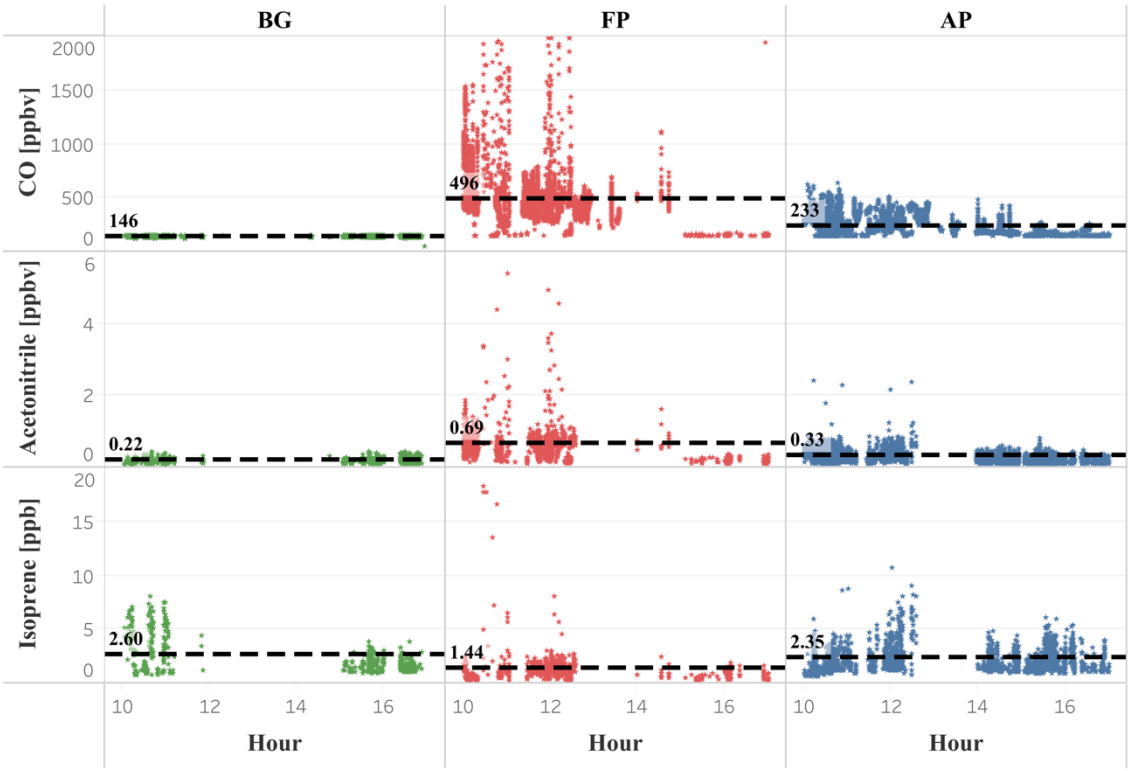

Source: Author's production.

In contrast, FP had the highest value in the boundary layer (7.0) and free troposphere (6.1), similar to values reported by Kuhn et al. (2007), in the tropical forest in Brazil (north of Manaus). Above the PBL, we did not find any substantial variation in [MVK+MACR+ISOPOOH]/[isoprene] ratio associated with the presence of smoke in AP (2.8), but an increase in the BG value (3.3) in the upper levels (> 1,200 m). The FP seems to be more active within the boundary layer than at upper levels, with the isoprene oxidation ratio about 6.1 above 1,200 m. Comparable with our results in FP, Kuhn et al. (2007), during the *Cooperative LBA Airborne Regional Experiment* (LBA-CLAIRE-2001) also found [MVK+MACR+ISOPOOH]/[isoprene] ratio values up to 2, below 1,000 m of altitude, and between 2 and 10, within the 1,000–2,000 m vertical layer.

Figure 4.8. Methanol (green dots), acetonitrile (orange dots), and acetaldehyde (blue dots) mixing ratios (ppbv), and the [MVK+MACR+ISOPOOH]/[Isoprene] ratio (gray bars), during a plume interception along the flight track B732 in different altitudes.

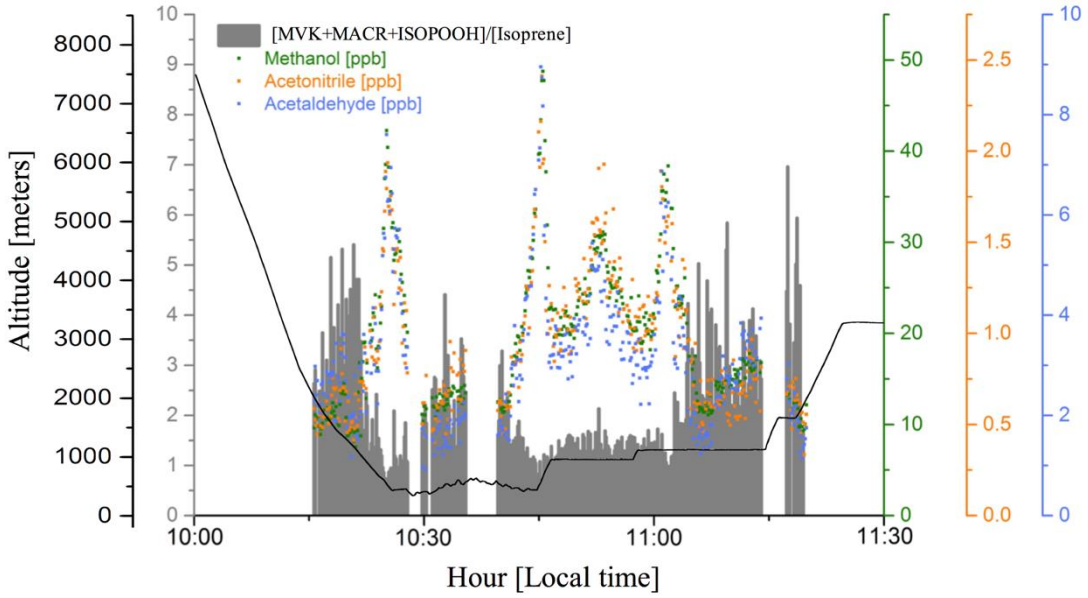

Source: Author's production

In summary, we found a strong increase in the isoprene oxidation ratio from surface to 2,000 m for FP relative to the BG and AP observed during SAMBBA, similar to other previous studies in biomass burning environments (Table 4.2).

We observed values of the [MVK+MACR+ISOPOOH]/[isoprene] ratio above 6 in BG above 1,800 m and between 12:00 pm and 13:30 pm. In contrast, in FP and AP, values in the range 4-6 are equally distributed in the vertical (Figure 4.6). Along the cloud layer (1,200–2,000 m), we found that the isoprene oxidation in BG environment tends to increase (94%) as in AP levels (Table 4.2). Karl et al. (2007) also reported evidence of an increase of the oxidizing power of the atmosphere in the transition from PBL to cloud layer (1,200–1,900 m) during TROFFEE experiment, with the [MVK+MACR+ISOPOOH]/[isoprene] ratio ranging from 0.39 up to 1.2 between 300 m and 1,800 m, already into the cloud layer (CL). Although lower values for the [MVK+MACR+ISOPOOH]/[isoprene] ratio were found during TROFFEE compared

with LBA-CLAIRE, both studies have suggested the occurrence of an oxidizing power in the transition from the PBL to the CL. In both cases, there was a positive gradient, increasing the [MVK+MACR+ISOPOOH]/[isoprene] ratio in the CL. Furthermore, Helmig et al. (1998) reported similar behavior in a remote Peruvian Amazonia site, with the [MVK]/[isoprene] ratio equal to 0.15, 0.19, and 0.48, near the surface (≅ 2 m), in the PBL (91–1,167 m), and above the PBL (1,481–1,554 m) respectively. The [MVK+MACR+ISOPOOH]/[isoprene] ratio increasing toward the top of the PBL and CL is likely to be due to the enhancement of the photolysis rates. Direct experimental data reported by Mauldin et al. (1997) also indicated significant changes above and inside cloud decks due to cloud edge effects on photolysis rates that have a major impact on OH production rates. Figure 4.9 presents the density distribution for the [MVK+MACR+ISOPOOH]/[isoprene] ratio along several altitude layers during SAMBBA. In FP, the average [MVK+MACR+ISOPOOH]/[isoprene] ratio was equal to 6.3 at 500–1,000 m, 7.6 at 1,000–1,500 m, and returning to 5.9 at 1,500–2,000 m. These results are consistent with the increase of the oxidative capacity in the transition from the PBL to the CL, reported by Mauldin et al. (1997) and Karl et al. (2007), with the SAMBBA measurements showing average [MVK+MACR+ISOPOOH]/[isoprene] ratio constantly increasing in BG and the highest value at 500 – 1,000 m in AP. The results showed the isoprene oxidation reaction is enhanced at higher altitudes in the BG environment, increasing from 1.4 at the first 500 m to 3.4 at 2,000 m.

Figure 4.9. Density distributions of the ratio [MVK+MACR+ISOPOOH]/[isoprene], at the altitude layers (a) 1,500 - 2,000 m, (b) 1,000 - 1,500 m, (c) 500 - 1,000 m and (d) 0 - 500 m. The Kernel analysis was carried out considering the classification for background (BG), aged smoke (AP), and fresh smoke plumes (FP). The number of samples and mean values for each group are depicted near the color bars.

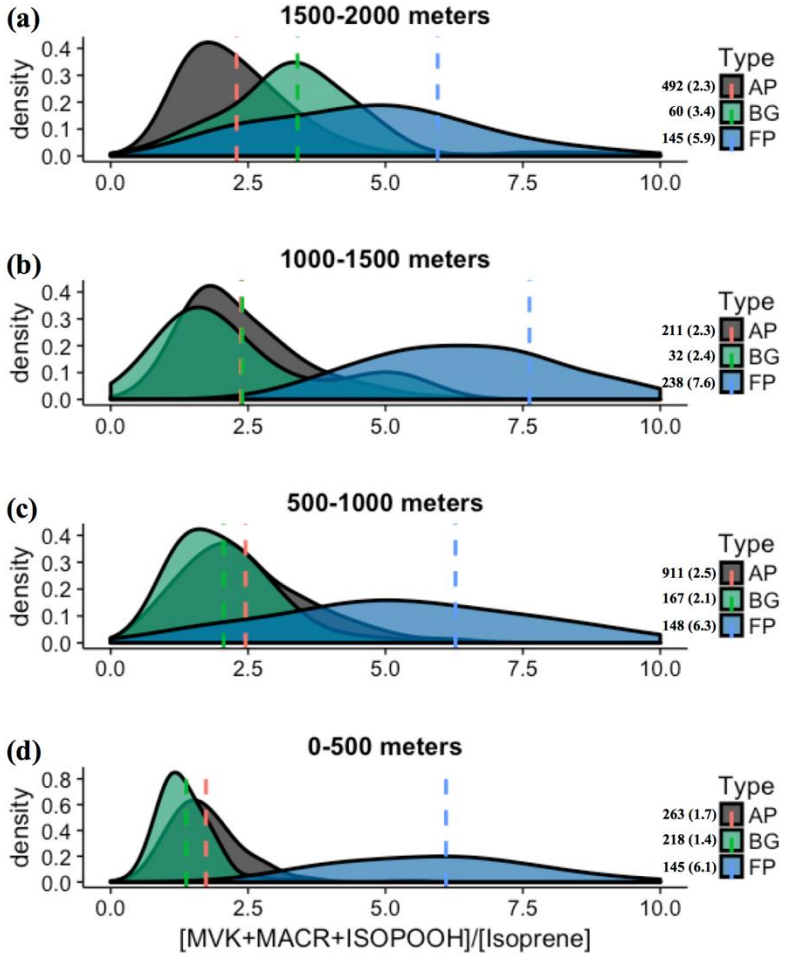

Source: Author's production.

4.2.4. OH estimated using the sequential reaction approach

The abundance of OH in the atmosphere is determined by a balance of its production and loss. Due to the absence of OH measurements during SAMBBA, we inferred the OH concentrations using a sequential reaction model with the observed profiles of the [MVK+MACR+ISOPOOH]/[Isoprene] ratio. Table 4.2 presents the average values of estimated OH concentration in the PBL and CL for the sequential reaction model approaches of Karl et al. (2007) and the modified approach proposed in this study. In FP, the estimated OH concentration reached the highest value within the PBL (1.4×10^{-6} molecules cm^{-3}), when compared with AP or even for the BG environment, both with OH concentration ~0.1×10^{-6} molecules cm^{-3}. The photochemical environment in young biomass burning plumes differs considerably from the clean conditions, especially near the surface. Hobbs et al. (2003) found OH concentrations of about 1×10^{-7} molecules cm^{-3} for a fresh plume from a savanna fire in South Africa, a value higher than found in our estimation. In CL, the estimated OH in FP reduced to 15% relative to the BG (0.5×10^{-6} molecules cm^{-3}) environment, in contrast to the increased pattern in AP (0.3×10^{-6} molecules cm^{-3}).

Figure 4.10 shows the vertical profile of estimated OH concentration in different chemical regimes, comparing the sequential reaction model according to the original approach of Karl et al. (2007) with the new approach used in this work. Throughout the entire altitude range (0 – 2,000 m), the difference in OH calculation between the two methods was approximately 2 orders of magnitude, although presenting a similar pattern in the different chemical regimes. Flight tracks classified as BG tend to increase the OH concentration along the altitude, with the inflection point occurring before the 1,000 m. Differing from BG environments, FP present a decreasing OH concentration above 1,000 m of altitude, with the AP in an intermediate state. In the flights tracks classified as BG, we observed the widest variation in the average OH concentration using the revised sequential reaction model (Figure 4.10, on bottom), especially in upper levels ($5 - 1 \times 10^{6}$ molecules cm^{-3}), although these results are associated with higher uncertainties due to a reduced number of samples. In all three different chemical regimes, the vertical profile of OH concentration presented an increase near to CL

(~1,000 m), in agreement with previous studies (MAULDIN et al., 1997; LANGFORD et al., 2005; KARL et al., 2007; KUHN et al., 2007).

Figure 4.10. Vertical profile of OH concentration (molecules cm^{-3}) for the different chemical regimes: background environment (BG), fresh smoke plume (FP), and aged smoke plume (AP). On top, the sequential reaction model according to the original approach of Karl et al. (2007), and on bottom, the new approach used in this work. Blues lines are the trend lines and grey interval represents the level of confidence (0.95) used.

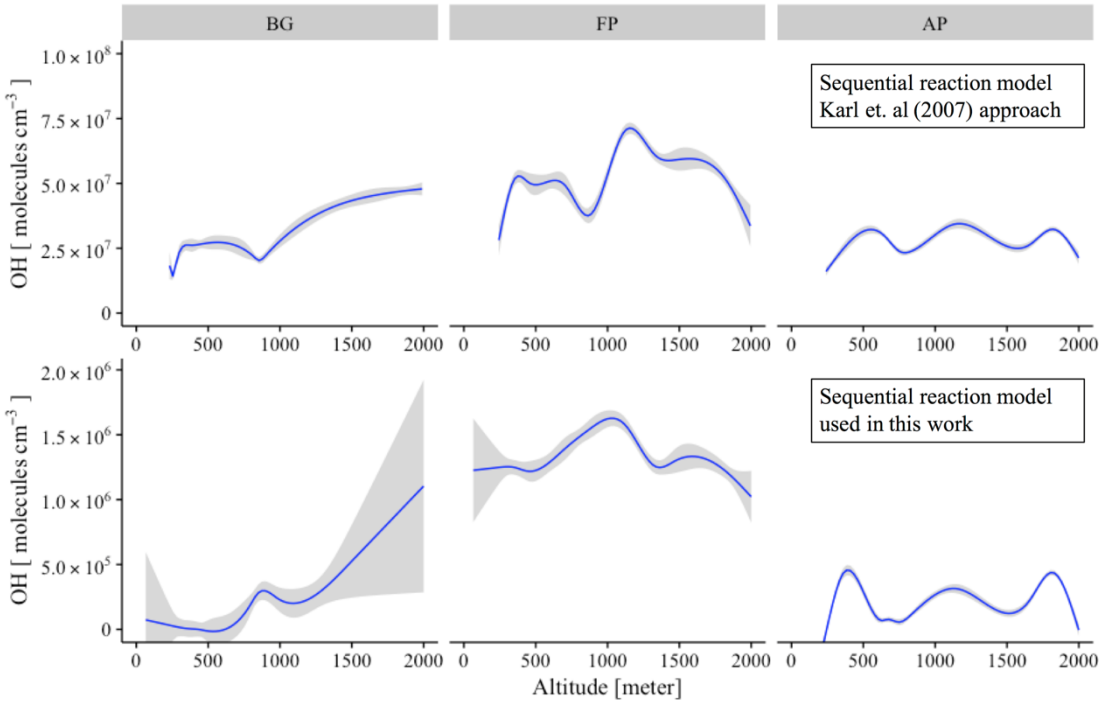

Source: Author's production.

In terms of absolute values, the estimated OH concentration values presented in this study agree within an order of magnitude with most of the observational values previously reported for Amazonia and other forest areas. For example, prediction studies conducted by Warneke et al. (2001) estimated the concentration of OH around 1-3 x 10^5 molecules cm^{-3} (24 h average), and Williams et al. (2001) found a range of 0.6-1.1 x 10^6 molecules cm^{-3} during day daytime. During the Guyanas Atmosphere-Biosphere exchange and Radicals Intensive Experiment with a Learjet (GABRIEL) experiment, the average OH concentrations in the boundary layer (<1 km) over the

Suriname rainforest in the afternoon was 4.4 x 10^6 molecules cm^{-3} (KUBISTIN et al., 2010). Dreyfus et al. (2002) reported high levels of OH concentration (3-5 x 10^6 molecules cm^{-3}) in the free troposphere over a forest area in Sierra Nevada, California.

4.3. Model coupling: BRAMS+MEGAN

In this section, we present the modeling results for isoprene and OH from the two experiments using the MEGAN model online and off-line with BRAMS during SAMBBA, as described in section 3.3.

Figure 4.11 presents the average emissions of isoprene for two settings of the BRAMS model, BRAMS-MEGAN off-line (a) and BRAMS-MEGAN online (b). BRAMS-MEGAN off-line during SAMBBA period. BRAMS-MEGAN off-line presented low values (10-150 µg m^{-2} day^{-1}) for isoprene emission in the southeast part of the Amazon basin, with the highest values (peaking 1,500 µg m^{-2} day^{-1}) in the central and west part. On the other hand, simulations using BRAMS-MEGAN online showed low levels of isoprene emissions when compared with off-line configuration, typically ranging from 10 – 300 µg m^{-2} day^{-1}. The BRAMS-MEGAN online results are comparable with the most recent isoprene emission estimates from aircraft eddy covariance measurements over the Amazonian forest (GU et al., 2017), close to 200 mg m^{-2} day^{-1}. Some discrepancy in the results can be related with the assumption that grid domain has the same PFT (broadleaf evergreen tropical tree) in the settings of BRAMS-MEGAN online, impacting in the results of southeast part of Amazon basin.

Figure 4.12 show the time series of isoprene mixing ratio in the first model layer (~40 m de altitude) between 14 September and 03 October 2012. The isoprene from BRAMS-MEGAN online has a diurnal cycle varying from 1 to 10 ppbv, which is the same order of magnitude of the isoprene levels measured at the K-34 tower and reported in previous studies (KARL et al., 2007; KUHN et al., 2007; YÁÑEZ-SERRANO et al., 2015). On the other hand, BRAMS-MEGAN off-line tends to overestimate the isoprene mixing ratio near the top of the canopy. Moreover, the overestimation of the isoprene as predicted by BRAMS-MEGAN off-line occurs not only during the daytime. The lower

values of isoprene mixing ratio during the nighttime are around 10 ppbv, which is up to five times higher than the values typically observed in Amazonia during this time of the year (YÁÑEZ-SERRANO et al., 2015). Therefore, the results of the coupled model are improved not only regarding the mean daily values of isoprene mixing ratio but also regarding the diurnal cycle, ranging from 3 to 12 ppbv during the daytime and 0.5 to 3 ppbv during the nighttime.

Figure 4.11. Average isoprene emissions rate from the model simulations during the SAMBBA period from 14 September to 03 October 2012: (a) Off-line BRAMS-MEGAN and (b) Online BRAMS-MEGAN.

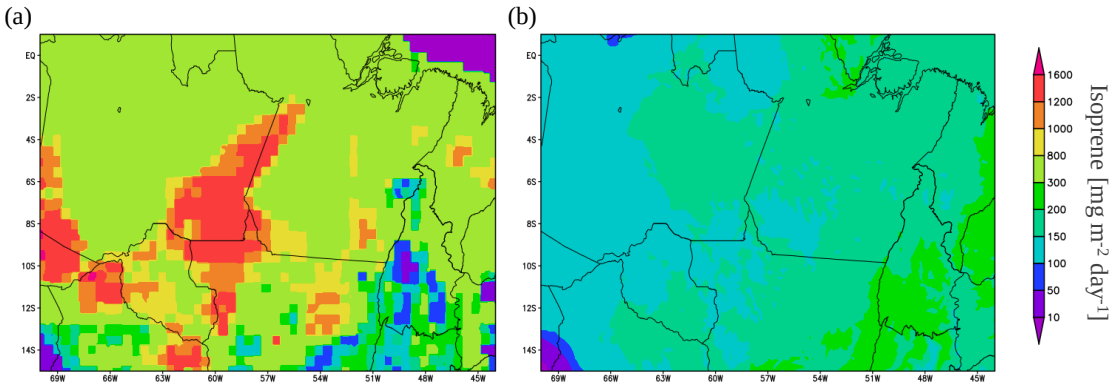

Source: Author's production.

Figure 4.13 represents the mean diurnal cycle of isoprene mixing ratio at the first model layer from the two model simulations during SAMBBA at the K-34 tower. In average, the isoprene mixing ratio from the off-line model peaks 20 ppbv around 12 UTC (9:00 local time). In addition, the off-line model results are offset for about 3 hours compared to the online model results. Previous measurements in Amazonia towers showed that the isoprene tend to peak around 2 – 8 ppbv between 13-17 local time, depending on the dry or wet season (KARL et al., 2007; KUHN et al., 2007; YÁÑEZ-SERRANO et al., 2015). Therefore, the online model also corrects the diurnal cycle of the isoprene mixing ratio at the top of the canopy.

Figure 4.12. Time series of the isoprene mixing ration (ppbv) from the numerical simulations during SAMBBA field campaign in the tower K-34 site at the first model vertical layer. Black line represents BRAMS-MEGAN off-line and green lines BRAMS-MEGAN coupled online.

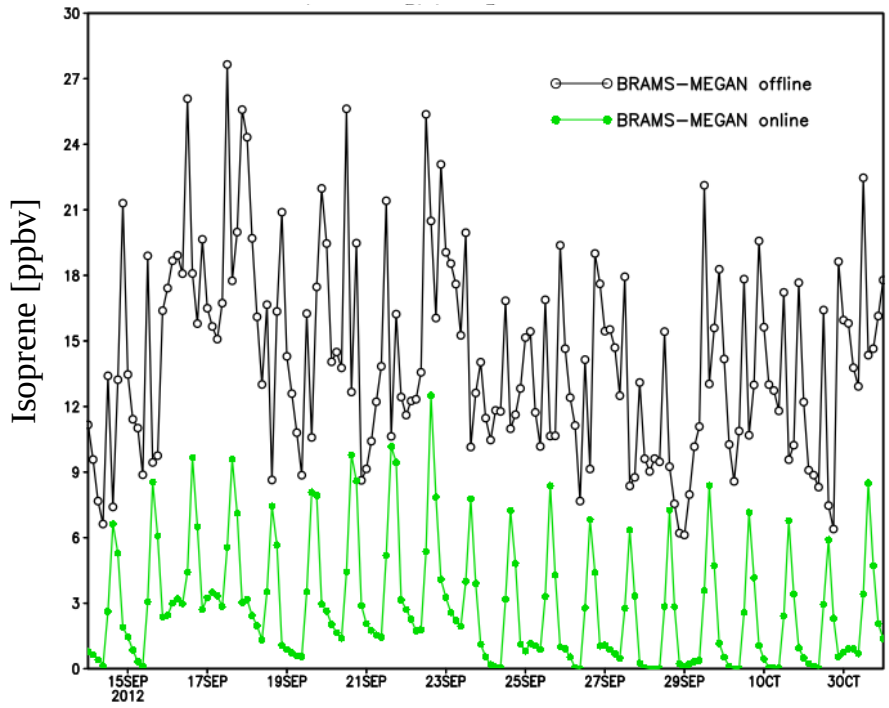

Source: Author's production.

Figure 4.13. Mean diurnal cycle of isoprene mixing ratio from the model simulations at the K-34 tower during the SAMBBA period from 14 September to 03 October 2012.

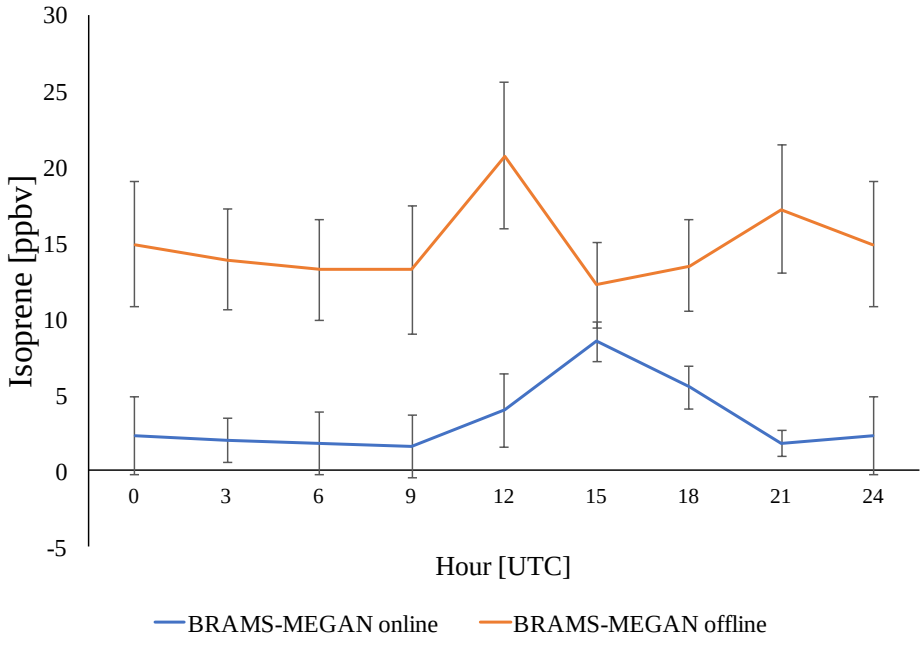

Source: Author's production.

The isoprene emission depends of several factors, such as LAI, solar radiation, temperature, moisture, CO_2, and source type (Plant Functional Type and the corresponding Emission Factor). To assess the factors that influence the isoprene concentration patterns near the surface, we opted for the Pearson correlation analysis for each version of the numerical model BRAMS. Table 4.3 shows the main factors that drive the isoprene emissions in MEGAN model. For light dependent emissions, MEGAN includes a light response that is based on electron transport (Guenther et al., 1991), a temperature response based on enzymatic activity (Guenther et al., 1991), and an inhibition response for CO_2 based on changes in metabolite pools, enzyme activity, and gene expression (Wilkinson et al., 2009). As expected, the isoprene from the simulation of the BRAMS-MEGAN online presented a high correlation with the short-wave radiation (0.95), surface temperature (0.62), and, a negative correlation with CO_2.

On the other hand, the isoprene from the BRAMS-MEGAN off-line does not respond to the MEGAN dependence basic formulation of isoprene emissions with the aforementioned variables (Table 4.3) and therefore constitutes a limitation.

Table 4.3. Pearson correlation coefficient before and after BRAMS-MEGAN coupling.

Isoprene	**Pearson correlation coefficient**		
	CO_2	**Surface temperature**	**Short-wave radiation**
BRAMS-MEGAN off-line	0.37	-0.34	-0,16
BRMAS-MEGAN online	-0.42	0.62	0.95

Even near the surface, the isoprene concentration depends not only on the isoprene emissions, several other chemical compounds and the air masses transport can also alter its concentration. With the aim to investigate the impact of polluted areas surrounding forest areas in Amazon basin, also sought to compare pristine regions with those

impacted by anthropogenic emissions, either by burning sources or by urban emissions. Figure 4.14 presents the number of fires detected from MODIS onboard AQUA during SAMBBA field campaign. We selected two sectors (1 and 2) located, respectively, in clean and polluted areas to assess the impact of biomass burning emission on isoprene levels. Important to note that both sectors have the isoprene emissions ranging between 100 and 150 µg $m^{-3}h^{-1}$ in the online model setting. On contrast, the emissions for the off-line model are typically around 300 µg $m^{-3}h^{-1}$ in sector 1, and ranging between 300 and 1,500 µg $m^{-3}h^{-1}$ in sector 2. So, when comparing the isoprene concentrations in these two sectors, must keep in mind that the differences are not only related with biomass burning emissions but also with the differences in terms of model representation of the biogenic emissions itself. In fact, the time series of isoprene mixing ratios in sectors 1 and 2, according to the online and off-line models, reflect these differences (Figure 4.15). The off-line model in polluted region resulted in values for isoprene mixing ration near surface about twice higher than in clean region, which was already overestimated. On the other side, the online resulted on value for the isoprene mixing ratio in sector 1 only slightly above the values in sector 2 on specific days. The results of the online model are consistent with the magnitude of the isoprene mixing ratios observed during SAMBBA and previous studies.

Figure 4.14. Selected sectors based on number of fires detected from MODIS onboard AQUA during SAMBBA campaign in 2012.

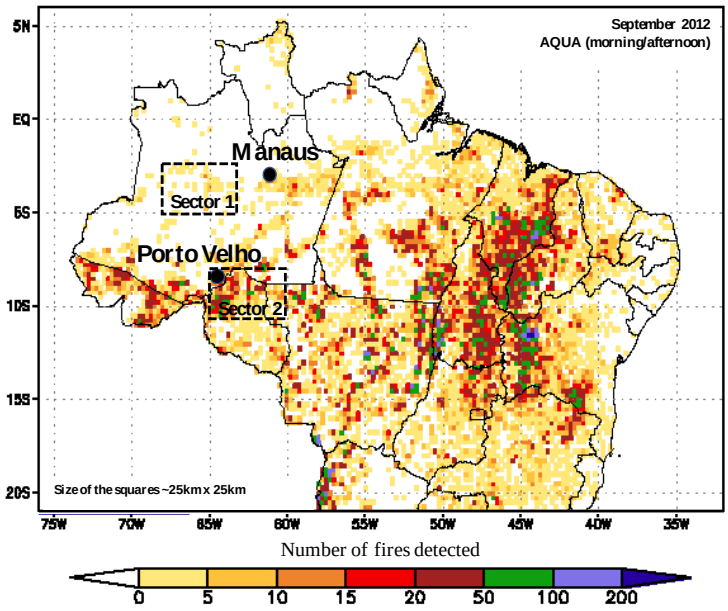

Source: Adapted from https://queimadas.dgi.inpe.br/. Accessed on 05 April 2017

Figure 4.15. Time series of the isoprene mixing ratio from the numerical simulations during SAMBBA field campaign in clean and polluted area (see Figure 4.14) at the first model vertical layer.

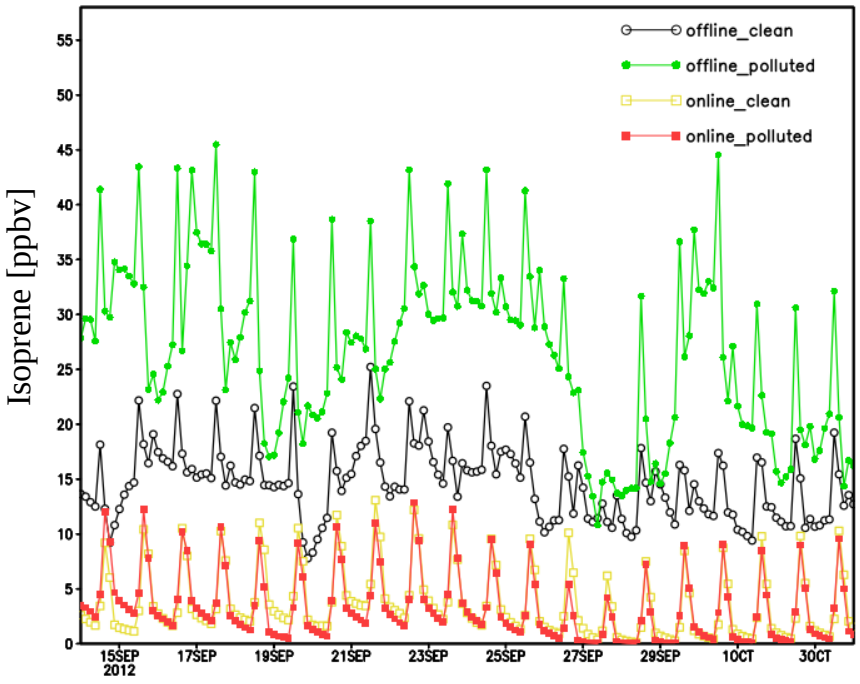

Source: Author's production.

Figure 4.16. Vertical profile of the isoprene mixing ration from the numerical simulations during SAMBBA field campaign in clean and polluted area (see Figure 4.14).

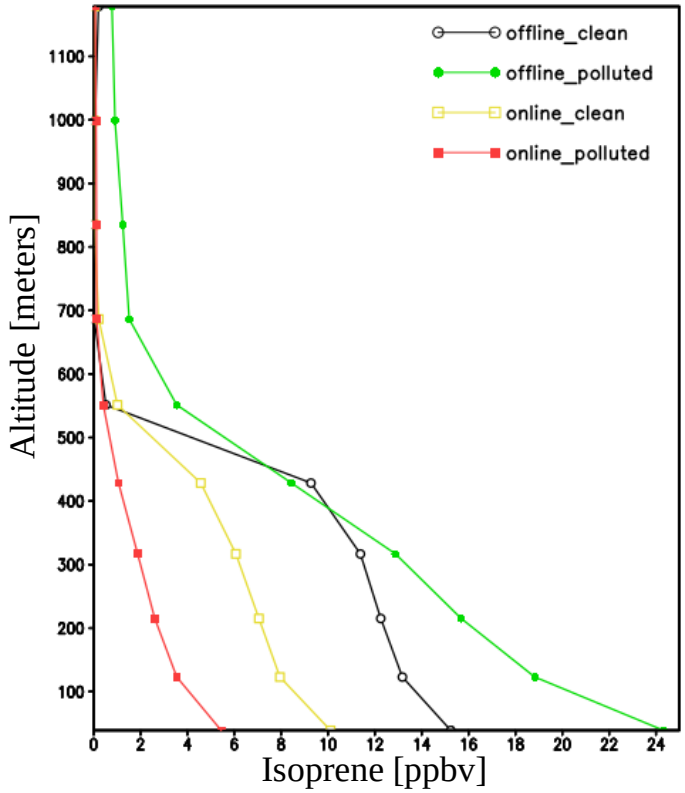

Source: Author's production.

Figure 4.17 show the time series of OH mixing ratio in the first model layer (~40 m de altitude) between 14 September and 03 October 2012. In general, BRAMS-MEGAN online presented higher values for OH than BRAMS-MEGAN off-line during the SAMBBA field campaign. This pattern was evident during the last days, 28 September to 4 October, with a difference of up to one order of magnitude. BRAMS-MEGAN off-line presented values of OH close those estimated in fresh smoke plumes (1.5×10^6 molecules cm^{-3}) and higher than aged smoke plumes (5×10^5 molecules cm^{-3}) in SAMBBA.

Figure 4.17. Time series of the OH mixing ratio from the numerical simulations during SAMBBA field campaign in clean and polluted area (see Figure 4.14) at the first model vertical layer.

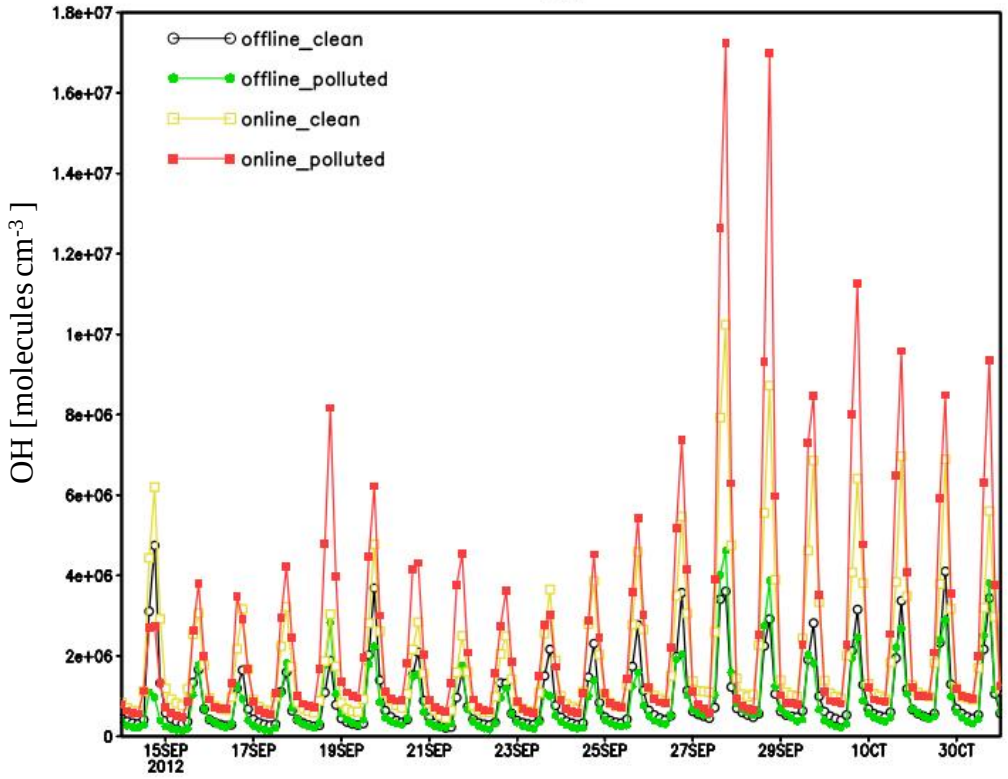

Figure 4.18 shows the OH vertical profile up to 1200 m altitude for BRAMS-MEGAN online and offline configurations. BRAMS-MEGAN online showed high values along the vertical profile when compared to BRAMS-MEGAN off-line, achieving an OH concentration of ~3 x 10^7 molecules cm^{-3} at 1,200 m of altitude.

This observed increase in OH near to 1,100 – 1,200 meters of altitude, both in the online and offline model, was also detected in the OH estimated in a fresh smoke plume and clean area environment. In all three different chemical regimes, the vertical profile of estimated OH also presented an increase near to the cloud layer, in agreement with model results and previous studies (MAULDIN et al., 1997; LANGFORD et al., 2005; KARL et al., 2007; KUHN et al., 2007).

Figure 4.18. Vertical profile of the OH mixing ratio from the numerical simulations during SAMBBA field campaign in clean and polluted area (see Figure 4.14).

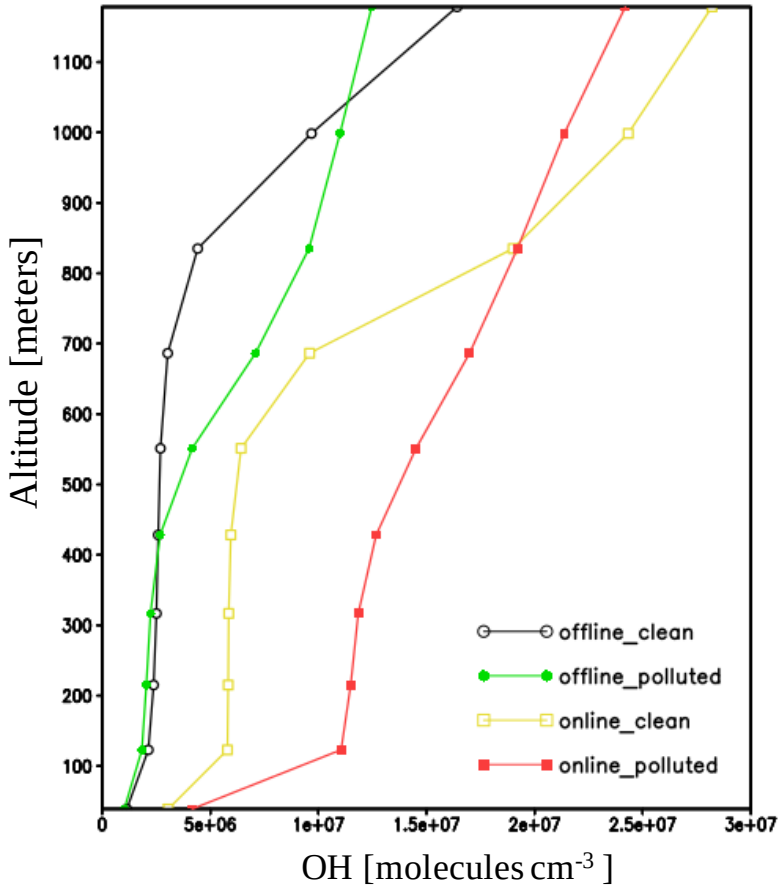

5 CONCLUSIONS

We present a concise chemical characterization of the atmosphere of Brazilian Amazonia during the SAMBBA airborne experiment from 14th September to 3rd October 2012, comprising the transition period from the dry to wet season. The flights were carried out in remote areas, as well as areas under the influence of biomass burning that commonly occurs in the region. The flight classification method adopted in this study prioritized the chemical classification, using CO mixing ratios and the enhancement ratio of O_3 to CO to categorize different flight tracks to include BG flights, and FP and AP flights.

Measurements of CO, NO_x, and O_3 performed in areas not directly affected by local fire emissions reveals the signature of biomass burning in the chemical composition of the background of the Amazonian atmosphere, due to long-range transport of biomass burning tracers both from Africa and the eastern part of Amazonia. The CO and O_3 mixing ratios exceeded the background values reported in other studies. Satellite-derived data, however, indicate there was a significant inflow of smoke tracer from Africa. Corroborating previous studies (AZEVEDO et al., 2010; LANGFORD et al., 2010; SRIVASTAVA; NAJA; THOURET, 2015), we found evidence of long-range transport events of O_3 during SAMBBA experiment, considering the high levels of O_3 in aged plumes at high altitudes (5,500 – 6,500 m), and the AIRS detection of an O_3 inflow in the Amazon basin from Africa. These findings support the hypothesis that the long-range transport events can be an important source of O_3 into the troposphere in the Amazon basin, which could even alter the atmospheric composition within the planetary boundary layer. We also emphasize the importance of further studies about the long-range ozone transport in the southern hemisphere, focusing on long-term records of vertical ozone profile to reduce the uncertainty especially related with seasonality and representativeness of the SAMBBA measurements.

In our analysis, we highlight the importance of photochemical age in areas influenced by biomass burning emission, with distinct results for FP and AP. Fresh smoke plumes had the highest mixing ratios of CO and NO_x, showing up the strength of vertical

transport through the detection of biomass burning products in upper levels (> 1,200 m). In AP, we detected up to 80 ppbv of O_3 at 1,300 m altitude, showing the O_3 levels in the transition from a remote site impacted by fresh smoke plumes to an urban site in Palmas-TO.

Regarding isoprene, we showed that there is an indication of the heat released from vegetation fires affecting the nearby plants which consequently also significantly increases amount of isoprene released to the atmosphere especially in AP environment. In contrast with BG condition (1.5 ppbv), the isoprene mixing ratio in AP was 2.4 ppbv in the free troposphere, followed by 1.6 ppbv in FP. The FP also presented a higher [MVK+MACR+ISOPOOH]/[isoprene] ratio (7.0), when compared with both AP (2.3) and BG (1.7), indicating a strong oxidation process within the boundary layer. Improving the simplified sequential reaction model used by Karl et al. (2007), we indirectly calculated the OH concentration in different chemical regimes and the results are comparable with observations. The highest value for OH in FP within the PBL (1.4 x 10^{-6} molecules cm^{-3}) corroborate the results from [MVK+MACR+ISOPOOH]/[isoprene] ratio, confirming that the photochemical environment in young biomass burning plumes differs considerably from background conditions. We also detected the strong signal in the oxidative capacity at higher levels (~1,000 m), characteristic of the cloud layer existence, as reported by others studies (MAULDIN et al., 1997; KARL et al., 2007).

Looking for a synergistic analysis between observations and numerical modeling, a coupling of the MEGAN model was developed in the numerical model BRAMS. The coupled model was able to reproduce the typical diurnal concentrations of isoprene on the surface, including corrections in the period of emission. Improvements were also observed in the isoprene concentrations at night, with values close to those obtained in recent observation studies in the Amazonian basin. Corroborating the improvement in the isoprene simulation, BRAMS-MEGAN online presented the expected correlation with the short-wave radiation, surface temperature, and a negative correlation with CO_2 during SAMBBA field campaign. Although the new version of the BRAMS model performed well in the simulations of the isoprene concentration, the model did not agree

with the estimated and observed results for OH. More tests are needed to investigate the possible causes of disagreement between the model result and the observations and estimates presented here. However, the results of the model also showed the influence of the cloud layer on increasing the oxidative capacity, as predicted in the estimated OH calculations.

In this thesis, we observed an improvement in the estimated OH concentration values using the modified sequential reaction model described in the section 3.1.4, for both biomass burning regimes and background environment. Both methods, column and plume approach, are useful to estimate the OH and some discrepancies may be associated with uncertainties in dynamic factors in the simplified analytical expression, such as vertical and horizontal transport, convective velocity above different vegetation cover, as well as the radiation regime influenced by clouds at high altitudes which are likely to affect the OH concentrations. We also assessed the impact of the model improvement in isoprene concentration and OH modeled, with a reasonable agreement for isoprene concentration and more investigation needed for the OH simulation.

The findings corroborate the influence of biomass burning activity not only on direct emissions of particulate matter, but also in the oxidative capacity to produce secondary organic aerosol through the gas-particle conversion that occurs in the atmosphere. The author highlights the potential use of the research results to improve the numerical model simulation with a better representativeness of the chemistry processes, which can impact on the global climate prediction.

For future studies, we recommend further investigation of the impact of the dynamic factors, such as horizontal transport, convective velocity above different vegetation cover, in the estimation of OH mixing ratios, as well as the effect of the radiation regime influenced by clouds at high altitudes altering photolysis rates. Considering the recent updates in the oxidative capacity of the atmosphere, we also expect a reduction in the uncertainties associated with the OH concentrations.

REFERENCES

AGHEDO, A. M.; SCHULTZ, M. G.; RAST, S. The influence of African air pollution on regional and global tropospheric ozone. **Atmospheric Chemistry and Physics**, v. 7, p. 1193–1212, 1 jan. 2007.

ALONSO, M. F.; LONGO, K. M.; FREITAS, S. R.; MELLO DA FONSECA, R.; MARÉCAL, V.; PIRRE, M.; KLENNER, L. G. An urban emissions inventory for South America and its application in numerical modeling of atmospheric chemical composition at local and regional scales. **Atmospheric Environment**, v. 44, n. 39, p. 5072–5083, 2010.

ANDREAE, M. O.; ANDERSON, B. E.; BLAKE, D. R.; BRADSHAW, J. D.; COLLINS, J. E.; GREGORY, G. L.; SACHSE, G. W.; SHIPHAM, M. C. Influence of Plumes from Biomass Burning on Atmospheric Chemistry over the Equatorial and Tropical South-Atlantic during Cite-3. **Journal of Geophysical Research-Atmospheres**, v. 99, n. D6, p. 12793–12808, 1994a.

ANDREAE, M. O.; ANDERSON, B. E.; BLAKE, D. R.; BRADSHAW, J. D.; COLLINS, J. E.; GREGORY, G. L.; SACHSE, G. W.; SHIPHAM, M. C. Influence of plumes from biomass burning on atmospheric chemistry over the equatorial and tropical South Atlantic during CITE 3. **Journal of Geophysical Research**, v. 99, n. 94, p. 0–1, 1994b.

ANDREAE, M. O.; ARTAXO, P.; BECK, V.; BELA, M.; FREITAS, S.; GERBIG, C.; LONGO, K.; MUNGER, J. W.; WIEDEMANN, K. T.; WOFSY, S. C. Carbon monoxide and related trace gases and aerosols over the Amazon Basin during the wet and dry seasons. **Atmospheric Chemistry and Physics**, v. 12, n. 13, p. 6041–6065, 2012.

ANDREAE, M. O.; GARSTANG, M.; GREGORY, G. L.; HARRISS, R. C.; PEREIRA, M. C.; SACHSE, G. W.; SETZER, A. W.; TALBOT, R. W.; TORRES, A. L.; WOFSY, S. C. Biomass-Burning Emissions and Associated Haze Layers Over Amazonia. **Journal of Geophysical Research**, v. 93, p. 1509–1527, 1988.

ARNETH, A.; SCHURGERS, G.; LATHIERE, J.; DUHL, T.; BEERLING, D. J.; HEWITT, C. N.; MARTIN, M.; GUENTHER, A. Global terrestrial isoprene emission models: Sensitivity to variability in climate and vegetation. **Atmospheric Chemistry and Physics**, v. 11, n. 15, 2011.

ARTAXO, P.; RIZZO, L. V; BRITO, J. F.; BARBOSA, H. M. J.; ARANA, A.; SENA, E. T.; CIRINO, G. G.; BASTOS, W.; MARTIN, S. T.; ANDREAE, M. O. Atmospheric aerosols in Amazonia and land use change: from natural biogenic to biomass burning conditions. **Faraday Discussions**, v. 165, p. 203–235, 2013.

AUMANN, H. H.; MILLER, C. C. R. C. Atmospheric infrared sounder (AIRS) on the

Earth Observing System. In: SATELLITE REMOTE SENSING II, 15 dez. 1995, **Anais...** SPIE, 15 dez. 1995Disponível em: <http://proceedings.spiedigitallibrary.org/proceeding.aspx?articleid=1008572%5Cnhttp://link.aip.org/link/?PSISDG/2583/332/1>

AZEVEDO, J. M.; GON?ALVES, F. L. T.; DE F?TIMA ANDRADE, M.; GONÇALVES, F. L. T.; DE FÁTIMA ANDRADE, M. Long-range ozone transport and its impact on respiratory and cardiovascular health in the north of Portugal. **International Journal of Biometeorology**, v. 55, n. 2, p. 187–202, 1 jul. 2010.

BARKET, D. J.; GROSSENBACHER, J. W.; HURST, J. M.; SHEPSON, P. B.; OLSZYNA, K.; THORNBERRY, T.; CARROLL, M. A.; ROBERTS, J.; STROUD, C.; BOTTENHEIM, J.; BIESENTHAL, T. A study of the NOx dependence of isoprene oxidation. **Journal of Geophysical Research D: Atmospheres**, v. 109, n. 11, 2004.

BARKLEY, M. P.; PALMER, P. I.; GANZEVELD, L.; ARNETH, A.; HAGBERG, D.; KARL, T.; GUENTHER, A.; PAULOT, F.; WENNBERG, P. O.; MAO, J.; KUROSU, T. P.; CHANCE, K.; MÜLLER, J. F.; DE SMEDT, I.; VAN ROOZENDAEL, M.; CHEN, D.; WANG, Y.; YANTOSCA, R. M.; GREGORY, G. L.; HARRISS, R. C.; TALBOT, R. W.; BROWELL, E. V.; BECK, S. M.; SEBACHER, D. I.; RASMUSSEN, R. A.; GARSTANG, M.; ANDREAE, M. O.; HINTON, R. R. Air chemistry over the tropical forest of Guyana. **Journal of Geophysical Research**, v. 91, n. D8, p. 8603–8612, 1 jan. 1986.

BELA, M. M.; LONGO, K. M.; FREITAS, S. R.; MOREIRA, D. S.; BECK, V.; WOFSY, S. C.; GERBIG, C.; WIEDEMANN, K.; ANDREAE, M. O.; ARTAXO, P. Ozone production and transport over the Amazon Basin during the dry-to-wet and wet-to-dry transition seasons. **Atmospheric Chemistry and Physics**, v. 14, n. 2, p. 757–782, 1 jan. 2014.

BELL, M.; ELLIS, H. Sensitivity analysis of tropospheric ozone to modified biogenic emissions for the Mid-Atlantic region. **Atmospheric Environment**, v. 38, n. 13, p. 1879–1889, 2004.

BERTSCHI, I.; HAO, W. M.; WARD, D. E.; YOKELSON, R. J.; GOODE, J. G.; BABBITT, R. E.; SUSOTT, R. A.; APEL, E. C. Measurement and interpretation of isoprene fluxes and isoprene, methacrolein, and methyl vinyl ketone mixing ratios at the PROPHET site during the 1998 Intensive. **Journal of Geophysical Research**, v. 107, n. D3, p. 1–15, 1 jan. 2002.

BERTSCHI, I. T.; JAFFE, D. A.; JAEGLÉ, L.; PRICE, H. U.; DENNISON, J. B. PHOBEA/ITCT 2002 airborne observations of transpacific transport of ozone, CO, volatile organic compounds, and aerosols to the northeast Pacific: Impacts of Asian anthropogenic and Siberian boreal fire emissions. **Journal of Geophysical Research D: Atmospheres**, v. 109, n. 23, p. 1–16, 2004.

BERTSCHI, I.; YOKELSON, R. J.; WARD, D. E.; BABBITT, R. E.; SUSOTT, R. A.; GOODE, J. G.; HAO, W. M. Trace gas and particle emissions from fires in large

diameter and belowground biomass fuels. **Journal of Geophysical Research-Atmospheres**, v. 108, n. D13, p. 8472, 2003.

BLAKE, N. J.; BLAKE, D. R.; SIVE, B. C.; CHEN, T.-Y.; ROWLAND, F. S.; COLLINS JR., J. E.; SACHSE, G. W.; ANDERSON, B. E.; COLLINS, J. E.; SACHSE, G. W.; ANDERSON, B. E. Biomass burning emissions and vertical distribution of atmospheric methyl halides and other reduced carbon gases in the South Atlantic region. **Journal of Geophysical Research**, v. 101, n. D19, p. 24151, 1 out. 1996.

BONAN, G. B. Forests and climate change: forcings, feedbacks, and the climate benefits of forests. **Science**, v. 320, n. 5882, p. 1444–1449, 2008.

BOWLING, D. R.; TURNIPSEED, A. A.; DELANY, A. C.; BALDOCCHI, D. D.; GREENBERG, J. P.; MONSON, R. K. The use of relaxed eddy accumulation to measure biosphere-atmosphere exchange of isoprene and other biological trace gases. **Oecologia**, v. 116, n. 3, p. 306–315, 3 set. 1998.

BYUN, D. W.; KIM, S.; CZADER, B.; NOWAK, D.; STETSON, S.; ESTES, M. Estimation of biogenic emissions with satellite-derived land use and land cover data for air quality modeling of Houston-Galveston ozone nonattainment area. **Journal of Environmental Management**, v. 75, n. 4, p. 285–301, 1 jun. 2005.

CARVALHO, L. R. F.; VASCONCELLOS, P. C.; MANTOVANI, W.; POOL, C. S.; PISANI, S. O. Measurements of biogenic hydrocarbons and carbonyl compounds emitted by trees from temperate warm Atlantic rainforest, Brazil. **Journal of environmental monitoring : JEM**, v. 7, n. 5, p. 493–499, 2005.

CICCIOLI, P.; CENTRITTO, M.; LORETO, F. Biogenic volatile organic compound emissions from vegetation fires. **Plant Cell Environ**, v. 37, n. 8, p. 1810–1825, 1 abr. 2014.

COTTON, W. R.; PIELKE SR., R. A.; WALKO, R. L.; LISTON, G. E.; TREMBACK, C. J.; JIANG, H.; MCANELLY, R. L.; HARRINGTON, J. Y.; NICHOLLS, M. E.; CARRIO, G. G.; MCFADDEN, J. P. RAMS 2001: Current status and future directions. **Meteorology and Atmospheric Physics**, v. 82, n. 1–4, p. 5–29, 2003.

CRASSIER, V.; SUHRE, K.; TULET, P.; ROSSET, R. Development of a reduced chemical scheme for use in mesoscale meteorological models. **Atmospheric Environment**, v. 34, n. 16, p. 2633–2644, jan. 2000.

CRUTZEN, P. J.; DELANY, A. C.; GREENBERG, J.; HAAGENSON, P.; HEIDT, L.; LUEB, R.; POLLOCK, W.; SEILER, W.; WARTBURG, A.; ZIMMERMAN, P. Tropospheric Chemical-Composition Measurements in Brazil During the Dry Season. **Journal of Atmospheric Chemistry**, v. 2, n. 3, p. 233–256, 1985.

CURCI, G.; BEEKMANN, M.; VAUTARD, R.; SMIATEK, G.; STEINBRECHER, R.; THELOKE, J.; FRIEDRICH, R. Modelling study of the impact of isoprene and terpene biogenic emissions on European ozone levels. **Atmospheric Environment**, v. 43, n. 7, p. 1444–1455, 2009.

DAMIAN, V., SANDU, A., DAMIAN, M., CARMICHAEL, G. R., AND POTRA, F. A.; F A DAMIAN, V. S. A. D. M. C. G. R. AND P. KPP – A symbolic preprocessor for chemistry kinetics – User's guide. **Technical report**, v. IA52246, 1 jan. 1995.

DARBYSHIRE, E.; JOHNSON, B. **The SAMBBA campaign :** a summary of research flights. 2012.

DE FREITAS, E. D.; MARTINS, L. D.; DA SILVA DIAS, P. L.; DE F??TIMA ANDRADE, M. A simple photochemical module implemented in RAMS for tropospheric ozone concentration forecast in the metropolitan area of S??o Paulo, Brazil: Coupling and validation. **Atmospheric Environment**, v. 39, n. 34, p. 6352–6361, 2005.

DEE, D. P.; UPPALA, S. M.; SIMMONS, A. J.; BERRISFORD, P.; POLI, P.; KOBAYASHI, S.; ANDRAE, U.; BALMASEDA, M. A.; BALSAMO, G.; BAUER, P.; BECHTOLD, P.; M BELJAARS, A. C.; VAN DE BERG, L.; BIDLOT, J.; BORMANN, N.; DELSOL, C.; DRAGANI, R.; FUENTES, M.; GEER, A. J.; HAIMBERGER, L.; HEALY, S. B.; HERSBACH, H.; OLM, E. V; ISAKSEN, L.; KÅLLBERG, P.; KÖHLER, M.; MATRICARDI, M.; MCNALLY, A. P.; MONGE-SANZ, B. M.; MORCRETTE, J.; PARK, B.; PEUBEY, C.; DE ROSNAY, P.; TAVOLATO, C.; THÉPAUT, J.; VITART, F.; ACM, B.; DE BERG, VAN L.; J-J, M.; B-K, P.; ROSNAY, DE P.; BELJAARS, A. C. M.; VAN DE BERG, L.; BIDLOT, J.; BORMANN, N.; DELSOL, C.; DRAGANI, R.; FUENTES, M.; GEER, A. J.; HAIMBERGER, L.; et al. The ERA-Interim reanalysis: configuration and performance of the data assimilation system. **Quarterly Journal of the Royal Meteorological Society**, v. 137, n. 656, p. 553–597, 28 abr. 2011.

DJOUAD, R.; SPORTISSE, B.; AUDIFFREN, N. Numerical simulation of aqueous-phase atmospheric models: use of a non-autonomous Rosenbrock method. **Atmospheric Environment**, v. 36, n. 5, p. 873–879, 2002.

DREYFUS, G. B.; SCHADE, G. W.; GOLDSTEIN, A. H. Observational constraints on the contribution of isoprene oxidation to ozone production on the western slope of the Sierra Nevada, California. **Journal of Geophysical Research Atmospheres**, v. 107, n. 19, p. 1–17, 2002.

ELSHORBANY, Y. F.; KURTENBACH, R.; WIESEN, P.; LISSI, E.; RUBIO, M.; VILLENA, G.; GRAMSCH, E.; RICKARD, A. R.; PILLING, M. J.; KLEFFMANN, J. Oxidation capacity of the city air of Santiago, Chile. n. 3, p. 2257–2273, 2009.

FAST, J. D.; GUSTAFSON, W. I.; EASTER, R. C.; ZAVERI, R. A.; BARNARD, J. C.; CHAPMAN, E. G.; GRELL, G. A.; PECKHAM, S. E. Evolution of ozone, particulates, and aerosol direct radiative forcing in the vicinity of Houston using a fully coupled meteorology-chemistry-aerosol model. **Journal of Geophysical Research Atmospheres**, v. 111, n. 21, 2006.

FELDMAN, M. S.; HOWARD, T.; MCDONALD-BULLER, E.; MULLINS, G.; ALLEN, D. T.; HANSEL, A.; WISTHALER, A. Applications of satellite remote

sensing data for estimating biogenic emissions in southeastern Texas. **Atmospheric Environment**, v. 44, n. 7, p. 917–929, 2010.

FREITAS, E. D.; ROZOFF, C. M.; COTTON, W. R.; SILVA DIAS, P. L.; DIAS, P. L. S. Interactions of an urban heat island and sea-breeze circulations during winter over the metropolitan area of São Paulo, Brazil. **Boundary-Layer Meteorology**, v. 122, n. 1, p. 43–65, 21 out. 2006.

FREITAS, S.; GEVAERD, R. Estimativa operacional da umidade do solo para iniciação de modelos de previsão numérica da atmosfera. parte i: descrição da metodologia e validação. **Revista Brasileira de Meteorologia**, 2006.

FREITAS, S. R.; LONGO, K. M.; ALONSO, M. F.; PIRRE, M.; MARECAL, V.; GRELL, G.; STOCKLER, R.; MELLO, R. F.; SÁNCHEZ GÁCITA, M. PREP-CHEM-SRC - 1.0: A preprocessor of trace gas and aerosol emission fields for regional and global atmospheric chemistry models. **Geoscientific Model Development**, v. 4, n. 2, p. 419–433, 2011.

FREITAS, S. R.; LONGO, K. M.; ANDREAE, M. O. Impact of including the plume rise of vegetation fires in numerical simulations of associated atmospheric pollutants. **Geophysical Research Letters**, v. 33, n. 17, p. 951–955, 1 jan. 2006.

FREITAS, S. R.; LONGO, K. M.; CHATFIELD, R.; LATHAM, D.; DIAS, M. A. F. S.; ANDREAE, M. O.; PRINS, E.; UNESP, F. E. G. and Physics Including the sub-grid scale plume rise of vegetation fires in low resolution atmospheric transport models. p. 3385–3398, 2007.

FREITAS, S. R.; LONGO, K. M.; SILVA DIAS, M. A. F.; CHATFIELD, R.; SILVA DIAS, P.; ARTAXO, P.; ANDREAE, M. O.; GRELL, G.; RODRIGUES, L. F.; FAZENDA, A.; PANETTA, J. The Coupled Aerosol and Tracer Transport model to the Brazilian developments on the Regional Atmospheric Modeling System (CATT-BRAMS) – Part 1: Model description and evaluation. **Atmospheric Chemistry and Physics**, v. 9, n. 8, p. 2843–2861, 2009.

FREITAS, S. R.; LONGO, K. M.; TRENTMANN, J.; LATHAM, D. Technical note: sensitivity of 1-D smoke plume rise models to the inclusion of environmental wind drag. **Atmospheric Chemistry and Physics**, v. 10, n. 2, p. 585-594, jan. 2010.

FREITAS, S. R.; PANETTA, J.; LONGO, K. M.; RODRIGUES, L. F.; MOREIRA, D. S.; ROSÁRIO, N. E.; SILVA DIAS, P. L.; SILVA DIAS, M. A. F.; SOUZA, E. P.; FREITAS, E. D.; LONGO, M.; FRASSONI, A.; FAZENDA, A. L.; SANTOS E SILVA, C. M.; PAVANI, C. A. B.; EIRAS, D.; FRANÇA, D. A.; MASSARU, D.; SILVA, F. B.; CAVALCANTE, F.; PEREIRA, G.; CAMPONOGARA, G.; FERRADA, G. A.; CAMPOS VELHO, H. F.; MENEZES, I.; FREIRE, J. L.; ALONSO, M. F.; GÁCITA, M. S.; ZARZUR, M.; FONSECA, R. M.; LIMA, R. S.; SIQUEIRA, R. A.; BRAZ, R.; TOMITA, S.; OLIVEIRA, V.; MARTINS, L. D. The Brazilian developments on the Regional Atmospheric Modeling System (BRAMS 5.2): an integrated environmental model tuned for tropical areas. **Geoscientific Model**

Development, v. 10, p. 189-222, Jan. 2017. DOI: <10.5194/gmd-10-189-2017>. Disponível em: <http://dx.doi.org/10.5194/gmd-10-189-2017>.

GENT, P. R.; DANABASOGLU, G.; DONNER, L. J.; HOLLAND, M. M.; HUNKE, E. C.; JAYNE, S. R.; LAWRENCE, D. M.; NEALE, R. B.; RASCH, P. J.; VERTENSTEIN, M.; WORLEY, P. H.; YANG, Z.-L.; ZHANG, M.; GENT, P. R.; DANABASOGLU, G.; DONNER, L. J.; HOLLAND, M. M.; HUNKE, E. C.; JAYNE, S. R.; LAWRENCE, D. M.; NEALE, R. B.; RASCH, P. J.; VERTENSTEIN, M.; WORLEY, P. H.; YANG, Z.-L.; ZHANG, M.; LAWRENCE, D. M.; GENT, P. R.; DONNER, L. J.; DANABASOGLU, G.; RASCH, P. J.; HOLLAND, M. M.; HUNKE, E. C.; JAYNE, S. R.; VERTENSTEIN, M.; YANG, Z.-L.; ZHANG, M. The Community Climate System Model Version 4. **Journal of Climate**, v. 24, n. 19, p. 4973–4991, 1 out. 2011.

GREENBERG, J. P.; GUENTHER, A. B.; PETRON, G.; WIEDINMYER, C.; VEGA, O.; GATTI, L. V.; TOTA, J.; FISCH, G. Biogenic VOC emissions from forested Amazonian landscapes. **Global Change Biology**, v. 10, n. 5, p. 651–662, maio 2004.

GREENBERG, J. P.; ZIMMERMAN, P. R. Nonmethane hydrocarbons in remote tropical, continental, and marine atmospheres. **Journal of Geophysical Research**, v. 89, n. D3, p. 4767, 1984.

GREENBERG, J. P.; ZIMMERMAN, P. R.; GREENBERG, J. P.; WESTBERG, C. E. Measurements of Atmospheric Hydrocarbons and Biogenic Emission Fluxes in the Amazon Boundary Layer Trade Wind Convective. **Journal of Geophysical Research: Atmospheres**, v. 93, n. D2, p. 1407–1416, 1 jan. 1988.

GREENSLADE, J. W.; ALEXANDER, S. P.; SCHOFIELD, R.; FISHER, J. A.; KLEKOCIUK, A. K. Stratospheric ozone intrusion events and their impacts on tropospheric ozone. **Atmospheric Chemistry and Physics Discussions**, n. January, p. 1–28, 2017.

GRELL, G. A.; PECKHAM, S. E.; SCHMITZ, R.; MCKEEN, S. A.; FROST, G.; SKAMAROCK, W. C.; EDER, B. Fully coupled "online" chemistry within the WRF model. **Atmospheric Environment**, v. 39, n. 37, p. 6957–6975, 2005.

GU, D.; GUENTHER, A. B.; SHILLING, J. E.; YU, H.; HUANG, M.; ZHAO, C.; YANG, Q.; MARTIN, S. T.; ARTAXO, P.; KIM, S.; SECO, R.; STAVRAKOU, T.; LONGO, K. M.; TÓTA, J.; DE SOUZA, R. A. F.; VEGA, O.; LIU, Y.; SHRIVASTAVA, M.; ALVES, E. G.; SANTOS, F. C.; LENG, G.; HU, Z. Airborne observations reveal elevational gradient in tropical forest isoprene emissions. **Nature Communications**, v. 8, n. May, p. 15541, 2017.

GUENTHER, A.; HEWITT, C. N.; ERVIN, D.; NICHOLAS, C.; FALL, R.; KLINGER, L.; MCKAY, W. A; SCHOLES, B.; STEINBRECHER, R.; TALLAMRAJU, R.; TAYLOR, J.; ZIMMERMAN, P.; HEWITT, C. N.; ERICKSON, D.; FALL, R.; GERON, C.; GRAEDEL, T.; HARLEY, P.; KLINGER, L.; LERDAU, M.; MCKAY, W. A; PIERCE, T.; SCHOLES, B.; STEINBRECHER, R.;

TALLAMRAJU, R.; TAYLOR, J.; ZIMMERMAN, P.; ERVIN, D.; NICHOLAS, C.; FALL, R.; KLINGER, L.; MCKAY, W. A; SCHOLES, B.; STEINBRECHER, R.; TALLAMRAJU, R.; TAYLOR, J.; ZIMMERMAN, P. A global model of natural volatile organic compound emissions. **Journal of Geophysical Research**, v. 100, n. D5, p. 8873–8892, 1 jan. 1995.

GUENTHER, A.; KARL, T.; HARLEY, P.; WIEDINMYER, C.; PALMER, P. I.; GERON, C. Estimates of global terrestrial isoprene emissions using MEGAN (Model of Emissions of Gases and Aerosols from Nature). **Atmospheric Chemistry and Physics Discussions**, v. 6, n. 1, p. 107–173, 3 jan. 2006.

GUENTHER, A. B.; JIANG, X.; HEALD, C. L.; SAKULYANONTVITTAYA, T.; DUHL, T.; EMMONS, L. K.; WANG, X. The Model of Emissions of Gases and Aerosols from Nature version 2.1 (MEGAN2.1): an extended and updated framework for modeling biogenic emissions. **Geoscientific Model Development**, v. 5, n. 6, p. 1471–1492, 12 nov. 2012.

GUIMARÃES, C. S.; CUSTODIO, D.; DE OLIVEIRA, R. C. S.; VARANDAS, L. S.; ARBILLA, G. Comparative Study of Automotive, Aircraft and Biogenic Emissions of Aldehydes and Aromatic Compounds. **Bulletin of Environmental Contamination and Toxicology**, v. 84, n. 2, p. 180–184, 6 out. 2009.

HARLEY, P.; VASCONCELLOS, P.; VIERLING, L.; PINHEIRO, C. C. D. S. .; GREENBERG, J.; GUENTHER, A.; KLINGER, L.; ALMEIDA, S. S. DE; NEILL, D.; BAKER, T.; PHILLIPS, O.; MALHI, Y.; DIVISION, A. C.; CITY, R.; LOUIS, S.; MANAGEMENT, R. Variation in potential for isoprene emissions among Neotropical forest sites. **Global Change Biology**, v. 10, n. 5, p. 630–650, 1 maio 2004.

HELMIG, D.; BALSLEY, B.; DAVIS, K.; KUCK, L. R.; JENSEN, M.; BOGNAR, J.; SMITH, T.; ARRIETA, R. V.; RODRÍGUEZ, R.; BIRKS, J. W. Vertical profiling and determination of landscape fluxes of biogenic nonmethane hydrocarbons within the planetary boundary layer in the Peruvian Amazon. **Journal of Geophysical Research: Atmospheres**, v. 103, n. D19, p. 25519–25532, 1998.

HERMANSSON, E.; ROLDIN, P.; RUSANEN, A.; MOGENSEN, D.; KIVEKÄS, N.; BOY, M.; SWIETLICKI, E. Biogenic SOA formation through gas-phase oxidation and gas-to-particle partitioning – comparison between process models of varying complexity. **Atmospheric Chemistry and Physics Discussions**, v. 14, n. 8, p. 11001–11040, 1 jan. 2014.

HESS, P. G.; GUENTHER, A.; PFISTER, G. G.; LAMARQUE, J.-F. F.; EMMONS, L. K.; ORLANDO, J. J.; WALTERS, S.; PALMER, P. I.; LAWRENCE, P. J.; HESS, P. G.; LAMARQUE, J.-F. F.; ORLANDO, J. J.; WALTERS, S.; GUENTHER, A.; PALMER, P. I.; LAWRENCE, P. J. Contribution of isoprene to chemical budgets: A model tracer study with the NCAR CTM MOZART-4. **Journal of Geophysical Research**, v. 113, n. D5, p. n/a-n/a, 8 mar. 2008.

HOBBS, P. V.; SINHA, P.; YOKELSON, R. J.; CHRISTIAN, T. J.; BLAKE, D. R.;

GAO, S.; KIRCHSTETTER, T. W.; NOVAKOV, T.; PILEWSKIE, P. Evolution of gases and particles from a savanna fire in South Africa. **Journal of Geophysical Research**, v. 108, n. D13, p. 8485, 2003.

HOFFMANN, T.; ODUM, J. R.; BOWMAN, F.; COLLINS, D.; KLOCKOW, D.; FLAGAN, R. C.; SEINFELD, J. H. Formation of Organic Aerosols from the Oxidation of Biogenic Hydrocarbons. **Journal of Atmospheric Chemistry**, v. 26, n. 2, p. 189–222, 1997.

IACONO, M. J.; DELAMERE, J. S.; MLAWER, E. J.; SHEPHARD, M. W.; CLOUGH, S. A.; COLLINS, W. D.; IACONO, M. J.; DELAMERE, J. S.; MLAWER, E. J.; MLAWER, E. J.; SHEPHARD, M. W.; CLOUGH, S. A.; CLOUGH, S. A.; COLLINS, W. D. Radiative forcing by long-lived greenhouse gases: Calculations with the AER radiative transfer models. **Journal of Geophysical Research**, v. 113, n. D13, p. 233, 2 jul. 2008.

IM, U.; POUPKOU, A.; INCECIK, S.; MARKAKIS, K.; KINDAP, T.; UNAL, A.; MELAS, D.; YENIGUN, O.; TOPCU, S.; ODMAN, M. T.; TAYANC, M.; GULER, M. The impact of anthropogenic and biogenic emissions on surface ozone concentrations in Istanbul. **Science of the Total Environment**, v. 409, n. 7, p. 1255–1265, 2011.

JACOB, D. J.; WOFSY, S. C.; GREENBERG, J. P.; ZIMMERMAN, P. R. Photochemistry of biogenic emissions over the Amazon forest. **Journal of Geophysical Research: Atmospheres**, v. 93, n. D2, p. 1477–1486, 1 jan. 1988.

JANSSENS-MAENHOUT, G.; CRIPPA, M.; GUIZZARDI, D.; DENTENER, F.; MUNTEAN, M.; POULIOT, G.; KEATING, T.; ZHANG, Q.; KUROKAWA, J.; WANKMÜLLER, R.; DENIER VAN DER GON, H.; KUENEN, J. J. P.; KLIMONT, Z.; FROST, G.; DARRAS, S.; KOFFI, B.; LI, M. HTAP-v2.2: A mosaic of regional and global emission grid maps for 2008 and 2010 to study hemispheric transport of air pollution. **Atmospheric Chemistry and Physics**, v. 15, n. 19, p. 11411–11432, 2015.

JONQUIÈRES, I.; MARENCO, A.; MAALEJ, A.; ROHRER, F. Study of ozone formation and transatlantic transport from biomass burning emissions over West Africa during the airborne Tropospheric Ozone Campaigns TROPOZ I and TROPOZ II. **Journal of Geophysical Research**, v. 103, p. 19059, 1998.

JOST, C.; TRENTMANN, J.; SPRUNG, D.; ANDREAE, M. Trace gas chemistry in a young biomass burning plume over Namibia: observations and model simulations. **Journal of Geophysical Research**, v. 108, n. D13, p. 8482, 2003.

KARL, T.; GUENTHER, A.; YOKELSON, R. J.; GREENBERG, J.; POTOSNAK, M.; BLAKE, D. R.; ARTAXO, P. The tropical forest and fire emissions experiment: Emission, chemistry, and transport of biogenic volatile organic compounds in the lower atmosphere over Amazonia. **Journal of Geophysical Research**, v. 112, n. D18, p. D18302, 19 set. 2007.

KARLIK, J. F.; CHUNG, Y. J.; WINER, A. M. Biogenic emission inventory development: Field assessment of the GAP vegetation database in California. **Physics**

and Chemistry of the Earth, v. 28, n. 8, p. 315–325, 2003.

KAUFMAN, Y. J.; SETZER, A.; WARD, D.; TANRE, D.; HOLBEN, B. N.; MENZEL, P.; PEREIRA, M. C.; RASMUSSEN, R. Biomass Burning Airborne and Spaceborne Experiment in the Amazonas (Base-a). **Journal of Geophysical Research-Atmospheres**, v. 97, n. D13, p. 14581–14599, 1992.

KONDO, Y.; MORINO, Y.; TAKEGAWA, N.; KOIKE, M.; KITA, K.; MIYAZAKI, Y.; SACHSE, G. W.; VAY, S. A.; AVERY, M. A.; FLOCKE, F.; WEINHEIMER, A. J.; EISELE, F. L.; ZONDLO, M. A.; WEBER, R. J.; SINGH, H. B.; CHEN, G.; CRAWFORD, J.; BLAKE, D. R.; FUELBERG, H. E.; CLARKE, A. D.; TALBOT, R. W.; SANDHOLM, S. T.; BROWELL, E. V.; STREETS, D. G.; LILEY, B. Impacts of biomass burning in Southeast Asia on ozone and reactive nitrogen over the western Pacific in spring. **Journal of Geophysical Research D: Atmospheres**, v. 109, n. 15, p. 1–22, 2004.

KUBISTIN, D.; HARDER, H.; MARTINEZ, M.; RUDOLF, M.; SANDER, R.; BOZEM, H.; EERDEKENS, G.; FISCHER, H.; GURK, C.; KL??PFEL, T.; K??NIGSTEDT, R.; PARCHATKA, U.; SCHILLER, C. L.; STICKLER, A.; TARABORRELLI, D.; WILLIAMS, J.; LELIEVELD, J.; KLÜPFEL, T.; KÖNIGSTEDT, R.; PARCHATKA, U.; SCHILLER, C. L.; STICKLER, A.; TARABORRELLI, D.; WILLIAMS, J.; LELIEVELD, J. Hydroxyl radicals in the tropical troposphere over the Suriname rainforest: Comparison of measurements with the box model MECCA. **Atmospheric Chemistry and Physics**, v. 10, n. 19, p. 9705–9728, 2010.

KUHN, U.; ANDREAE, M. O.; AMMANN, C.; ARAÚJO, A. C.; BRANCALEONI, E.; CICCIOLI, P.; DINDORF, T.; FRATTONI, M.; GATTI, L. V.; GANZEVELD, L.; KRUIJT, B.; LELIEVELD, J.; LLOYD, J.; MEIXNER, F. X.; NOBRE, A. D.; PÖSCHL, U.; SPIRIG, C.; STEFANI, P.; THIELMANN, A.; VALENTINI, R.; KESSELMEIER, J. Isoprene and monoterpene fluxes from Central Amazonian rainforest inferred from tower-based and airborne measurements, and implications on the atmospheric chemistry and the local carbon budget. **Atmospheric Chemistry and Physics**, v. 7, n. 11, p. 2855–2879, 11 jun. 2007.

LAMARQUE, J.-F. F.; EMMONS, L. K.; HESS, P. G.; KINNISON, D. E.; TILMES, S.; VITT, F.; HEALD, C. L.; HOLLAND, E. A.; LAURITZEN, P. H.; NEU, J.; ORLANDO, J. J.; RASCH, P.; TYNDALL, G.; TILMES, S.; EMMONS, L. K.; ORLANDO, J. J.; LAMARQUE, J.-F. F.; HESS, P. G.; KINNISON, D. E.; VITT, F.; HEALD, C. L.; LAURITZEN, P. H.; NEU, J.; RASCH, P.; TYNDALL, G. CAM-chem: description and evaluation of interactive atmospheric chemistry in CESM. **Geoscientific Model Development Discussions**, v. 4, n. 3, p. 2199–2278, 1 jan. 2011.

LANGFORD, A. O.; SENFF, C. J.; ALVAREZ, R. J.; BANTA, R. M.; HARDESTY, R. M. Long-range transport of ozone from the Los Angeles Basin: A case study. **Geophysical Research Letters**, v. 37, n. 6, p. n/a-n/a, 2010.

LANGFORD, A O.; SENFF, C. J.; ALVAREZ II, R. J.; BANTA, R. M.; HARDESTY,

R. M.; KLEFFMANN, J.; GAVRILOAIEI, T.; HOFZUMAHAUS, A.; HOLLAND, F.; KOPPMANN, R.; RUPP, L.; SCHLOSSER, E.; SIESE, M.; WAHNER, A. Daytime formation of nitrous acid: A major source of OH radicals in a forest. **Geophysical Research Letters**, v. 32, n. 5, p. 1–4, 1 jan. 2005.

LAOTHAWORNKITKUL, J.; TAYLOR, J. E.; PAUL, N. D.; HEWITT, C. N. Biogenic volatile organic compounds in the Earth system. **The New phytologist**, v. 183, n. 1, p. 27–51, jan. 2009.

LAWRENCE, D. M.; OLESON, K. W.; FLANNER, M. G.; THORNTON, P. E.; SWENSON, S. C.; LAWRENCE, P. J.; ZENG, X.; YANG, Z.; LEVIS, S.; SAKAGUCHI, K.; BONAN, G. B.; SLATER, A. G.; PETER, J.; ZENG, X.; YANG, Z.; LEVIS, S.; SAKAGUCHI, K.; BONAN, G. B.; SLATER, A. G. Parameterization improvements and functional and structural advances in Version 4 of the Community Land Model. **Journal of Advances in Modeling Earth Systems**, v. 3, n. 3, p. 1–27, 19 mar. 2011.

LELIEVELD, J.; BUTLER, T. M.; CROWLEY, J. N.; DILLON, T. J.; FISCHER, H.; GANZEVELD, L.; HARDER, H.; LAWRENCE, M. G.; MARTINEZ, M.; TARABORRELLI, D.; WILLIAMS, J. Atmospheric oxidation capacity sustained by a tropical forest. **Nature**, v. 452, n. 7188, p. 737–40, 10 abr. 2008.

LIU, Y.; BRITO, J.; DORRIS, M.; RIVERA-RIOS, J. C.; SECO, R.; BATES, K. H.; ARTAXO, P.; JUNIOR, S. D.; KEUTSCH, F.; KIM, S.; GOLDSTEIN, A. H.; GUENTHER, A. B.; MANZI, A.; SOUZA, R.; SPRINGSTON, S. R.; WATSON, T. B.; MCKINNEY, K. A.; MARTIN, S. T. Isoprene Photochemistry over the Amazon Rain Forest. **Proceedings of the National Academy of Sciences**, 2016.

LONGO, K. M.; FREITAS, S. R.; ANDREAE, M. O.; SETZER, A.; PRINS, E.; ARTAXO, P. The coupled aerosol and tracer transport model to the brazilian developments on the regional atmospheric modeling system (catt-brams)-part 2: Model sensitivity to the biomass burning inventories. **Atmospheric Chemistry and Physics**, v. 10, n. 13, p. 5785–5795, 2010.

LONGO, K. M.; FREITAS, S. R.; ANDREAE, M. O.; YOKELSON, R.; ARTAXO, P. Biomass burning in Amazonia: Emissions, long-range transport of smoke and its regional and remote impacts. **Geophysical Monograph Series**, v. 186, n. 4, p. 207–232, 1 jan. 2009.

LONGO, K. M. ; FREITAS, S. R. ; PIRRE, M., MARÉCAL; V., RODRIGUES; L. F., PANETTA, J. ; ALONSO, M. F. ; ROSÁRIO, N. E. ; MOREIRA, D. S. ; GÁCITA, M. S. ; ARTETA, J. ; FONSECA, R. ; STOCKLER, R. ; KATSURAYAMA, D. M. ; FAZENDA, A. AND BELA, M. The Chemistry CATT-BRAMS model (CCATT-BRAMS 4.5): A regional atmospheric model system for integrated air quality and weather forecasting and research. **Geoscientific Model Development**, v. 6, n. 5, p. 1389–1405, 9 set. 2013.

MASSON, V. A physically-based scheme for the urban energy budget in atmospheric

models. **Boundary-Layer Meteorology**, v. 94, n. 3, p. 357–397, 2000.

MASTIN, L. G.; GUFFANTI, M.; SERVRANCKX, R.; WEBLEY, P.; BARSOTTI, S.; DEAN, K.; DURANT, A.; EWERT, J. W.; NERI, A.; ROSE, W. I.; SCHNEIDER, D.; SIEBERT, L.; STUNDER, B.; SWANSON, G.; TUPPER, A.; VOLENTIK, A.; WAYTHOMAS, C. F. A multidisciplinary effort to assign realistic source parameters to models of volcanic ash-cloud transport and dispersion during eruptions. **Journal of Volcanology and Geothermal Research**, v. 186, n. 1, p. 10–21, 2009.

MAULDIN, R. L. I.; MADRONICH, S.; FLOCKE, S. J.; EISELE, F. L.; FROST, G. J.; PREVOT, A. S. H. New insights on OH: Measurements around and in clouds. **Geophysical Research Letters**, v. 24, n. 23, p. 3033–3036, 1997.

MAUZERALL, D. L.; LOGAN, J. A.; JACOB, D. J.; ANDERSON, B. E.; BLAKE, D. R.; BRADSHAW, J. D.; HEIKES, B.; SACHSE, G. W.; SINGH, H.; TALBOT, B. Photochemistry in biomass burning plumes and implications for tropospheric ozone over the tropical South Atlantic. **Journal of Geophysical Research**, v. 103, n. D7, p. 8401, 1998.

MELLOR; YAMADA, T. Development of a turbulence closure model for geophysical fluid problems. **Rev. Geophys. Space Phys.**, v. 20, n. C2, 1982.

MEYERS, M. P.; WALKO, R. L.; HARRINGTON, J. Y.; COTTON, W. R. New RAMS cloud microphysics parameterization. Part II: The two-moment scheme. **Atmospheric Research**, v. 45, n. 1, p. 3–39, ago. 1997.

MISZTAL, P. K.; AVISE, J. C.; KARL, T.; SCOTT, K.; JONSSON, H. H.; GUENTHER, A. B.; GOLDSTEIN, A. H. Evaluation of regional isoprene emission factors and modeled fluxes in California. **Atmospheric Chemistry and Physics**, v. 16, n. 15, p. 9611–9628, 1 jan. 2016.

MLAWER, E. J.; TAUBMAN, S. J.; BROWN, P. D.; IACONO, M. J.; CLOUGH, S. A. Radiative transfer for inhomogeneous atmospheres: RRTM, a validated correlated-k model for the longwave. **Journal of Geophysical Research**, v. 102, n. D14, p. 16663–16682, 1 jul. 1997.

MONKS, P. S. Gas-phase radical chemistry in the troposphere. **Chemical Society reviews**, v. 34, n. 5, p. 376–95, maio 2005.

MOREIRA, D. S.; FREITAS, S. R.; BONATTI, J. P.; MERCADO, L. M.; ROSÁRIO, N. M. É.; LONGO, K. M.; MILLER, J. B.; GLOOR, M.; GATTI, L. V. Coupling between the JULES land-surface scheme and the CCATT-BRAMS atmospheric chemistry model (JULES-CCATT-BRAMS1.0): applications to numerical weather forecasting and the CO_2 budget in South America. **Geoscientific Model Development**, v. 6, n. 4, p. 1243–1259, 22 ago. 2013.

MÜLLER, M.; ANDERSON, B. E. ; BEYERSDORF, A. J. ; CRAWFORD, J. H. ; DISKIN, G. S. ; EICHLER, P. ; FRIED, A. ; KEUTSCH, F. N. ; MIKOVINY, T. ; THORNHILL, K. L. ; WALEGA, J. G. ; WEINHEIMER, A. J. ; YANG, M. ;

NÖLSCHER, A C.; SINHA, V.; BOCKISCH, S.; KLÜPFEL, T.; WILLIAMS, J.; MÜLLER, M.; GRAUS, M.; RUUSKANEN, T. M.; SCHNITZHOFER, R.; BAMBERGER, I.; KASER, L.; TITZMANN, T.; HÖRTNAGL, L.; WOHLFAHRT, G.; KARL, T.; HANSEL, A. First eddy covariance flux measurements by PTR-TOF. **Atmospheric Measurement Techniques**, v. 2, n. 6, p. 3265–3290, 1 jan. 2009.

OLIVIER, J. G. J.; BLOOS, J. P. J.; BERDOWSKI, J. J. M.; VISSCHEDIJK, A. J. H.; BOUWMAN, A. F. A 1990 global emission inventory of anthropogenic sources of carbon monoxide on 1°×1° developed in the framework of EDGAR/GEIA. **Chemosphere - Global Change Science**, v. 1, n. 1, p. 1–17, 1999.

PARRISH, D. D.; HOLLOWAY, J. S.; TRAINER, M.; MURPHY, P. C.; FEHSENFELD, F. C.; FORBES, G. L. Export of North American Ozone Pollution to the North Atlantic Ocean. **Science**, v. 259, n. 5100, p. 1436–1439, 5 mar. 1993.

PIELKE, R. A.; COTTON, W. R.; WALKO, R. L.; TREMBACK, C. J.; LYONS, W. A.; GRASSO, L. D.; NICHOLLS, M. E.; MORAN, M. D.; WESLEY, D. A.; LEE, T. J.; COPELAND, J. H. A comprehensive meteorological modeling system-RAMS. **Meteorology and Atmospheric Physics**, v. 49, n. 1–4, p. 69–91, 1992.

PIERCE, T.; GERON, C.; BENDER, L.; DENNIS, R.; TONNESEN, G.; GUENTHER, A. Influence of increased isoprene emissions on regional ozone modeling. **Journal of Geophysical Research**, v. 103, n. D19, p. 25611, 1998.

POTTER, C. S.; ALEXANDER, S. E.; COUGHLAN, J. C.; KLOOSTER, S. A. Modeling biogenic emissions of isoprene: exploration of model drivers, climate control algorithms, and use of global satellite observations. **Atmospheric Environment**, v. 35, n. 35, p. 6151–6165, 2001.

PRINN, R. THE CLEANSING CAPACITY OF THE ATMOSPHERE. **Annu Rev Env Resour**, v. 28, n. 1, p. 29–57, 2003.

PRINN, R. G. **Ozone, hydroxyl radical, and oxidative capacity**. 2. ed. [s.l.] Elsevier Ltd., 2014. v. 5 1-18 p. ISBN(9780080983004).

RASMUSSEN, R. A.; KHALIL, M. A. K. Isoprene over the Amazon Basin. **Journal of Geophysical Research**, v. 93, n. D2, p. 1417–1421, 1 jan. 1988.

GRANIER, C.; ARTAXO NETTO, P. E.; REEVES, C. E. **Emissions of atmospheric trace compounds**. Springer Netherlands, 2004. 545p.

REID, J. S.; HOBBS, P. V; FEREK, R. J.; BLAKE, D. R.; MARTINS, J. V; DUNLAP, M. R.; LIOUSSE, C. Physical, chemical, and optical properties of regional hazes dominated by smoke in Brazil. **Journal of Geophysical Research**, v. 103, n. D24, p. 32059–32080, 1998.

RIBEIRO, J. E. L. S. **Flora da Reserva Ducke**: guia de identificação das plantas vasculares de uma floresta de terra-firme na Amazônia Central. p. 793p, 1 jan. 1999.

RIVERA-RIOS, J. C.; NGUYEN, T. B.; CROUNSE, J. D.; JUD, W.; ST. CLAIR, J. M.; MIKOVINY, T.; GILMAN, J. B.; LERNER, B. M.; KAISER, J. B.; DE GOUW, J.; WISTHALER, A.; HANSEL, A.; WENNBERG, P. O.; SEINFELD, J. H.; KEUTSCH, F. N.; LIN, G.; PENNER, J. E.; ZHOU, C. Conversion of hydroperoxides to carbonyls in field and laboratory instrumentation: Observational bias in diagnosing pristine versus anthropogenically controlled atmospheric chemistry. **Geophysical Research Letters**, v. 41, n. 23, p. 8645–8651, 8 dez. 2014.

SALEEBY, S.; COTTON, W. A large-droplet mode and prognostic number concentration of cloud droplets in the {…}. **Journal of Applied Meteorology**, v. 44, p. 1912-1929, 2004.

SALEEBY, S. M.; COTTON, W. R.; SALEEBY, S. M.; COTTON, W. R. A Binned Approach to Cloud-Droplet Riming Implemented in a Bulk Microphysics Model. **Journal of Applied Meteorology and Climatology**, v. 47, n. 2, p. 694–703, 1 fev. 2008.

SARTELET, K. N.; COUVIDAT, F.; SEIGNEUR, C.; ROUSTAN, Y. Impact of biogenic emissions on air quality over Europe and North America. **Atmospheric Environment**, v. 53, p. 131–141, 2012.

SHARKEY, T. D.; WIBERLEY, A. E.; DONOHUE, A. R. Isoprene emission from plants: Why and how. **Annals of Botany**, Ann Bot. v.101, n.1, p.5-18, 2008.

SIMMON, R. **Map of the rainforests in the world**. Disponível em: <https://earthobservatory.nasa.gov/Features/Deforestation/>. Acesso em: 25 abr. 2017.

SINGH, H. B. Atmospheric peroxyacetyl nitrate measurements over the Brazilian Amazon Basin during the wet season: relationships with nitrogen oxides and ozone. **Journal of Geophysical Research**, v. 95, n. D10, p. 16,916-945,954, 1990.

SINGH, H. B.; VIEZEE, W.; CHEN, Y.; BRADSHAW, J.; SANDHOLM, S.; BLAKE, D.; BLAKE, N.; HEIKES, B.; SNOW, J.; TALBOT, R.; BROWELL, E.; GREGORY, G.; SACHSE, G.; VAY, S. Biomass burning influences on the composition of the remote South Pacific troposphere: analysis based on observations from PEM-Tropics-A. **Atmospheric Environment,** v. 34, p. 635 – 644, 2000.

SOLMON, F.; SARRAT, C.; SERÇA, D.; TULET, P.; ROSSET, R. Isoprene and monoterpenes biogenic emissions in France: modeling and impact during a regional pollution episode. **Atmospheric Environment**, v. 38, n. 23, p. 3853–3865, 2004.

SRIVASTAVA, S.; NAJA, M.; THOURET, V. Influences of regional pollution and long range transport over Hyderabad using ozone data from MOZAIC. **Atmospheric Environment**, v. 117, p. 135–146, 2015.

ST CLAIR, J. M.; RIVERA-RIOS, J. C.; CROUNSE, J. D.; KNAP, H. C.; BATES, K. H.; TENG, A. P.; JØRGENSEN, S.; KJAERGAARD, H. G.; KEUTSCH, F. N.; WENNBERG, P. O.; ST. CLAIR, J. M.; RIVERA-RIOS, J. C.; CROUNSE, J. D.; KNAP, H. C.; BATES, K. H.; TENG, A. P.; JØRGENSEN, S.; KJAERGAARD, H. G.;

KEUTSCH, F. N.; WENNBERG, P. O.; JORGENSEN, S.; KJAERGAARD, H. G.; KEUTSCH, F. N.; WENNBERG, P. O.; ST CLAIR, J. M.; RIVERA-RIOS, J. C.; CROUNSE, J. D.; KNAP, H. C.; BATES, K. H.; TENG, A. P.; JØRGENSEN, S.; KJAERGAARD, H. G.; KEUTSCH, F. N.; WENNBERG, P. O. Kinetics and Products of the Reaction of the First-Generation Isoprene Hydroxy Hydroperoxide (ISOPOOH) with OH. **Journal of Physical Chemistry A**, v. 120, n. 9, p. 1441–1451, 10 mar. 2016.

STOCKWELL, W. R.; KIRCHNER, F.; KUHN, M.; SEEFELD, S. A new mechanism for regional atmospheric chemistry modeling. **Journal of Geophysical Research: Atmospheres**, v. 102, n. 97, p. 25847–25879, 1997.

STOCKWELL, W. R.; LAWSON, C. V.; SAUNDERS, E.; GOLIFF, W. S. A Review of Tropospheric Atmospheric Chemistry and Gas-Phase Chemical Mechanisms for Air Quality Modeling. **Atmosphere**, v. 3, n. 4, p. 1–32, 21 dez. 2011.

STOHL, A.; THELOKE, J.; GRANIER, C.; ORLANDO, J. J. J.; HOFZUMAHAUS, A.; JENKIN, M. E. E.; BAKLANOV, A.; LIOUSSE, C.; LEE, J. D. D.; PETZOLD, A.; PÖSCHL, U.; PALMER, P. I. I.; BLAKE, N.; DENTENER, F.; MONKS, P. S. S.; PREVOT, A S. H.; MOUSSIOPOULOS, N.; FROST, G. J. J.; BALTENSPERGER, U.; FUZZI, S.; WILLIAMS, M. L. L.; AKIMOTO, H.; AMANN, M.; BEY, I.; BLAKE, R. S. S.; CARSLAW, K.; COOPER, O. R. R.; FOWLER, D.; FRAGKOU, E.; GENEROSO, S.; GINOUX, P.; GREWE, V.; GUENTHER, A.; HANSSON, H.-C. H. C.; HENNE, S.; HJORTH, J.; HUNTRIESER, H.; ISAKSEN, I. S. A. S. A.; KAISER, J.; KANAKIDOU, M.; KLIMONT, Z.; KULMALA, M.; LAJ, P.; LAWRENCE, M. G. G.; MAIONE, M.; MCFIGGANS, G.; METZGER, A.; MIEVILLE, A.; O'DOWD, C. D. D.; PARRISH, D. D. D.; et al. Atmospheric composition change – global and regional air quality. **Atmospheric Environment**, v. 43, n. 33, p. 5268–5350, 1 out. 2009.

STROUD, C. A.; ROBERTS, J. M.; GOLDAN, P. D.; KUSTER, W. C.; MURPHY, P. C.; WILLIAMS, E. J.; HEREID, D.; PARRISH, D.; SUEPER, D.; TRAINER, M.; FEHSENFELD, F. C.; APEL, E. C.; RIEMER, D.; WERT, B.; HENRY, B.; FRIED, A.; MARTINEZ-HARDER, M.; HARDER, H.; BRUNE, W. H.; LI, G.; XIE, H.; YOUNG, V. L.; APEL, C.; RIEMER, D.; WERT, B.; HENRY, B.; FRIED, A. Isoprene and its oxidation products, methacrolein and methylvinyl ketone, at an urban forested site during the 1999 Southern Oxidants Study. **Journal of Geophysical Research**, v. 106, n. D8, p. 8035–8046, 1 abr. 2001.

THOMPSON, G.; EIDHAMMER, T. A Study of Aerosol Impacts on Clouds and Precipitation Development in a Large Winter Cyclone. **Journal of the Atmospheric Sciences**, v. 71, n. 10, p. 3636–3658, 2014.

THOMPSON, G.; FIELD, P. R.; RASMUSSEN, R. M.; HALL, W. D. Explicit Forecasts of Winter Precipitation Using an Improved Bulk Microphysics Scheme. Part II: implementation of a new snow parameterization. **Monthly Weather Review**, v. 136, n. 12, p. 5095–5115, 2008.

THUNIS, P.; CUVELIER, C. Impact of biogenic emissions on ozone formation in the

Mediterranean area – a BEMA modelling study. **Atmospheric Environment**, v. 34, n. 3, p. 467–481, 2000.

TOLL, I.; BALDASANO, J. M. Modeling of photochemical air pollution in the Barcelona area with highly disaggregated anthropogenic and biogenic emissions. **Atmospheric Environment**, v. 34, n. 19, p. 3069–3084, 2000.

TOON, O. B.; MCKAY, C. P.; ACKERMAN, T. P.; SANTHANAM, K. Rapid calculation of radiative heating rates and photodissociation rates in inhomogeneous multiple scattering atmospheres. **Journal of Geophysical Research**, v. 94, n. D13, p. 16287, 1989.

TORRES, A. L.; BUCHAN, H. Tropospheric nitric oxide measurements over the Amazon Basin. **Journal of Geophysical Research: Atmospheres**, v. 93, n. D2, p. 1396–1406, 1988.

TRENTMANN, J.; ANDREAE, M. Chemical processes in a young biomass-burning plume. **Journal of Geophysical Research**, v. 108, n. D22, p. 4705, 2003.

TURNIPSEED, A. A.; PRESSLEY, S. N.; KARL, T.; LAMB, B.; NEMITZ, E.; ALLWINE, E.; COOPER, W. A.; SHERTZ, S.; GUENTHER, A. B. The use of disjunct eddy sampling methods for the determination of ecosystem level fluxes of trace gases. **Atmospheric Chemistry and Physics**, v. 9, n. 3, p. 981–994, 9 fev. 2009.

WALKO, R. L.; BAND, L. E.; BARON, J.; KITTEL, T. G. F.; LAMMERS, R.; LEE, T. J.; OJIMA, D.; PIELKE, R. A.; TAYLOR, C.; TAGUE, C.; TREMBACK, C. J.; VIDALE, P. L. Coupled Atmosphere–Biophysics–Hydrology Models for Environmental Modeling. **Journal of Applied Meteorology**, v. 39, n. 6, p. 931–944, 2000.

WARNEKE, C.; HOLZINGER, R.; HANSEL, A.; JORDAN, A. Isoprene and its oxidation products methyl vinyl ketone, methacrolein, and isoprene related peroxides measured online over the tropical rain forest of Surinam in …. **Journal of Atmospheric …**, 2001.

WHALLEY, L. K.; STONE, D.; HEARD, D. E.; WHALLEY, L. K. New Insights into the Tropospheric Oxidation of Isoprene. **TripleC**, v. 11, n. 1, p. 13–35, 1 jan. 2013.

WILLIAMS, J.; POSCHL, U.; CRUTZEN, P. J.; HANSEL, A.; HOLZINGER, R.; WARNEKE, C.; LINDINGER, W.; LELIEVELD, J. An atmospheric chemistry interpretation of mass scans obtained from a proton transfer mass spectrometer flown over the tropical rainforest of Surinam. **Journal of Atmospheric Chemistry**, v. 38, n. 2, p. 133–166, 2001.

XU, Y.; WESELY, M. L.; PIERCE, T. E. Estimates of biogenic emissions using satellite observations and influence of isoprene emission on O3 formation over the eastern United States. **Atmospheric Environment**, v. 36, n. 38, p. 5819–5829, 2002.

YÁÑEZ-SERRANO, A. M.; NÖLSCHER, A C.; WILLIAMS, J.; WOLFF, S.;

ALVES, E.; MARTINS, G. A; BOURTSOUKIDIS, E. Diel and seasonal changes of biogenic volatile organic compounds within and above an Amazonian rainforest. **Atmos Chem Phys**, v. 15, p. 3359–3378, 2015.

YARWOOD, G.; RAO, S.; YOCKE, M.; WHITTEN, G. Z. **Updates to the carbon bond chemical mechanism**: CB05 - Final Report to US EPA. 1 jan. 2005.

YIN, D.; JIANG, W.; ROTH, H.; GIROUX, É. Improvement of biogenic emissions estimation in the Canadian Lower Fraser Valley and its impact on particulate matter modeling results. **Atmospheric Environment**, v. 38, n. 4, p. 507–521, 2004.

YOKELSON, R.; BERTSCHI, I.; CHRISTIAN, T.; HOBBS, P.; WARD, D.; HAO, W. Trace gas measurements in nascent, aged, and cloud-processed smoke from African savanna fires by airborne Fourier transform infrared spectroscopy {(AFTIR)}. **J Geophys Res Atmospheres 1984 2012**, v. 108, n. D13, p. n/a-n/a, 2003.

YOKELSON, R.; CROUNSE, J. D.; DECARLO, P. F.; KARL, T.; URBANSKI, S.; ATLAS, E. Emissions from biomass burning in the Yucatan. **Atmospheric Chemistry and Physics**, n. October 2008, p. 5812, 2009.

YOKELSON, R. J.; KARL, T.; ARTAXO, P.; BLAKE, D. R.; CHRISTIAN, T. J.; GRIFFITH, D. W. T.; GUENTHER, A.; HAO, W. M. The Tropical Forest and fire emissions experiment: overview and airborne fire emission factor measurements. **Atmospheric Chemistry and Physics Discussions**, v. 7, n. 3, p. 6903–6958, 2007.

YOKELSON, R. J.; WISTHALER, A. In situ measurements and modeling of reactive trace gases in a small biomass burning plume. **Atmospheric Chemistry and Physics**, v. 16, n. 6, p. 3813–3824, 2016.

ZANNONI, N.; GROS, V.; LANZA, M.; SARDA, R.; BONSANG, B.; KALOGRIDIS, C.; PREUNKERT, S.; LEGRAND, M.; JAMBERT, C.; BOISSARD, C.; LATHIÈRE, J.; VOGEL, B.; VOGEL, H.; BÄUMER, D.; BANGERT, M.; LUNDGREN, K.; RINKE, R.; STANELLE, T. The comprehensive model system COSMO-ART – radiative impact of aerosol on the state of the atmosphere on the regional scale. **Atmospheric Chemistry and Physics**, v. 9, n. 4, p. 14483–14528, 1 jan. 2009.

APPENDIX – SUPLEMENTAR INFORMATION

Data availability

The SAMBBA field experiment data are available at Centre for Environmental Data Analysis (http://browse.ceda.ac.uk/browse/badc/sambba/data/faam-bae146) and complementary data are available on request.

S1**.** Interpolation grid used in the Figures 21 and 25

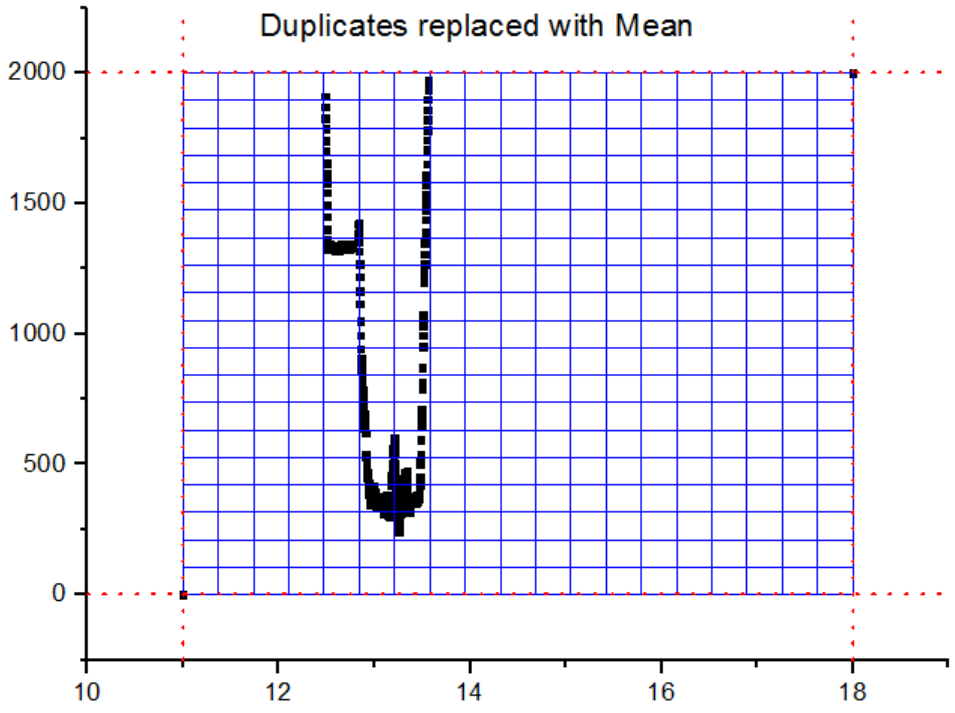

Interpolation grid (0 - 2000m and 11 - 18h)

S2**.** The kinetic rate constant measurements for OH + ISOPOOH (1,2- and 4,3-ISOPOOH), at 297 K, is 7.5 x 10^{-11} cm^3 $molecule^{-1}$ s^{-1} for (1,2)-ISOPOOH and 1.18 x 10^{-10} cm^3 $molecule^{-1}$ s^{-1} for (4,3)-ISOPOOH (ST CLAIR et al., 2016). The kinetic rate

constant of MVK + OH = 1.88 x 10^{-11} cm^3 $molecule^{-1}$ s^{-1} and MACR + OH = 3.35 x 10^{-11} cm^3 $molecule^{-1}$ s^{-1} (BERTSCHI et al., 2002).

K_{prod} Average kinetic rate constant = 6.1325 $_x$ 10^{-11}

$K_{iso} - K_{prod}$ = (1.1 x 10^{-10}) – (6.1325 $_x$ 10^{-11}) = 4.8675 $_x$ 10^{-11}

S3. Estimated the processing time as $t = 5.3e^{5.4 * ER_{[\Delta O_3]/[\Delta CO]}}$ (seconds), based on the fitting function of previous measurements of $ER_{[\Delta O_3]/[\Delta CO]}$ and plume age observations in tropical and subtropical sites.

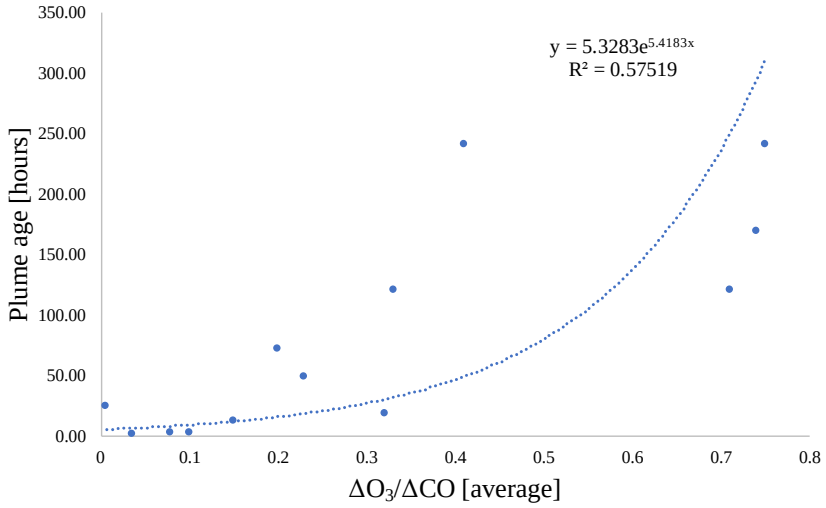

Figure S4. Flight Plots for sorties within/near the Rondônia Region

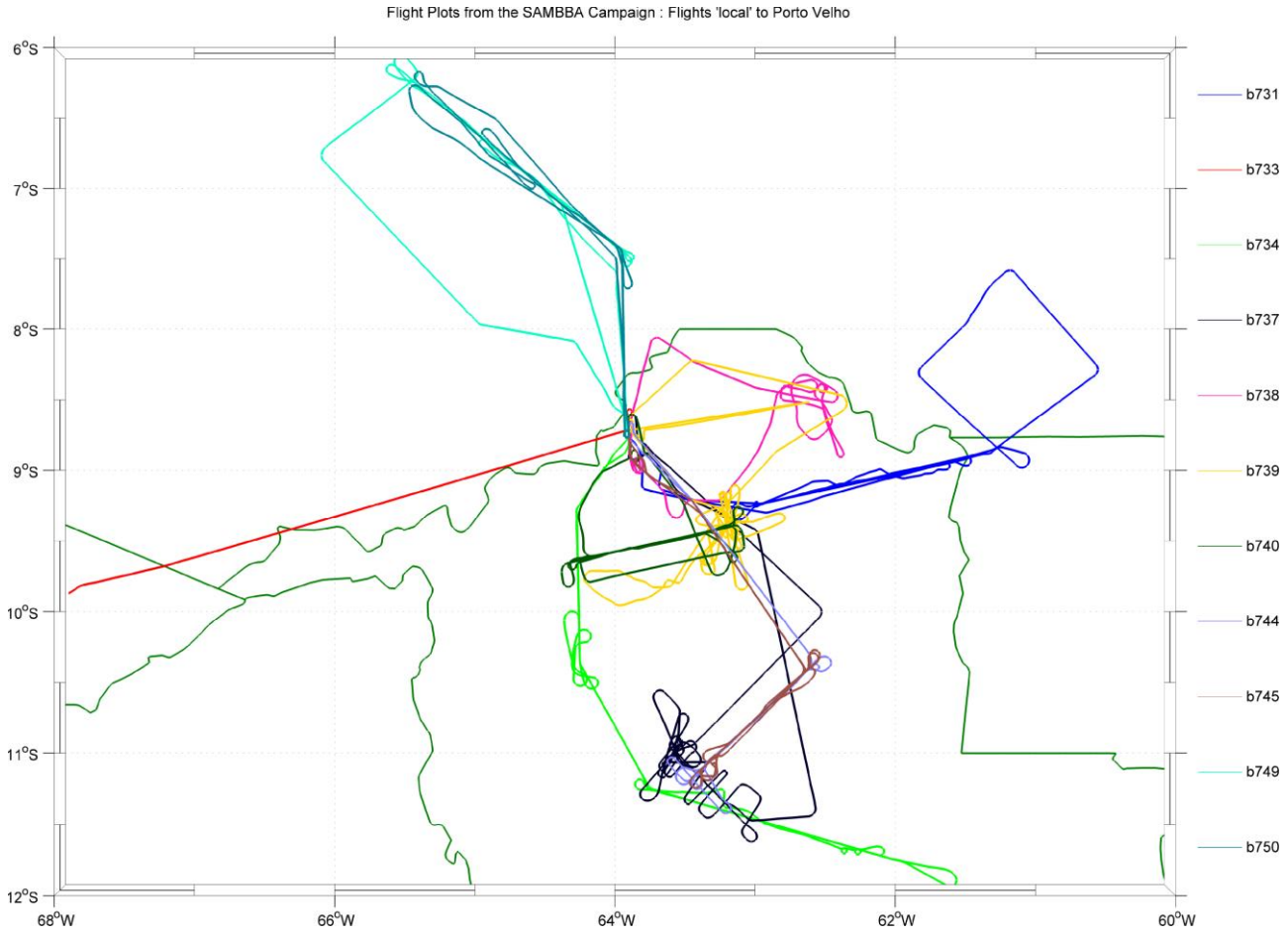

Source: Adapted from Johnson, B. (2012).

Figure S5. Flight plots for long range, regional scale sorties

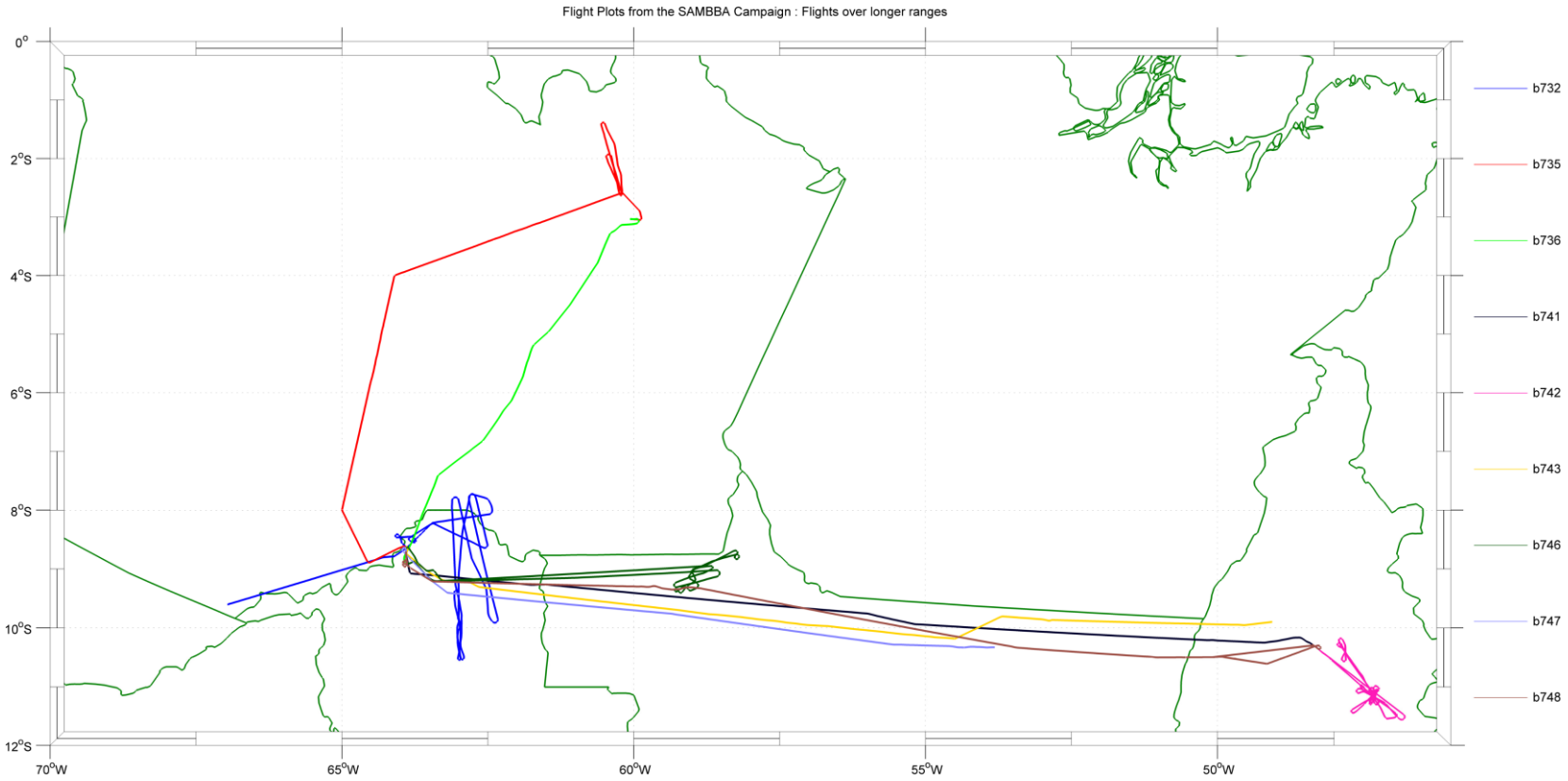

Source: Adapted from Johnson, B. (2012).

PUBLICAÇÕES TÉCNICO-CIENTÍFICAS EDITADAS PELO INPE

Teses e Dissertações (TDI)

Teses e Dissertações apresentadas nos Cursos de Pós-Graduação do INPE.

Manuais Técnicos (MAN)

São publicações de caráter técnico que incluem normas, procedimentos, instruções e orientações.

Notas Técnico-Científicas (NTC)

Incluem resultados preliminares de pesquisa, descrição de equipamentos, descrição e ou documentação de programa de computador, descrição de sistemas e experimentos, apresentação de testes, dados, atlas, e documentação de projetos de engenharia.

Relatórios de Pesquisa (RPQ)

Reportam resultados ou progressos de pesquisas tanto de natureza técnica quanto científica, cujo nível seja compatível com o de uma publicação em periódico nacional ou internacional.

Propostas e Relatórios de Projetos (PRP)

São propostas de projetos técnico-científicos e relatórios de acompanhamento de projetos, atividades e convênios.

Publicações Didáticas (PUD)

Incluem apostilas, notas de aula e manuais didáticos.

Publicações Seriadas

São os seriados técnico-científicos: boletins, periódicos, anuários e anais de eventos (simpósios e congressos). Constam destas publicações o Internacional Standard Serial Number (ISSN), que é um código único e definitivo para identificação de títulos de seriados.

Programas de Computador (PDC)

São as sequências de instruções ou códigos, expressos em uma linguagem de programação compilada ou interpretada, a ser executada por um computador para alcançar um determinado objetivo. São aceitos tanto programas fonte quanto executáveis.

Pré-publicações (PRE)

Todos os artigos publicados em periódicos, anais e como capítulos de livros.